„Physiologische Untersuchung neuronaler Signalmechanismen im olfaktorischen und vomeronasalen System der Maus“

Von der Fakultät für Mathematik, Informatik und Naturwissenschaften der RWTH Aachen Universität zur Erlangung des akademischen Grades einer Doktorin der Naturwissenschaften genehmigte Dissertation

vorgelegt von

Daniela Patrizia Flügge (M.Sc.)
geboren in Mainz

Berichter: Universitätsprofessor: Prof. Dr. Marc Spehr
Universitätsprofessor: Prof. Dr. Dr. Frank Zufall

Tag der mündlichen Prüfung: 08.10.2010

Diese Dissertation ist auf den Internetseiten der Hochschulbibliothek online verfügbar.

“Physiological investigation of neuronal signaling mechanisms in the mouse olfactory and vomeronasal system”

Faculty for mathematics, informatics and natural science
A thesis submitted for the degree of Doctor in Biology
at the RWTH Aachen University

Daniela Patrizia Flügge (M.Sc.)
born in Mainz

I Content

1 Introduction

1.1 The olfactory system 1

1.1.1 Anatomy of the main olfactory epithelium 2

1.1.2 Anatomy of the accessory olfactory system 3

1.2 Pheromones 4

1.3 Chemoreceptors in olfactory epithelia 6

1.4 Physiology of the olfactory system 10

1.4.1 Signal transduction cascade of the MOE 10

1.4.2 Signal transduction cascade of the VNO 11

1.5 Physiological role of calcium 13

1.6 Mitochondria 14

Aims 17

2 Materials & Methods

2.1 Chemicals and enzymes 19

2.2 Solutions and buffers 22

2.3 Consumables 23

2.4 Antibodies and sera 24

2.5 Cultured cells 24

2.6 Mouse strains 24

2.7 Equipment 24

2.8 Primer 25

2.9 Molecular cloning 26

2.9.1 Chemical transformation 26

2.9.2 Plasmid purification using Qiagen Plasmid Maxi Kit 26

2.9.3 Determination of nucleic acid concentration 26

2.9.4 Polymerase chain reaction, PCR 27

2.9.5 Restriction of DNA 27

2.9.6 Dephosphorylation of DNA-fragments 28

2.9.7 Fill in reaction with Klenow-enzyme 28

2.9.8 Agarose gelelectrophorese 28

2.9.9 Ligation 29

2.9.10 RT- qPCR 29
2.9.11 DNA sequencing 29
2.10 Cell culture 30
2.10.1 Cultivation of HEK293 cells 30
2.10.2 Transient transfection with Lipofectamine™ reagent 30
2.10.3 Lumio™ In-Cell Labeling 30
2.11 Cryostat sections of VNO/MOE 31
2.12 Immunocytochemistry 31
2.13 In situ hybridizations 32
2.14 Expression profiling 32
2.15 Animal preparation 34
2.15.1 Dissociation of vomeronasal sensory neurons 34
2.15.2 Dissociation of olfactory sensory neurons 34
2.15.3 MOE coronal vibratome slices 35
2.15.4 En face preparation of the VNO sensory epithelium 35
2.16 Ca^{2+} imaging 35
2.16.1 Ratiometric calcium imaging in HEK293 cells 35
2.16.2 Ca^{2+} imaging in isolated vomeronasal neurons 36
2.16.3 Ca^{2+} imaging MOE slices 37
2.16.4 Bioluminescence imaging MOE slices 37
2.16.5 *En face* confocal Ca^{2+} imaging of the VNO sensory epithelium 37
2.17 Labeling of Mitochondria in OSNs using MitoTracker® 38
2.18 Statistical Analysis 38

3 Results
3.1 Formyl peptide receptor-like proteins are a novel family of VNO chemosensors 39
3.1.1 FPR-like receptors in olfactory sensory neurons 39
3.1.2 In vitro agonists of FPR-rs receptors 42
3.1.3 Vomeronasal responses to FPR-rs agonists 43
3.2 Functional characterization of vomeronasal receptor V1RD3 49
3.2.1 Functional characterization of the vomeronasal receptor V1RD3 50
3.2.2 4-Ethylphenol evokes Ca^{2+} signals and firing of action potentials in intact VSNs 55
3.2.3 4-Ethylphenol is actively produced by the body and added to urine before secretion 56

3.3 The role of mitochondrial Ca^{2+} in mouse olfactory sensory neurons 58
3.3.1 Odor responses are mediated by canonical OSNs 61
3.3.2 Odor responses depend on extracellular Ca^{2+} 63
3.3.3 Inhibition of SERCA prolongs odor response duration 64
3.3.4 Inhibition of mitochondrial NCX prolongs odor response duration 65
3.3.5 Inhibition of mitochondrial Ca^{2+} sequestration (MiCa) extends odor response duration 66
3.3.6 Both ER and mitochondria function synergistically as Ca^{2+} buffer systems in OSNs 68
3.3.7 Mitochondria modulate odor-dependent Ca^{2+} rise time 69
3.3.8 Mitochondria modulate Ca^{2+} signaling in primary signal transduction 70
3.3.9 Mitochondria show odor-dependent translocation to dendritic compartments 70

4 Discussion
4.1 Formyl peptide receptor-like proteins are a novel family of VNO chemosensors 73
4.1.1 Body odors and immune system 79
4.2 Functional characterization of vomeronasal receptor V1RD3 81
4.2.1 The receptive field of V1RD3 83
4.3 The role of mitochondrial Ca^{2+} in mouse olfactory sensory neurons 85
4.3.1 Measurements of mitochondrial Ca^{2+} 85
5 Summary 91
6 Abbreviations 93
7 References 96
8 Acknowledgement 116
9 Curriculum vitae 117

1 Introduction

1.1 The olfactory system

The detection of environmental chemical signals is essential for the survival of both the individual and the species. The chemical senses can be divided into the sense of smell (olfactory system) and the sense of taste (gustatory system). These senses enable animals to locate food sources as well as suitable mating partners and to avoid both predators and toxic substances. The chemical senses detect molecules of immense structural variety. This task requires a massive repertoire of receptors to match the diversity in chemical structures. 1,037 (Zhang and Firestein, 2002; Buck and Axel, 1991) and 390 (Olender *et al*., 2008) functional members of olfactory receptors (ORs) in mice and humans, respectively, are specialized in the detection of volatile chemical compounds (odors). Each olfactory neuron apparently expresses only one member of the OR gene family in a monoallelic and mutually exclusive manner (Serizawa *et al.*, 2004; 2005). This 'one receptor – one neuron' hypothesis, however, is still far from being proven (Mombaerts, 2004; Spehr and Leinders-Zufall, 2005). An indication of the importance of the olfactory system is that, in mammals, up to 4% of the genome is devoted to encode proteins of smell (Firestein *et al.,* 2001). The olfactory system in rodents is classically divided into two anatomically separate and morphologically distinct sensory systems: the main and accessory olfactory system (Zufall and Munger, 2001; Breer *et al.*, 2006). The main olfactory epithelium (MOE) is responsible for sensing and discriminating a variety of volatile odor compounds, whereas the accessory olfactory system and its peripheral sensory structure - the vomeronasal organ (VNO) - plays a major role in the detection of conspecific cues involved in social communication (Munger *et al.*, 2009; Ma 2007; Breer *et al.*, 2006). These chemosignals provide information about social hierarchy, reproductive status, gender, aggression or genetic individuality but the principle molecular and cellular mechanisms of pheromone detection remain largely unknown. However, the two systems show a certain overlap with respect to the chemosignals they detect and the effects they mediate (Restrepo *et al.*, 2004; Spehr *et al.*, 2006; Zufall and Leinders-Zufall, 2007).

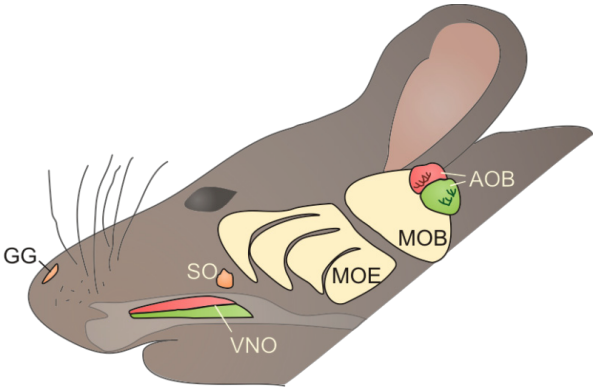


Fig. 1.1: Schematic diagram showing the localization of the different olfactory subsystems with the main olfactory epithelium (MOE), vomeronasal organ (VNO), septal organ (SO), and Grueneberg ganglion (GG) (adapted from Spehr *et al.*, 2006).

1.1.1 Anatomy of the main olfactory epithelium

In mammals, the MOE covers cartilaginous lamellae (turbinates) in the posterior nasal cavity, comprising a few million olfactory sensory neurons (OSNs). There are three principal cell types in the MOE: OSNs, sustentacular cells and basal cells (Graziadei and Monti-Graziadei, 1979; Moulton and Beidler, 1967). OSNs are bipolar neurons with a single dendrite that extends to the epithelial surface of the tissue and ends in a dendritic knob carrying 20 – 30 long nonmotile cilia embedded in the nasal mucus. The ciliary membrane of OSNs is enriched for OR proteins (Buck and Axel, 1991) and proteins of the olfactory signal transduction machinery (Menco, 1997). OSNs extend thin unmyelinated axons. These project through the basal lamina and cribiform plate and terminate in the brain‘s main olfactory bulb (MOB). Neurons that express the same OR send their axons to one or a few glomeruli in each hemisphere of the MOB (Ressler *et al.,* 1994; Mombaerts *et al.,* 1996). Glomeruli are neuropil networks of synaptic interaction between the axon terminals of OSNs and the dendrites of the olfactory bulb projection neurons, the mitral / tufted cells (Fig.1.2). The axons of mitral cells project to higher brain regions e.g. to the primary olfactory cortex (Dulac *et al*., 2006). Basal cells are the second cell type found in the MOE. When OSNs die throughout life at a regular rate, they are replaced by differentiating basal cells (Graziadei, 1973, Caggiano *et al.,* 1994). As they mature, OSNs move apically in the epithelium, permitting rough determination of neuronal age by position. Mature OSNs express the olfactory marker protein (OMP) (Margolis, 1980). Sustentacular cells, the third type of cells found in the MOE, are generally considered as supportive cells and share features with glia cells. They stretch from the epithelial surface to the basal lamina, where they maintain foot processes and produce growth factors important for OSNs development (Getchell 1986; Getchell *et al.,* 1985).

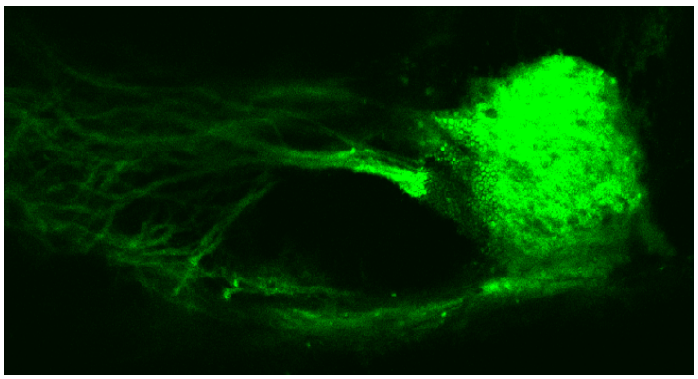


Fig. 1.2: Confocal fluorescence image of a GFP-labeled glomerulus in the MOB of a transgenic mOR-EG mouse (Oka *et al*., 2006). This glomerulus was prepared using the whole-mount preparation. Right side: the glomerulus. Left side: the axons of mOR-EG neurons of the MOE.

1.1.2 Anatomy of the accessory olfactory system

Most mammals possess a well-developed accessory olfactory system (AOS), which is frequently considered a 'specialized nose' for detecting chemical signals, emitted by other animals, that convey specific information concerning species, gender and identity. The vomeronasal sensory neurons (VSNs) within the VNO are able to detect so-called pheromones (Karlson and Lüscher, 1959; Tirindelli et al., 2009). The VNO was first described in 1813 by Ludvig Jacobson. Jacobson provided detailed descriptions of the VNO, but could only speculate about the function of this organ based on its anatomical appearance (Jacobson *et al.,* 1813). Jacobson studied the VNO in a variety of animals. A VNO is present in most amphibians, reptiles and mammals. However, it is absent in fish, crocodiles and exclusively marine mammals. Although, there are well developed VNOs in new world monkeys, the VNO appears to be absent in old world monkeys such as gorillas, chimpanzees and orangutans (Bhatnagar *et al.,* 1998). Do humans possess a functional VNO? Human societies and relationships are extremely complex, requiring flexible behavior that does not come under the obligatory regulation of one sense (Keverne 1983). Chemosensory cues undoubtedly influence human sexual behavior via the olfactory system (Doty, 2003). However, it is unlikely that responses elicited by vomeronasal stimuli play an important role in humans. Studies that use microanatomical methods reported that humans do not have functional vomeronasal sensory neurons (Witt and Hummel, 2006). There is no evidence for nerve and axon connections between potentially existing sensory receptor cells in an adult human VNO-like structure and the brain (Wysocki and Preti, 2004). Furthermore, there is no evidence for any accessory olfactory bulb in adult humans (Bhatnagar et al., 1987), and the key genes involved in VNO function in other mammals have pseudogeneized in humans (Rodriguez and Mombaerts, 2002).

The vomeronasal system differs anatomically from the MOE at both the peripheral and the central level. The vomeronasal organ is a bilateral organ enclosed in a cartilaginous capsule and located at the base of the nasal cavity (Døving and Trotier, 1998; Keverne, 1999; Breer *et al.*, 2006). The lumen of the VNO is filled with fluid from vomeronasal glands. The VSNs are isolated from the airstream that passes through the nasal cavity during normal respiration and conveys largely volatile odorants to the MOE. Therefore stimulus access to the VNO requires some form of vascular pumping mechanism (Meredith and O'Connell, 1979; Pankevich *et al*., 2003). The vomeronasal organ can be divided into a nonsensory and a sensory part (Brennan, 2004). The nonsensory part of the organ, lateral to the lumen, is characterized by large blood vessels and sinuses which are innervated by the autonomic nervous system. The vomeronasal sensory epithelium contains three different cell types: the VSNs, the supporting cells and the basal cells. The basal cells are stem cells, which are located along the basement membrane and replace dying VSNs. Supporting cells have

supportive function for VSN development and they are found in the more superficial layer of the sensory epithelium. The vomeronasal sensory neurons are the chemosensory cells, which detect chemical compounds from conspecifics (Leinders-Zufall *et al*., 2000; Chamero *et al*., 2007; Holy *et al.,* 2000; Stowers *et al.,* 2002) as well as sensory cues emitted by predators (Papes *et al.,* 2010). VSNs are bipolar cells and possess microvilli at the tip of the dendrite (dendritic knob) and long unmyelinated axons that fasiculate and form the vomeronasal nerve. This nerve runs along the septum, passes the cribriform plate and enters the accessory olfactory bulb (AOB) at the posterior site of the MOB (Døving and Trotier, 1998; Keverne, 1999). Cells in the AOB project to the amygdala (Licht and Meredith, 1987, Meredith, 1998) and hypothalamus (Cowan et al., 1965; Heimer, 1972; Scalia and Winans, 1976), areas that are control behavioral and neuroendocrine output. Much information about VNO function has been obtained by investigating the behavioral consequences of surgical lesions. Mice with complete anatomical removal of the VNO show a variety of deficits in social and reproductive behaviors, including intermale aggression, male sexual behavior and maternal aggression (Wysocki *et al.,* 1991).

1.2 Pheromones

The term pheromone was first used by Karlson and Lüscher 1959 and comes from the assembly of two Greek roots ‘pherein’, meaning to transfer, and ‘hormone’, meaning to excite. Pheromones are defined as ‘substances, which are secreted to the outside by an individual of one species and elicit a specific response in a second individual of the same species’ (Karlson and Luscher, 1959). Pheromones are used by most species, from single-cell organisms to mammals (Bassler, 2002). In insects, pheromone-induced behaviors include territory marking, colony identification, social hierarchy and mating rituals (Regnier and Wilson, 1971). Insect sex attractants comprise a well-defined group of pheromones that are detected in minimal concentrations (Dulac and Torello*,* 2003). Initially, it was assumed that mammalian pheromones are exclusively non-volatile. This concept was based on the fact that most vertebrates detect pheromonal cues upon direct physical contact with the stimulus source, e.g. by licking or inhaling minimal amounts of bodily fluids. Stimuli are thought to gain access to the VNO by a vascular pumping mechanism that is activated in arousing situations (Brennan and Zufall*,* 2006). Detailed studies in rodents, however, showed that volatile (Novotny *et al*., 1999; Leinders-Zufall *et al*., 2000) as well as non-volatile (Cheetham *et al*., 2007; Sherborne *et al.,* 2007; Kimoto *et al*., 2005; Kimchi *et al.,* 2007; Leinders-Zufall *et al.,* 2004) substances play an important role in pheromone-based communication. While it is true that the MOE mainly respond to conventional odorants and the VNO mainly respond to social cues, it appears that the converse also occurs (Restrepo

et al., 2004; Spehr *et al.*, 2006; Zufall and Leinders-Zufall, 2007). Experiments indicate that not all pheromone-dependent behaviors are mediated by the VNO. Mice which lack the transient receptor potential cation channel 2 (TRPC2) show impaired VNO activity, but continue to display some pheromone-mediated behaviors such as pup suckling (Leypold *et al.,* 2002; Stowers *et al.,* 2002; Kelliher *et al*., 2006). However, this pup suckling behavior is defective in mutant mice lacking an important ion channel for MOE activity (the cyclic nucleotide-gated channel subunit A2 (CNGA2)) (Brunet *et al.,* 1996).

The main sources for pheromones are bodily fluids such as urine, anogenital gland secretions, saliva and vaginal secretions (Vandenbergh et al., 1975; Singer et al., 1986; Novotny et al., 1999). It has been proposed that VSN populations exist which respond differentially to male and female urine, respectively (Holy *et al*., 2000). In 2008, He et al. confirmed these findings by recording from two populations of VSNs that were selectively activated by male and female urine, respectively. Moreover, their results showed that these VSN populations are essential for sex identification (He *et al*., 2008). Two years later, the same group showed a complex concentration-dependent activation of the VNO. Urine at low and high concentrations activates distinct subsets of VSNs (He *et al.,* 2010).

Urine contains high levels of macromolecules, for example the major urinary proteins (MUPs). MUPs are 18-20 kDa members of the lipocalin family of ligand-binding proteins, thought to act as olfactory binding proteins that deliver small volatile molecules through the mucosa to the chemosensory receptor neurons (Shaw *et al.,* 1983; Cavaggioni *et al.* 1990; Cavaggioni *et al.,* 2000). Cavaggioni *et al.* have studied ligand binding by MUPs. Their findings are consistent with the suggestion that MUPs function in pheromone transport in urine (Cavaggioni *et al.,* 1987).

A second class of macromolecules likely present in urine (Singh *et al.,* 1987) and able to activate VNO neurons are the major-histocompatibility-complex class I (MHC class I) peptides (Leinders-Zufall *et al.,* 2004). The classical class Ia MHC molecules are expressed in association with β2-microglobulin (β2m). In the immune system, their main function is to signal the presence of foreign invaders by presenting intracellular peptides to immune cells (Janeway and Golstein, 1993; Maenaka and Jones, 1999). MHC peptides are excellent candidates for social recognition signals that convey information about genetic individuality (Leinders-Zufall *et al.,* 2004). Behavioral studies in mice show that vomeronasal detection of MHC peptides mediates the formation of an olfactory memory that is required for mate recognition in the context of selective pregnancy failure (the Bruce effect (Fig.1.3)) (Brennan, 2004). The Bruce effect (Bruce, 1959) describes the following phenomenon: If an unfamiliar male is introduced to the home cage of a recently copulated female mouse, the fertilized eggs will fail to implant in the uterine wall and pregnancy is blocked (Brennan, 2004). Since the unfamiliar male would likely kill the foreign offspring, it is energetically advantageous for

the female not to commit metabolic resources to a potentially sacrificed set of offspring. Female mice build up an olfactory memory (Kaba and Nakanishi, 1995; Binns and Brennan, 2005) specific to the MHC class I peptide profile (Leinders-Zufall *et al.,* 2004) of the mating partner. This memory of the original mating partner's 'pheromone' signature (MHC peptides) is thought to be 'stored' in the AOB and compared with the pheromonal signal of the unfamiliar male. This demonstrates that the MHC peptides intrinsically alter behavior (Stowers *et al.*, 2005).

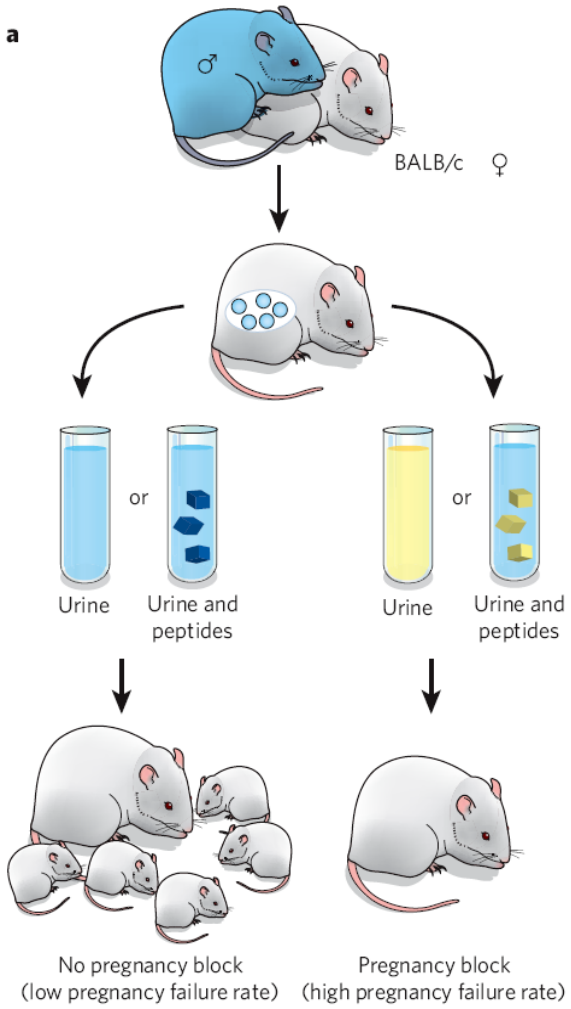


Fig. 1.3: The Bruce effect. Urine from unfamiliar males (yellow) or familiar urine (blue) supplemented with unfamiliar (disparate) MHC class-I peptide ligands activates neuroendocrine mechanisms leading to pregnancy failure (adapted from Brennan and Zufall, 2006)

1.3 Chemoreceptors in olfactory epithelia

In the mammalian nose, five types of chemosensory G protein–coupled receptors (GPCRs) have been identified. Mammalian GPCRs are classified into three main classes based on protein sequence similarity: the rhodopsin receptor-like family (A), the secretin receptor-like receptor family (B) and the metabotropic glutamate receptor-like family (C) (Bockaert and Pin, 1999; Josefsson, 1999; Graul and Sadee, 2001; Joost and Methner, 2002). The main role of GPCRs is to recognize extracellular ligands and translate receptor-ligand interactions

into amplified intracellular signals. Upon ligand binding, these receptors change their conformation (e.g. in transmembrane domain 3 and 6) and, thereby, activate heterotrimeric G-proteins (Bockaert and Pin, 1999). The majority of known mammalian GPCRs are expressed in sensory systems, functioning as specialized receptors for external sensory cues such as odors, pheromones or tastants (Mombaerts, 1999; 2004; Spehr and Munger, 2009). Until now, five different receptor classes are found in the mammalian nose. Odorant receptors (ORs) and trace-amine-associated-receptors (TAARs) are found in the MOE (Buck and Axel, 1991; Liberles *et al.,* 2006), whereas vomeronasal receptor type 1 (V1R) (Dulac and Axel, 1995; Rodriguez *et al.,* 2002), vomeronasal receptor type 2 (V2R) (Herrada and Dulac, 1997; Ryba and Tirindelli, 1997; Matsunami and Buck, 1997) and formyl peptide receptors (FPRs) (Riviére *et al.,* 2009; Liberles *et al.,* 2009) are found in the VNO.

Odorant receptors (ORs)

Olfactory sensory neurons (OSNs) are located in the MOE and express a single type of OR (Buck and Axel, 1991; Chess *et al*., 1994), most abundantly found in the ciliary compartments of these cells (Menco *et al*., 1997). There are more than 1000 genes for ORs in the mammalian genome. Mice express almost 1300 different ORs. Olfactory receptors consist of seven transmembrane domains, an extracellular amino terminus and an intracellular carboxyl terminus, similar to those known from neurotransmission and photoreception. Vertebrate ORs share many features with other GPCRs. Within the OR family, amino-acid similarity ranges from 40% to 90%. In the third, fourth and fifth transmembrane regions, ORs show a region of high variability. These domains may control the ligand accessibility to the binding pocket of ORs (Zhang and Firestein, 2002; Mombaerts, 2004).The high variability provides a molecular basis for understanding the diversity and large number of olfactory ligands that can be detected and discriminated.
Moreover, OR genes coding regions lack introns. Structural analysis predicts seven α-helical membrane-spanning domains connected by intracellular and extracellular loops and numerous conserved short sequences (Buck and Axel, 1991).

Trace-amine-associated-receptors (TAARs)

Recently, a second family of OSN chemosensory receptors was identified in the MOE. These trace-amine-associated-receptors (TAARs) are expressed in a small subpopulation of neurons (~1/1000 OSNs), coexpress $G\alpha_{olf}$, and recognize volatile amines *in vitro* (Liberles and Buck, 2006). TAARs can increase cAMP levels when activated by ligands in heterologous cells, suggesting that they activate a similar cAMP second-messenger pathway in OSNs as classical odorant receptors (Liberles *et al.,* 2006). They relate to biogenic amine receptors such as serotonin and dopamine receptors that regulate a range of behavioral and

emotional states (Borowsky *et al.,* 2001). TAARs are found in diverse vertebrates. There are 15 genes in mouse, 17 in rat, 6 in humans, and 109 in zebrafish (Zucchi *et al*., 2006; Hussain *et al*., 2009; Lewin, 2006).

Vomeronasal receptor type 1 (V1R)

VSNs that express V1Rs, members of the class A GPCR family, are located in the more apical zone of the VNO epithelium and send their projections to the anterior part of the AOB. The *V1r*s comprise a family of 137 genes that are divided into 12 subfamilies (*V1r*a-l) and organized in gene clusters at multiple chromosomal locations (Dulac and Axel, 1995; Rodriguez *et al.,* 2002). V1Rs are coexpressed with the G protein $G\alpha_{i2}$. V1Rs have relatively short extracellular amino terminals and high sequence diversity in their transmembrane domains, which presumably constitute the ligand binding-site (Dulac and Axel, 1995). In contrast to ORs, which are relatively broadly tuned to odors, the V1R-expressing cells were shown to be selective pheromone sensors (Leinders-Zufall *et al.,* 2000). Until now, little is known about V1R function. A study by Del Punta *et al.,* 2002 shed first light to the role of V1Rs in the VNO. To determine if V1Rs are involved in pheromone responses, a cluster of 16 intact *V1r* genes (*V1r*a and *V1r*b family) was deleted in the germ line of mice. Mutant male mice show a reduced sexual drive and mutant females display a reduced level of maternal aggression. Deficits in pheromonal sensitivity were also observed in electrophysiological recordings of the VNO, indicating a role of V1Rs as pheromone receptors. The first V1R receptor-agonist pair was identified by Boschat *et al.* (2002). To link the detection of a known pheromone to a specific V1R, the authors combined electrophysiological and Ca^{2+} imaging recordings in a transgenic mouse model, in which the *V1rb2* gene was linked to the expression of a green fluorescent protein (GFP). V1RB2 positive cells responded to 2-heptanone by increasing intracellular Ca^{2+} and generating a reversible inward current. 2-heptanone is a male urinary pheromone that extends oestrus in female mice (Novotny, 2003). The discovery of the first receptor agonist pair in the VNO was expected to provide a valuable tool for understanding the signal transduction cascade in the VNO. However, no follow-up studies that utilize this receptor-ligand pair have been published.

Vomeronasal receptor type 2 (V2R)

V2Rs are members of the class C GPCR family. VSNs that express V2Rs are located in the basal zone of the vomeronasal epithelium and send projections to the posterior part of the AOB (Fig.1.5) (Herrada and Dulac, 1997; Matsunami and Buck, 1997; Ryba and Tirindelli, 1997). The V2Rs are coexpressed with $G_{\alpha o}$ and comprise a family of about 120 genes (Young and Trask, 2007). The *V2r*s can be grouped into four families (*V2r*a-d). The ligand-

binding site of V2Rs is likely built by the large and highly variable extracellular amino terminal domain. Some V2R positive VSNs express members of another multigene family, *H2-Mv* that encode nonclassical MHC class I genes (Loconto *et al.,* 2003; Ishii *et al*., 2003). V2R positive VSNs respond to several nonvolatile peptide and protein pheromones that require direct physical contact between the nose and the stimulus source (Leinders-Zufall *et al.,* 2004). Ca^{2+} imaging of V2R positive VSNs in VNO tissue slices demonstrated, that the major histocompatibility complex (MHC) class I peptides are ligands for V2Rs (Leinders-Zufall *et al.,* 2004). In 2009, Leinders-Zufall *et al*. showed that VSNs expressing V2R1b detect MHC peptides and distinguish peptides differing in their amino-acid residue (Leinders-Zufall *et al*., 2009). Additional ligands for V2Rs have also been identified. A male-specific exocrine gland-secreting peptide 1 (ESP1), which is secreted from the extraorbital lacrimal gland, functions as a sensory cue for V2R positive neurons (Kimoto *et al.,* 2005). ESP1 is a member of a multigene family that encodes peptides of various lengths consisting of 38 members in mice and 10 members in rat but is absent from the human genome (Kimoto *et al.,* 2007). Major urinary proteins (MUPs) represent another set of proteins which act as ligands for the V2Rs. MUPs are thought to be involved in chemosensory communication including identity recognition (Cheetham *et al.,* 2007). MUPs promote aggressive behavior (Chamero *et al.,* 2007) and signal danger, thus, mediating interspecies defensive behaviors (Papes *et al*., 2010).

Formyl peptide receptors (FPRs)

FPRs belong to the seven-transmembrane domain, $G_{\alpha i}$ protein-coupled receptor family (Gierschik *et al.,* 1989; Klinker *et al.,* 1994). FPRs are expressed at high levels by cells of the immune system and mediate chemotaxis. Due to their capacity to interact with bacterial formylated peptides, these receptors play a role in host defense against microbial infection (Schiffman *et al*., 1975). The murine FPR gene family has at least seven members: FPR1, FPR-rs1; FPR-rs2; FPR-rs3; FPR-rs4; FPR-rs6 and FPR-rs7, which form a cluster on chromosome 17 (Gao *et al.,* 1998, Migeotte *et al*., 2006). Intrafamily sequence identity among FPRs ranges from 67% to 96%. Mouse FPR1 is expressed in neutrophils, dendritic cells, microglia and liver. FPR-rs1 is expressed in neutrophils, liver and heart. FPR-rs2 is coexpressed with FPR1 except for liver (Le *et al*., 2002; Lee *et al*., 2004). FPR-rs3 was only found in skeletal muscle (Le *et al.,* 2002). FPR-rs6 is expressed in testis, brain and skeletal muscle and FPR-rs7 was found in heart, liver, smooth muscle and pancreas. Functionally, the first described FPR ligand is *N*-formyl-methionyl-leucyl-phenylalanine (fMLF), a classical chemoattractant derived from bacteria. It activates FPR1 at picomolar to low nanomolar concentrations. On agonist binding, FPR coupled $G_{\alpha i}$ proteins dissociate into α and βγ subunits, resulting in the activation of a phospholipase C (PLC) pathway (Camps *et al*.,

1992). Stimulation of phagocytic leukocytes by fMLF can elicit shape change, chemotaxis, adhesion, phagocytosis and release of superoxide anions (Le *et al.,* 2001). fMLF has been shown to stimulate the activation of specific transcription factors, such as nuclear factor 'kappa-light-chain-enhancer' of activated B-cells (NFκB) (Browning *et al.*, 1997), and the production of inflammatory cytokines by phagocytes (Murphy *et al.,* 1992).

The hypothesis that the N-formyl group of a ligand is essential for agonist binding has been disproven by findings that non-formylated peptides can also chemoattract immune cells via FPR receptor activation (Murphy, 1996; Prossnitz and Ye, 1997). Recent studies continued to identify additional ligands for FPRs, e.g. lipoxin A4 (Takano *et al.,* 1997), urokinase plasminogen activator (uPAR) (Resnati *et al*., 2002), an acute phase protein serum amyoloid A (SAA) (Su *et al.,* 1999), and the antimicrobial peptide CRAMP (Kurosaka *et al*., 2005). The *in vivo* importance of FPRs in host defense against bacteria was demonstrated by targeted gene disruption of FPR1 in mice (Gao *et al*., 1999). Mice lacking FPR1 had decreased resistance to bacteria (*Listeria monocytogenes*). Compared to wildtype littermates, the FPR1-deficient mice showed increased bacterial load in spleen and liver two days after infection. Neutrophil chemotaxis and cell mobilization were both absent in FPR1 deficient mice (Gao *et al*., 1999) confirming that FPRs play a crucial role for host anti-bacterial responses.

1.4 Physiology of the olfactory system

1.4.1 Signal transduction cascade of the MOE

Olfactory transduction begins with the binding of an odor to an olfactory receptor protein, initiating a signal transduction cascade that transforms the chemical energy into an electrical signal. The individual steps of the olfactory signal transduction cascade are relatively well understood in mammals. Binding of an odor molecule to the binding pocket of the OR leads to activation and dissociation of the trimeric G_{olf}-protein into a guanosine-5'-triphosphate (GTP)-bound G_{α}-subunit and the $G_{\beta\gamma}$-complex (Jones and Reed, 1989; Belluscio *et al*., 1998). The G_{α}-subunit stimulates a specific enzyme, the adenylate-cyclase III (ACIII) (Bakalyar and Reed, 1990; Wong *et al*., 2000). This ACIII converts the intracellular molecule adenosine triphosphate (ATP) into a second messenger, the cyclic adenosine monophosphate (cAMP), a molecule with numerous signaling roles within cells (Pace et al., 1985; Breer et al., 1990; Ronett and Synder, 1992). As the ciliary cAMP concentration rises, cAMP molecules bind to the intracellular face of an ion channel, the cyclic nucleotide-gated channel (CNG) (Dhallan *et al.*, 1990; Zagotta and Siegelbaum, 1996; Bradley *et al*., 1994; Liman and Buck, 1994). CNG channel opening results in an influx of cations, Na^+ and Ca^{2+} (Nakamura and Gold, 1987; Firestein and Werblin, 1989; Zufall et al., 1994; Kleene, 2008).

Ca^{2+} ions entering via the CNG channel activate a Ca^{2+}-activated Cl^--channel (CaCC) which conducts a Cl^- outward current. The molecular identity of the CaCC was recently discovered. A member of the transmembrane 16 group of proteins (TMEM16B, also called Anoctamin 2 (ANO2)) was shown to form a recombinant CaCC that exhibits channel properties closely resembling the native olfactory CaCC (Stephan *et al.*, 2009; Pifferi *et al.*, 2009; Rasche *et al.*, 2009). The activation of the Cl^- channel leads to a Cl^- efflux out of the cell (Fig. 1.4). Due to influx of cations and efflux of anions across the cell membrane the inside of the membrane becomes electrically less negative (Kleene, 1993) resulting in the depolarization of the cell and action potential (AP) generation (Firestein, 2001). The APs are then propagated along the OSN axons and, thus, odor information is conveyed to mitral cells in the MOB (Fig. 1.5).

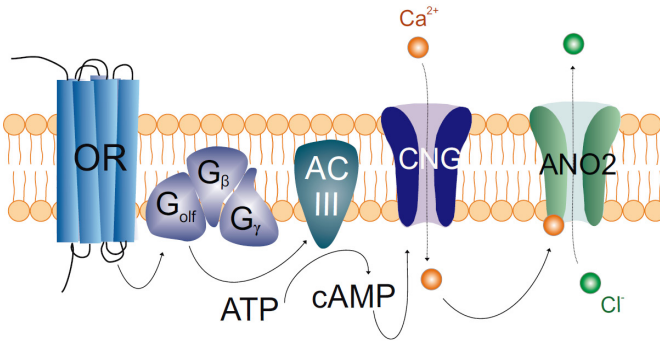


Fig. 1,4: Schematic diagram of the signal transduction cascade of canonical OSNs. The binding of an odor to an OR activates an associated, trimeric G-protein by exchanging its bound GDP for GTP. The G_α-subunit, together with the bound GTP, dissociates from the $G_{\beta\gamma}$-complex. The G_α subunit activates the adenylate-cyclase (AC III) which converts ATP to cAMP. The cAMP, in turn, opens a CNG channel through which Na^+ and Ca^{2+} flow into the cell. The entering Ca^{2+} ions activate Cl^- channels. Modified from Spehr *et al.,* 2006.

However, Ca^{2+} was also shown to play a critical role in olfactory adaptation (Zufall, 2000; Matthews and Reisert, 2003). Ca^{2+}/calmodulin-mediated negative feedback, a prototypical regulatory mechanism for Ca^{2+}-permeable ion channels, affects the open probability of the CNG channel (Zufall *et al.*, 1991; Chen and Yau, 1994; Liu *et al.*, 1994).

1.4.2 Signal transduction cascade of the VNO

The question how molecular cues are transduced into neural signaling in the vomeronasal system is not solved yet. Various signal transduction cascades have been proposed (Spehr *et al.*, 2002; Brann *et al.*, 2002; Lucas *et al.*, 2003). It is evident that the signal transduction cascade in VSNs clearly differs from the cascade in OSNs. Both VSNs and OSNs respond to stimulation by elevating intracellular Ca^{2+} and firing action potentials, but the underlying molecular mechanism in VSNs remains largely unclear.

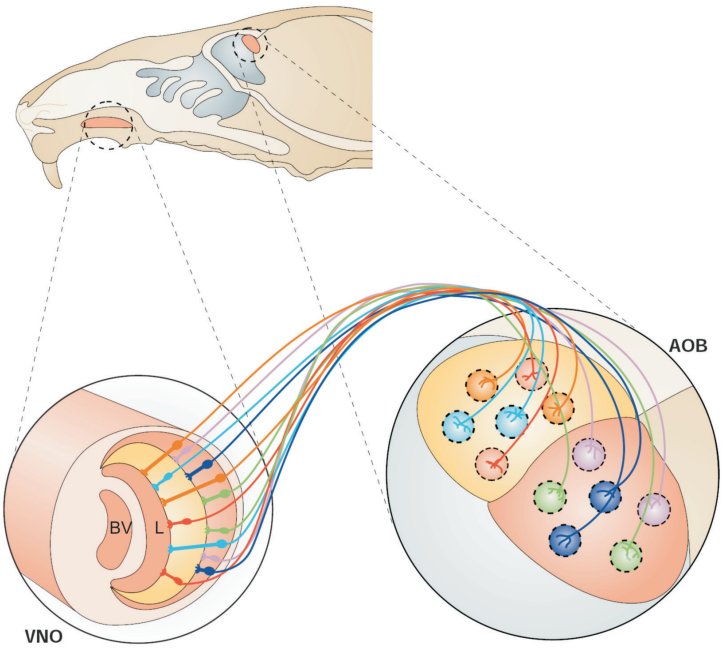


Fig. 1.5: Vomeronasal sensory neurons that express the same V1R or V2R project to multiple, small glomeruli in the AOB. The apical layer of the epithelium projects to the anterior half of the AOB. The basal layer projects to the posterior half of the AOB. BV = blood vessel / L = lumen (adapted from Mombaerts, 2004)

The following general signal transduction concept has been proposed: First, a vomeronasal receptor is activated by the binding of a specific ligand. This receptor activation leads to an activation of G proteins. Depending on receptor type, one of two different G proteins are activated (V1Rs activate $G_{\alpha i2}$, V2Rs activate $G_{\alpha o}$). Activated G proteins cause a conformational change in an effector enzyme, likely phospholipase C (PLC) (Wekesa and Anholt, 1997; Krieger *et al.*, 1999; Inamura *et al.*, 1999; Rossler *et al.*, 2000; Holy *et al.*, 2000; Leinders-Zufall *et al.*, 2000; Spehr *et al.*, 2002; Lucas *et al.*, 2003). PLC regulates synthesis of two second messengers: inositol 1,4,5-trisphosphate (IP_3) and diacylglycerol (DAG). IP_3, DAG as well as polyunsaturated fatty acids (PUFAs; DAG metabolites) have all been postulated in gating a Ca^{2+} permeable transduction channel (Spehr *et al.*, 2002; Brann *et al.*, 2002; Lucas *et al.*, 2003). DAG binds to and activates TRPC2 ion channels (Liman *et al.*, 1999), leading to Ca^{2+} influx into the cell (Fig. 1.6) (Lucas *et al.,* 2003). The resulting receptor potential generates action potentials which are conveyed to the AOB. Excitatory relay neurons of the AOB, the mitral cells, project their axons to areas are known to control innate behavior and the release of hormones by the pituitary gland, altering the endocrine status of the animal.

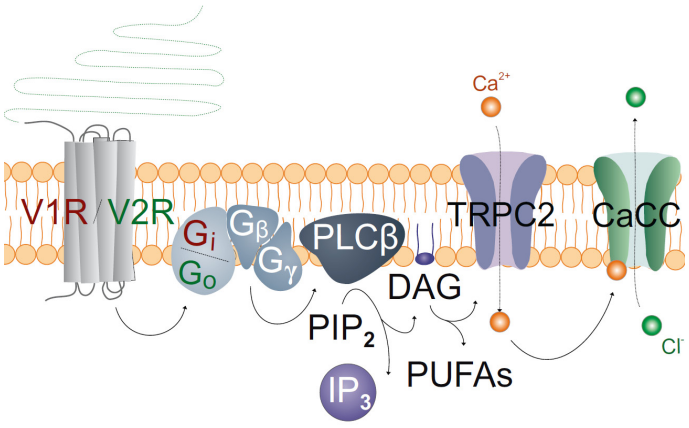


Fig. 1.6: Schematic diagram of the proposed signal transduction cascade of VSNs. The binding of a ligand to a member of one of the two receptor families (V1R / V2R) activates an associate, trimeric G-protein by exchanging its bound GDP for GTP. The $G_{\alpha i/o}$-subunit, together with the bound GTP, dissociates from the $G_{\beta\gamma}$-complex. The $G_{\alpha i/o}$ subunit activates PLC which catalyses the reaction from PIP_2 to DAG and IP_3. DAG, in turn, is hypothesized to open a TRPC2 channel through which Na^+ and Ca^{2+} flow into the cell. Ca^{2+} ions entering the neuron via the TRPC2 channel possibly activate Cl^- channels that lead to a Cl^- efflux (Yang and Delay, 2010). Modified from Spehr *et al.,* 2006.

Recently, the core model of vomeronasal signaling has been extended considerably. Spehr *et al.* showed that Ca^{2+}-calmodulin feedback mediates sensory adaptation by inhibiting pheromone sensitive ion channels in the VNO (Spehr *et al.,* 2009). Urine stimulation of VSNs activated large-conductance Ca^{2+}-activated K^+ (BK) channels (Uhkanov *et al*., 2007), potentially via arachidonic acid (Zhang *et al*., 2008). Furthermore, Yang and Delay postulated the existence of a Ca^{2+}-activated Cl^--channel (CaCC) in VSNs, which conducts an amplifying Cl^- outward current. Using electrophysiological recordings in isolated VSNs, they demonstrated that the Cl^- outward current contributes to urine responses in native VSNs and, thus, amplifies the primary signal (Yang and Delay, 2010).

1.5 Physiological role of Ca^{2+}

Ionized Ca^{2+} is one of the most important signal transduction elements in cells. To control Ca^{2+}, cells must chelate, compartmentalize or extrude it. The three main intracellular compartments in which Ca^{2+} accumulates are the cytoplasm, the endoplasmic reticulum (ER) and mitochondria (Gerasimenko *et al.,* 1996; Michelangeli *et al.*, 2005). Resting cytosolic Ca^{2+} levels at ~100 - 200 nM are 10,000-fold lower than the ~2 mM concentration found extracellularly (Pietrobon *et al.,* 1990). Two principle Ca^{2+} entry pathways mediate Ca^{2+} influx. First, voltage gated Ca^{2+} channels (VGCC) that are highly selective for Ca^{2+}. Upon plasma membrane depolarization, VGCC are activated (Hess and Tsien, 1984). When voltage-dependent Ca^{2+} channels are open ~1 million Ca^{2+} ions per seconds per channel flow into the cytoplasm (Clapham *et al.,* 2007). Second, ligand gated cation channels that are less selective for Ca^{2+} than VGCC. Their activation results in an unspecific increase of cytosolic Na^+ and Ca^{2+} (MacDermott *et al*., 1986; Murphy *et al.,* 1987; Hollmann *et al.,* 1991, Verdoorn *et al*., 1991). The low cytoplasmic Ca^{2+} concentration in cells is, in part, maintained by Ca^{2+} extrusion via plasma membrane Ca^{2+} ATPase (PMCA) (Strehler and Treiman, 2004) and plasma membrane Na^+/Ca^{2+} exchangers (Gunter *et al.*, 1994; White and Reynolds, 1997; Clapham *et al.,* 2007). PMCAs have a high affinity for Ca^{2+} but are of limited capacity (Pietrobon *et al.,* 1990, Pozzan *et al*., 1994). The Na^+/Ca^{2+} exchangers allow the entry of three Na^+ ions for the efflux of one Ca^{2+} ion (Eisner and Lederer, 1985).

Intracellular Ca^{2+} storage organelles, i.e. the ER and mitochondria, process Ca^{2+} in different ways. The ER acts as the largest cellular Ca^{2+} store, which dynamically establishes the spatial and temporal organization of Ca^{2+} signaling events (Park *et al*., 2000; Jones *et al.,* 2008). In the ER, Ca^{2+} accumulates via smooth endoplasmic reticular Ca^{2+} ATPase (SERCA) transporters, which transfer Ca^{2+} from the cytosol to the lumen of the ER (Pietrobon *et al.,* 1990). The second important intracellular Ca^{2+} store is represented by mitochondria, which are able to store Ca^{2+} in a millimolar range (Toescu, 2000; Nicholls, 2005). In mitochondria

however, Ca^{2+} is regulated by mechanisms distinct to those of the ER (Nicholls and Akerman, 1982). In addition to Ca^{2+} extrusion and storage, free cytosolic Ca^{2+} ions are bound by specific families of Ca^{2+} adaptor proteins (e.g. calmodulin), which have a high affinity for Ca^{2+} and act as short-term buffers (Lledo *et al.,* 1992). Calmodulin changes its conformation upon Ca^{2+} binding and modulates effector molecules such as enzymes and ion channels (Hoeflich and Ikura, 2002).

1.6 Mitochondria

Mitochondria are membrane enclosed organelles found in most eukaryotic cells. They have retained an independent genome, known as mitochondrial DNA (mtDNA). mtDNA only encodes for 13 proteins of the respiratory chain, while all other mitochondria-localized proteins are encoded by nuclear DNA and are post-translationally imported into the organelle (Neupert, 1997). A key role of mitochondria is to provide energy for the host cell in form of ATP by oxidative phosphorylation. But, mitochondria are also central in apoptotic cell death, generation of free radical species and steroid synthesis. In recent years, evidence has accumulated showing that mitochondria are much more than mere energy suppliers, but are also critically involved in intracellular Ca^{2+} signaling (Gunter *et al.,* 2000; Rizzuto *et al.,* 2004).

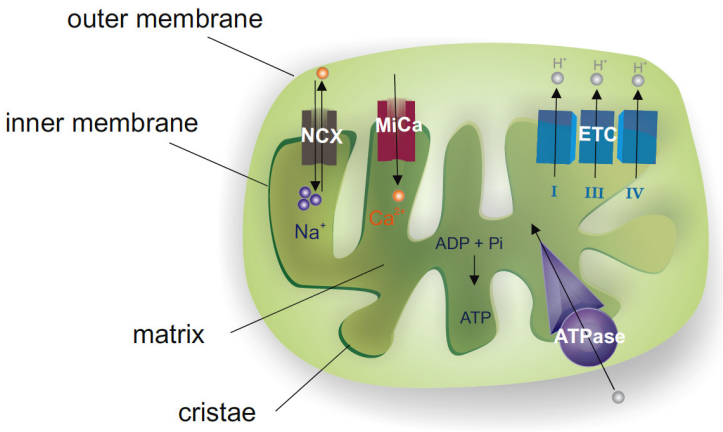


Fig. 1.7: Scheme of a mitochondrion with proteins located at the inner membrane. ETC = electron transfer chain, NCX = Na^+/Ca^{2+} exchanger, MiCa = mitochondrial Ca^{2+} channel, ATPase = ATP synthase

Mitochondria consist of inner and outer membranes, the intermembrane space and the matrix enclosed by the inner membrane. Infoldings of the inner mitochondrial membrane form numerous cristae. The outer membrane is permeable for ions and small molecules. The inner membrane is almost impermeable, equipped with a variety of distinct ion channels and transporters such as the mitochondrial Ca^{2+} channel (MiCa), Na^+/ Ca^{2+} exchanger (NCX) as well as proteins from the mitochondrial electron transport chain (ETC). The ETC consists of different complexes, complex I (NADH ubiquinone oxidoreductase), complex II (succinate dehydrogenase), complex III (ubiquinol cytochrome c oxidoreductase) and complex IV (cytochrome c oxidase). These complexes transfer electrons from NADH and $FADH_2$ to O_2.

These reactions also imply the transfer of protons from the mitochondrial matrix to the intermembrane space, thus, generating a huge negative membrane potential across the inner mitochondrial membrane. That negative membrane potential sets the driving force for protons that activate the ATP synthase (complex V) to generate ATP (Fig.1.7) (Wallace, 2005). MiCa is a highly selective ion channel for Ca^{2+} and allows Ca^{2+} influx along the electrochemical gradient without counter ion transport or the need for ATP hydrolysis (Gunter *et al.,* 2000). Ca^{2+} uptake into the mitochondrial matrix via MiCa critically depends on the electrical driving force that is established by the negative inner mitochondrial membrane potential. In respiring mitochondria, a membrane potential of approximately -180 mV is generated by the H^+ gradient (Mitchell *et al.,* 1961). During intracellular Ca^{2+} signaling, mitochondria are able to rapidly take up significant amounts of Ca^{2+} from the cytosol. This matrix Ca^{2+} elevation can trigger a variety of different processes (Gunter *et al.,* 2000).

Chemical uncouplers (protonophores) such as 4-(trifluoromethoxyl) s-phenyl-hydrazone (FCCP) immediately destroy the proton gradient and strongly reduce Ca^{2+} uptake into mitochondria (Trenker *et al.,* 2007). Protonophores, thus, rapidly provoke a severe morphological change in the structural organization of mitochondria (Graier *et al.,* 2007). Under physiological conditions, mitochondria form highly interconnected tubular networks, whereas, upon addition of FCCP, mitochondrial structure turns towards disconnected singular mitochondria (Fig.1.8). Such structural changes are accompanied with alterations in mitochondrial Ca^{2+} homeostasis (Graier *et al.,* 2007).

Recent studies suggest that mitochondria undergo continuous cycles of fission and fusion to form a highly dynamic interconnected network (Bereiter-Hahn and Voth, 1994; Nunnari *et al.*, 1994). Mitochondrial fission is the separation of long tubular mitochondria (Skulachev *et al.,* 2001), whereas mitochondrial fusion is the liaison of different mitochondria into a single organelle (Hermann *et al.,* 1998). Fission and fusion events allow the mixing of metabolites and mtDNA.

Mitochondria actively communicate, adapt to a cell's energy demands, and interact with each other and with other cellular organelles such as the endoplasmic reticulum (ER) (Manella *et al.,* 1998; Sharma *et al.,* 2000; Csordas *et al.,* 1999, 2006). Trafficking of mitochondria is, therefore, important for cellular function. Due to complex neuronal morphologies, including long axons and dendritic branches it is essential that mitochondria are effectively transported to regions of high energy demands (Hollenbeck and Saxton, 2005). Mitochondria can be actively transported along microtubules in both anterograde and retrograde directions by ATP-dependent motor-proteins (Rice and Gelfand, 2006).

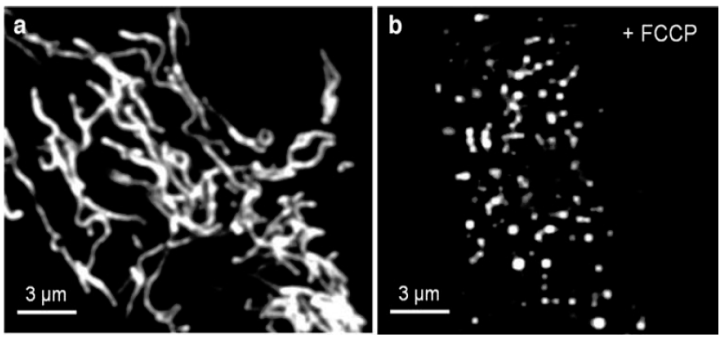


Fig. 1.8: Morphology and structural integrity of mitochondria of human endothelial cells, which transiently express mitochondrial-targeted DsRed. a) Under basal conditions, mitochondria consist as highly interconnected tubular networks. b) After treatment with 2 µM FCCP for 10 min, mitochondria fragment and form singular round mitochondria (adapted from Graier *et al.,* 2007).

Until now, Ca^{2+} measurements in mitochondria were mainly performed using a number of different Ca^{2+} dyes (e.g. Indo-1, Fura-2, Fura-2FF, Rhod-2-AM). These Ca^{2+} dyes accumulate in mitochondria, cytoplasm and other cell organelles (Mix *et al*., 1994; Hajnoczky *et al*., 1995). To measure Ca^{2+} in mitochondria, cells were treated with Mn^{2+} to quench most of the cytosolic indicator after loading with the Ca^{2+} dye (Gerasimenko *et al.,* 2005). Rhod-2-AM is the most used fluorescent probe for Ca^{2+} measurements in mitochondria. This dye carries a delocalized positive charge that causes preferential accumulation in mitochondria and reports Ca^{2+} concentration in the mitochondrial lumen. Although preferential mitochondrial localization was reported in a number of cell types, the presence of the indicator in the cytosol and other cell compartments creates problems for mitochondrial Ca^{2+} measurements (Rutter *et al.,* 1996). Different techniques have been established to remove the indicator from the cytosol, e.g. by using a patch pipette or selective permeabilization of the plasma membrane (Gerasimenko *et al.,* 2005). Rizzuto *et al.* (1993) established a powerful tool for investigating Ca^{2+} homoeostasis at the subcellular level. Using a genetic approach, the recombinant Ca^{2+}-sensitive photoprotein aequorin was targeted to defined intracellular locations, e.g. mitochondria, in different cultured cell lines to perform transient expression experiments. The photoprotein aequorin is well tolerated by the cell and may be expressed at high levels in numerous heterologous systems. While all these approaches provide a wealth of important insights into the Ca^{2+} homoeostasis of mitochondria, such tools were not transferable to observe Ca^{2+} homoeostasis in native neuronal tissue. Until now, experimental tools to observe Ca^{2+} homoeostasis in endogenously expressed mitochondria are not well established. So far, a single paper in 2007 described aequorin / GFP-based *in vivo* monitoring of mitochondrial Ca^{2+} (Rogers *et al*., 2007).

Aims

Olfaction is the most important sensory modality for chemical communication in the majority of vertebrates. The olfactory system consists of several subsystems. The MOE is responsible for detection and discrimination of a large variety of mostly volatile odor compounds. The VNO, a blind-ended tube at the ventral part of the nasal septum, is specialized for detection of information important for social behavior. Signaling mechanisms in the MOE are relatively well understood, whereas signaling pathways in the VNO still remain largely mysterious.

The overall aim of my thesis is to gain a deeper understanding of sensory signaling mechanisms in the mouse olfactory system. Specifically, my research focuses on three important aspects of vomeronasal and olfactory signaling: Identification of previously undescribed receptor proteins in the VNO, recombinant characterization of a vomeronasal receptor / ligand pair, and the role of mitochondria in Ca^{2+} signaling of olfactory sensory neurons. In this thesis, I use physiological recording methods (Ca^{2+} imaging) as well as molecular and biochemical techniques to experimentally target olfactory signaling processes in mice from complementary analytical angles.

As a first project, we will search for previously unidentified vomeronasal receptor proteins, establishing a collaborative approach with colleagues from the University of Geneva. Should we find novel vomeronasal receptors, we will characterize these proteins *in vitro*, followed by functional characterization *in situ*. Therefore, I aim to establish an *in situ* approach that combines a whole-mount VNO preparation with dendritic Ca^{2+} imaging in the intact vomeronasal sensory epithelium to validate and examine receptor signaling in native vomeronasal tissue.

In the second part of this thesis, I will characterize vomeronasal receptor-ligand interactions using both recombinant receptor expression in a heterologous cell system and physiological recording methods in the mouse model. With the use of the Affymetrix GeneChip® microarray platform, we expect to show regulated vomeronasal receptor expression after exposure of sexually naïve male mice to pheromonal stimulus mixtures. After identification, the receptor(s) will be cloned, recombinantly expressed and characterized *in vitro*. Next, I aim to use dendritic Ca^{2+} imaging in the intact VNO sensory epithelium to characterize putative ligands *in situ*. Following this experimental strategy, I aim to describe a prototypical cognate vomeronasal receptor / ligand pair that will provide novel insights into the chemical identity of mammalian pheromones and the coding logic underlying signaling processes in the AOS.

A parallel line of research will focus on the functional characterization of the mitochondrial role in Ca^{2+} signaling of OSNs. Using a combination of bioluminescence imaging and transgenic mice which stably express a Ca^{2+}-sensitive photoprotein selectively in mitochondria, I aim to establish a novel imaging approach to record mitochondrial Ca^{2+}

signals in OSNs. Employing this novel system, we envisage to obtain significant new insight into the role of mitochondrial Ca^{2+} signaling in the olfactory system.

2 Material

2.1 Chemicals and enzymes

N-(2-acetamido)-2-aminoethanesulfonic acid (ACES)	Sigma Aldrich
Agar	AppliChem
Agarose	Sigma Aldrich
Antimycin A	Sigma Aldrich
Ampicillin	Sigma Aldrich
ATP	Sigma Aldrich
Azulene	Aldrich
3-Amino-1,2,4-triazole	Aldrich
Bis(2-hydroxyethyl)-2-aminoethanesulfonic Acid (BES)	Sigma Aldrich
Bradford Reagent	PIERCE
2-Butyl-1-octanol	Aldrich
Calciumchloride	Sigma Aldrich
CGP 37157	Tocris
Coelenterazine	Proteinkinase
Concanavalin A	Sigma Aldrich
3-cyclohexen-1-methanol	Aldrich
2,4-dimethylphenol	Aldrich
2,5-dimethylpyrazine	Aldrich
2,4-di-tert-butylphenol	Aldrich
Edelfosine	Calbiochem
Ethylene diamine tetraacetic acid (EDTA)	Sigma Aldrich
Ethylene glycol tetraacetic acid (EGTA)	Sigma Aldrich
Ethanol	Sigma Aldrich, Fluka

Ethylbenzol	Fluka
2-ethylphenol	Aldrich
3-ethylphenol	Fluka
4-ethylphenol	Aldrich
Ethylcyclohexane	Sigma Aldrich, Fluka
Cis-4-ethylcyclohexanol	Sigma Aldrich
DNase	Promega
Glucose	Sigma Aldrich
2-Heptanone	Sigma Aldrich
1-Iodoundecane	Aldrich
KB-R7943	Tocris
Trifluoromethoxyphenylhydrazone (FCCP)	Sigma Aldrich
Fluo-4	Invitrogen GmbH
Fura-2/AM	Invitrogen GmbH
Gelatine	Sigma Aldrich
Geranylacetone	Aldrich
(2-hydroxyethyl)-1-piperazineethanesulfonic acid (HEPES)	Sigma Aldrich
Lumio ™	Invitrogen
Lipofectamine LTX ™	Invitrogen
Magnesiumchloride	Sigma Aldrich
MDL 12, 330A	Calbiochem
3-methyl-2-buten-1-ol	Aldrich
3-methylcyclopentanone	Aldrich
MitoTracker	Invitrogen GmbH
Oligomycine	Sigma Aldrich
Phenol	Sigma Aldrich

3-penten-2-on e	Aldrich
PFA (paraformaldehyde)	Sigma Aldrich
Potassiumchloride	Sigma Aldrich
Sodiumchlorid e	Sigma Aldrich
Sodiumhydrogensulfate	Sigma Aldrich
Sodiumhydroxide	Sigma Aldrich, Fluka
Thapsigargin	Axxora Deutschland GmbH
Tissue Freezing Medium	Jung, Leica Instruments GmbH
Triton-X 100	Sigma Aldrich
U-73122	Sigma Aldrich
U-73343	Sigma Aldrich
Wortmannin	Sigma Aldrich
p-xylol	Aldrich
2 x Power SYBR Green Master Mix	Applied Biosystems
SDS 7900 HT instrument	Applied Biosystems
SDS 2.2	Applied Biosystems
DABCO mounting medium	Sigma
Biotinyl-tyramide solution	PerkinElmer

2.2 Solutions and buffers

Blocking solution: 100 ml PBS, 1 g Gelatine, 2 % serum, 0.2 % Triton-X 100

Extracellular solution ($E_{regular}$):
145 mM NaCl, 5 mM KCl, 1 mM $CaCl_2$, 1 mM $MgCl_2$, 10 mM HEPES, pH 7.3, 300 mosmol

Extracellular solution (oxygenated, 95% O_2 / 5% CO_2) (E_{oxy}):
120 mM NaCl, 25 mM $NaHCO_3$, 5 mM KCl, 1 mM $CaCl_2$, 1 mM $MgSO_4$, 5 mM BES,
pH 7.3, 300 mosmol

High potassium solution:
100 mM NaCl, 50 mM KCl, 1 mM $CaCl_2$, 1 mM $MgCl_2$, 10 mM HEPES,
pH 7.3, 300 mosmol

Low Ca^{2+}- extracellular solution ($[Ca^{2+}]$ = 100 nM) (E_{lowCa}):
135 mM NaCl, 5 mM EGTA, 1,5 mM $CaCl_2$, 5 mM KCl, 10 mM NaOH, 1 mM $MgCl_2$,
10 mM HEPES, pH 7.3, 300 mosmol

Solution for preparation of dissociated VSNs / OSNs:
140 mM NaCl, 5 mM KCl, 4.25 mM $CaCl_2$, 1 mM $MgCl_2$, 10 mM HEPES,
5 mM EGTA, 0.09 mg/ml Papain, 1 unit/ml DNase, pH 7.3, 300 mosmol

0.05 % Triton-X 100 washing solution: 500 µl Triton-X 100/l in PBS^{--}

Agarose (4%), Typ VII-A: 4 g/100 ml in $E_{regular}$

Paraformaldehyde (PFA) 8%: 80g/l in $E_{regular}$, pH 7.3

2.3 Consumables

Coverslips (roundly, 30 mm)	Hecht-Assistent
Syringes	Henke Sass, Wolf GmbH
Eppendorf tubes, 0.5 ml	Eppendorf AG
Eppendorf tubes 1.5 ml	Eppendorf AG
Object plate, Superfrost	Menzel
Pasteur pipets	VWR International GmbH
Aseptic filter, 0.45 µm	Whatman GmbH
Sterile filters, 0.33 µm	Millipore GmbH
Cell culture bottles	BD Bioscience
Cell culture dishes (35 x 10 mm)	BD Bioscience
Cell culture dishes (145 x 20 mm)	BD Bioscience
Cell strainer, 70 µm Nylon	BD Bioscience

2.4 Antibodies and sera

2.4.1 Primary antibodies

Anti-olfactory-marker-protein (Anti- OMP)	Wako-Chemicals GmbH
Anti- V1RD3	immunoGlobe
Anti- V2R2	Dr. R. Tirindelli (University of Parma, Italy)

2.4.2 Secundary antibodies

Goat- anti- rabbit Alexa 488	Molecular Probes
Goat- anti- rabbit Alexa 633	Molecular Probes
Goat- anti- rabbit Alexa 532	Molecular Probes
Donkey- anti- goat Alexa 488	Molecular Probes

2.4.3 Sera

1 % NSG, normal serum goat	Invitrogen GmbH
1 % NSR, normal serum rabbit	Invitrogen GmbH
Fetale Bovine Serum (FBS)	Sigma Aldrich

2.4.4 Accessory materials

Fab-fragments	Sigma Aldrich

2.5 Cultured cells

HEK293	
CHO c-Photina® cells	Axxam Inc.

2.6 Mouse strains

OMP-GFP strain	kindly provided by Mombaerts
C57BL/6 strain	Charles River
c-Photina® strain (AXXAM)	Axxam Inc
mOR-EG	kindly provided by Touhara

2.7 Equipment

Animal behavior setup	Noldus
Binocular eyepiece S4E	Leica Microsystems
Bioluminescence microsope LV 200	Olympus Europa Holding GmbH
Calcium imaging setup	Carl Zeiss AG
Cell culture bench	Thermo Scientific
Centrifuge Fresco 17	HERAEUS
Centrifuge labofuge 400R	HERAEUS
Confocol laser scan microscope SP5	Leica Microsystems
Cryostat CM 1950	Leica Microsystems
Hotplate magnetic stirrer	Snijders
Incubator	Binder
Lab dancer	Ika® Werke
Lateral shaker mini-rocker MR-1	Lab4you
Macroscope M80	Leica Microsystems

Osmometer 030	Gonotec
PH meter	Hanna instruments
Scale	Kern Abs
Vibratome VT 1000S	Leica Microsystems
Water bath	Memmert

2.8 Primer

V1rd3 Fwd1 (5’ to 3’): CAC TGT CCA ACC TGA TCC TTA CAC CAC TGT G

V1rd3 Rev1 (5’ to 3’): GAT CAA GGC AGG ATC AGT CCT ACT CCT GCT G, T= 60°C

Methods

2.9 Molecular cloning

2.9.1 Chemical transformation of DNA

For chemical transformation, approximately 1 µg/µl plasmid was mixed with 75 µl of competent *E.coli*, incubated on ice for 30 min and then put a 42 °C heating pan for 45 s. Based on this 'heat shock', plasmid DNA can enter the bacteria.

2.9.2 Plasmid purification using Qiagen Plasmid Maxi Kit

The Qiagen plasmid purification Kit is based on a modified alkaline lysis procedure, followed by binding of plasmid DNA to anion-exchange resin under appropriate low-salt and pH-conditions. A single colony is picked from a freshly streaked selective plate and a starter culture of 2 ml LB medium is inoculated with the appropriately selective 1 antibiotic. The starter culture is incubated for 8 h at 37°C by vigorous shaking (300 rpm). The starter culture is then diluted 1: 500 in to selective LB-medium and incubated at 37°C for 12-16 h by vigorous shaking. Next, bacterial cells were harvested by centrifugation at 6000 x g for 15 min at 4°C. The pellet was resuspended in 10 ml of lysisbuffer P1. 10 ml of neutralization buffer P2 was added and the whole lysate was thoroughly shaken by inverting the tube 4-6 times. The lysate is incubated for 5 min at room temperature (RT). Subsequently, 10 ml of chilled Buffer P3 was added, mixed immediately and incubated for 20 min on ice. The lysate was then centrifuged at 20,000 x g for 30 min at 4°C. The supernatant containing plasmid DNA is removed. Meanwhile the Qiagentip column has to be equilibrated with 10 ml Buffer QBT. The supernatant containing plasmid DNA is applied to the column and enters the resin by gravity flow. Before eluting the plasmid DNA with 15 ml QF the column is washed twice with 30 ml of Buffer QC to remove all contaminants. The eluted DNA is precipitated by adding 0.7 volumes of RT isopropanol and immediately centrifuged at 15,000 x g for 30 min. The DNA pellet is washed with 70 % ethanol to remove precipitated salt and centrifuged again for 10 min at 15,000 x g. Finally the DNA pellet has to air-dry and can be dissolved in a suitable volume of buffer.

2.9.3 Determination of nucleic acid concentration

To determine the concentration of nucleid acids (DNA or RNA), suitable sample dilutions were prepared and analyzed by monitoring absorbance at a wavelength of 260 nm by a UV-Spectrophotometer. The concentrations of the samples were calculated according to the following formula. OD_{260} = 1 equates to 50 µg/ml double strand DNA. Single strand DNA or RNA equates to 40 µg/ml.

2.9.4 Polymerase chain reaction, PCR

PCR (Mullis et al., 1986) is used to amplify DNA. The reaction generally requires design of exact oligonucleotide primers at either end of the region of interest. Through a series of cycles of denaturation of the DNA template, annealing of the primers and elongation of DNA by a DNA polymerase, the region of DNA between the primers is exponentially amplified. The *Taq* DNA polymerase is isolated from *Thermus aquaticus* and it catalyzes the polymerization of nucleotides into duplex DNA in the 5'→3' direction in the presence of magnesium.

Reactions with:

10 µl	10x PCR-Puffer
3 µl	$MgCl_2$ (50 mM)
0,8 µl	dNTPs (25 mM)
2,5 U	Polymerase (0,5 µl)
10 ng	DNA-Template (1 µl)
50 pmol	Primer (0,5 µl)
ad 100 µl	A.dest

Standard protocol:

Step	Temperature	Time
1. Denaturation	94°C	5 min
2. Annealing	55° - 65°C	1 min
3. Elongation	72°C	1 min
4. Filling	72°C	10 min
5. Cooling	4°C	end

Steps 2 to 4 are repeated 20 to 30 times. To determine the annealing temperature of the used oligonucleotides, the following formula is used.

$T_M = 2°C \cdot (A + T) + 4°C \cdot (G + C)$

2.9.5 Restriction of DNA

Restriction enzymes recognize short, specific and double stranded DNA sequences. They cleave DNA at specific sites within or adjacent to their recognition sequences. Each restriction enzyme has specific requirements to achieve optimal activity. Conditions such as

temperature, pH, enzyme cofactors, salt composition and ionic strength affect enzyme activity and stability. An analytical scale restriction enzyme digest is usually performed in a volume of 20 µl on 0.1-0.5 µg of substrate DNA (preparative scale, 5-10 µg DNA, 20 - 50 µl), using a 2- to 10-fold excess of enzyme over DNA. For calculation of the amount of enzyme it was assumed that app. 1 U of enzyme cuts 1 µg DNA in a volume of 50 µl at 37°C in one hour.

2.9.6 Dephosphorylation of DNA-fragments

Alkaline phosphatases are used for the dephosphorylation of 5'-phosphorylated DNA ends. Dephosphorylation of a restriction enzyme digested plasmid (5 - 20 pmoles of 5' ends, 0.1-0.5 U / p moles 5' ends) reduces religation of the primers without insert. Shrimp Alkaline Phosphatase (SAP) is a high specific activity, heat-labile alkaline phosphatase for molecular biology applications. Vectors were linearized with the appropriate restriction enzymes. The phosphate that stays at the 5' end of the vector is cut by adding SAP buffer (Roche) to a final concentration of 1x and 1-5 U enzyme for 1 µg DNA. Incubation was done for 1 h at 37°C. 1/20th volume of 500 mM EDTA was added.

2.9.7 Fill in reaction with Klenow-enzyme

In some cases, a filling step using the DNA Polymerase I Large (Klenow) fragment was used to fill 5' protruding ends and rendering blunt ends. The fill in protocol was performed according to the product instructions. 1 - 10 µg of the digested DNA was mixed with 1 µl Klenow (5 U), 10x buffer, 40 µM of each dNTP in a final volume of 20 µl. The reaction was incubated at RT for 10 min and stopped by heating the mixture at 75°C for 10 min.

2.9.8 Agarose gelelectrophorese

Following amplification of DNA by PCR or linearization by restriction reactions, the size of the product was determined by agarose gel electrophoresis. Samples were mixed with loading buffer to a final concentration of 1x and loaded in the wells of the gel. The gel was then run in a gel chamber in 1x TBE buffer at a voltage of approximately 10 V / cm. The gel was supplied with ethidium bromide, an intercalating dye, to a final concentration of 40 ng / ml. At this concentration, DNA is visible under the UV-light (312 nm). To mark the size of a fragment, the 1 KB DNA marker was used.

2.9.9 Ligation

T4 DNA ligase catalyzes the formation of phosphodiester bonds in the presence of ATP between double-stranded DNAs with 3' hydroxyl and 5' phosphate termini. For the ligation reaction, 100-200 ng vector was used and 2-15 µl purified fragment was added. Both DNA molecules were incubated in a 20 µl volume containing 2 µl 5x ligation buffer and 1 µl ligase (5 U) over night at 4-20°C.

2.9.10 RT- qPCR

To avoid tissue contamination, in particular from circulating lymphocytes, animals were flushed from blood by perfusion before tissue collection. cDNA was synthesized from 1µg of total RNA using random hexamers using Supercript II reverse transcriptase (Invitrogen) following suppliers instructions. The following oligonucleotides were used: FPR1, ATC ATT GGG TTC AGC ACT CC and GCC CTG CCT GTG AAT TTT AG; FPR-rs1, TTT ATC TGT TGG TTT CCT TTC CA and ACC ACT AAA CTG CAT CTC TTT GAG; FPR-rs2, ACA GCA GTT GTG GCT TCC TT and AAC CAG ACT GTG CCC AAA AG; FPR-rs3, GAG CAC AGC AAC AGG AAT CA and ATA GCA GAC GGC AAT GAA GG; FPRrs4, GAC TAG TCC TTG ATG GAA AAT TCA GTC and AGT TGC TGT CTG TGT CAG TGC TC; FPRrs6, TGA CAC TCA TGA TGG CAT GG and GTA GGA TGA GAT GGG AAG TGA G; FPR-rs7, GAT TCA GCC CTG AAC AGT GAC and CAC CAC ACC TCT CAG GTC CTA. PCR reactions contained diluted cDNA, 2 x Power SYBR Green Master Mix, 300 nM of forward and reverse primers. PCRs were performed on a SDS 7900 HT instrument with the following parameters: 50°C for 2 min, 95°C for 10 min, and 45 cycles of 95°C 15 s-60°C 1 min. Each reaction was performed in three replicates on 384-well plate. Each sample was constituted by pooled tissues from two 6 week-old C57BL/6 mice (one male and one female). Since all experiments were realized in triplicates, i.e. three independent pools of two animals per tissue, nine values were obtained per tissue (except for kidney for which two samples of two animals each were used). Raw Ct values obtained with SDS 2.2 were imported in Excel; normalization factors and fold changes were calculated using the GeNorm method. Normalization genes were 18S, GusB and Tfrc, except for values corresponding to the 18S graph which were normalized with GusB and Tfrc.

2.9.11 DNA sequencing

Sequencing of DNA was done using the sequencing service of the Department of Molecular Biochemistry, Ruhr-University Bochum, Bochum. Sequencing reactions were carried out by the Sanger method using fluorescine-labelled primers or oligonucleotides.

2.10 Cell culture

2.10.1 Cultivation of HEK293 cells

HEK293 cells were originally generated by transformation of cultured human embryonic kidney cells with sheared adenovirus 5 DNA (Graham *et al*., 1977; Thomas und Smart, 2005). HEK293 cells were grown in DMEM-Medium (Dulbecco´s Modified Essential Medium) at 5% CO_2, 95% humidity at 37°C to a confluency of 80%. When confluenty was reached cells were splitted. First, the cells were washed with $PBS^{-/-}$ and then incubated with 500 µg/l trypsine and 200 µg/l EDTA (0,5 M, pH 8,0) for a few minutes. Cells were resuspended in DMEM and disseminated in a ratio of 1:10. To freeze cells, 10% of DMSO and 20% of FBS is added to the media and cell suspension is placed at -80°C over night and then transferred to liquid nitrogen.

2.10.2 Transient transfection with Lipofectamine™ reagent

HEK293 cells were grown to 90-95% confluence prior to transfection. The culture medium was changed at least 1hr prior to transfection. Lipofectamine was mixed with Opti-MEM media. After 5 min incubation in Opti-MEM, the Lipofectamine and DNA (0.5 µg *V1rd3* and 0.5 µg RTP1 per dish) were combined and incubated for 20 min with gentle shaking at RT. The DNA / Lipofectamine complexes were then added to the cells. The media was swirled to ensure even coverage and the cells were incubated overnight. Due to the low toxicity of Lipofectamine there was no need to remove the complexes after incubation.

2.10.3 Lumio™ In-Cell Labeling

To label V1RD3-transfected HEK293 cells, growth medium from transfected cells was removed and 2.5 µM Lumio™ Reagent was added to the cells. Cells were incubated for 30 min at RT, protected from light. After labeling the proteins, detection and localization of recombinant receptors was performed using a fluorescence microscope equipped with a FITC - Filter (Ex = 495, Em = 518nm, dichroic mirror).

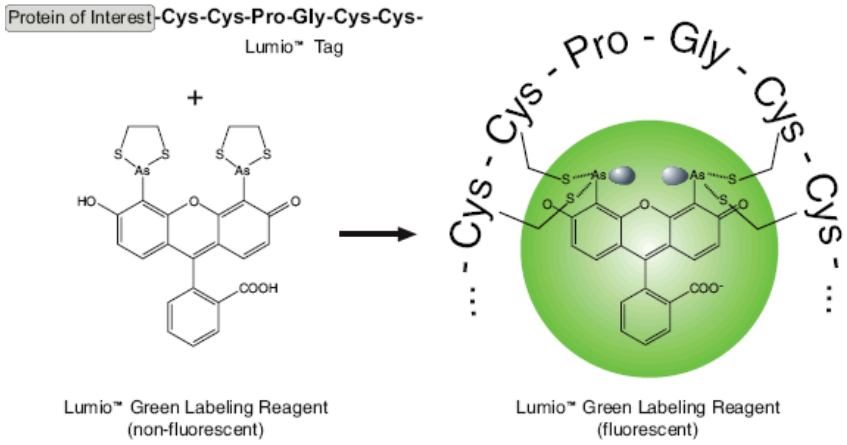


Fig. 2.1: When the Lumio Green Reagent is mixed with a Lumio fusion protein, the arsenic atoms of the reagent react with the tetracysteine motif of the protein and form four covalent bonds—the two arsenic groups of the Lumio Green Reagent each bind two thiols in the Lumio tag tetracysteine sequence. This binding hinders the free rotation of the arsenic atoms and the fluorescein molecule of the LumioGreen Reagent becomes fluorescent. Adapted from invitrogen.

2.11 Cryostat sections of VNO / MOE

For preparation of cryosections, the VNO was fixed for 2 h in 4% paraformaldehyde in PBS at 4°C, decalcified overnight in 0.5 M EDTA at 4°C and cryoprotected in PBS containing 30% sucrose at 4°C. The dehydrated VNO was embedded in Tissue Freezing Medium and sectioned at 15 µm on a cryostat.

To prepare cryostat sections of the MOE, mice were decapitated, the fur and the lower jaw was removed and the skull was fixed in 4% paraformaldehyde overnight at 4°C, decalcified for two days in 0.5 M EDTA at 4°C and cryoprotected in PBS containing 30% sucrose at 4°C. The dehydrated skull was embedded in Tissue Freezing Medium and sectioned at 15 µm on a cryostat.

2.12 Immunocytochemistry

Cryostat slices are marked with a Liquid Blocker (Super Pap Pen, Daido Sangyo, Tokyo) to draw a hydrophobic circle around slide-mounted tissue that prevents the waste of valuable reagents by keeping liquid pooled in a small droplet. Blocking was carried out in 1% Gelatin / 0.1% TritonX-100 (Blocking buffer) +/- 5% normal goat serum (NGS) for 1 hour at RT. All staining procedures were carried out in a humidified chamber to avoid sections drying out. Primary antibodies were applied in dilutions recommended by the manufacturer, over night at 4°C. Washes were carried out using $PBS^{-/-}$, 3 times for 15 min. Secondary antibodies were used in concentrations of 1:500 or 1:1000, in blocking solution, for 45 min at RT. Washes were repeated as above. Immunofluorescence was subsequently visualized using a laser scanning confocal microscope, Zeiss LSM 510 META.

2.13 In situ hybridizations

Cryostat slices (12-15 µm) of adult (7 to 9 week-old) mouse vomeronasal organs were arranged on SuperFrost slides (Menzel-Glaser), dried for 40 min , fixed for 20 min at 4ºC with 4% paraformaldehyde, and hybridized overnight at 65ºC with the following probes (position of nucleotides relative to the start ATG and origin is mouse if not stated otherwise): FPR1, nt 896-1357; FPR-rs1, nt 1070-1418; FPR-rs2, nt 784-1102; FPR-rs3, nt 710-1057; FPR-rs4, nt 841-1080; FPR-rs6, nt 854-1226; FPR-rs7, nt 967-1268; V1ra3, nt 249–839; V1rb2, nt 1–933; V1rc32, nt 103–467; V1rd16, nt 417–619; V1re4, nt 178–754; V1rf4, nt 397–920; V1rg1, nt 311–833; V1rh5, nt 163–740; V1ri8, nt 496–933; V1ri1, nt 313–750; V1rj3, nt 334–775; V1rl1, nt 433–876; V2R2, nt 1898–2733; Gαi2, nt 248–1138; rat FPR-rs3, nt 105-452. Fluorescein- and digoxigenin-labeled RNA probes were prepared using the DIG RNA labeling kit (Roche) following the manufacturer instructions. Hybridizations were performed in 1x salt buffer (in mM) (10 NaCl, 5 NaH2PO4, 5 Na2HPO4, 5 EDTA, pH 7.5), 50% formamide, 10% dextran sulfate, 1 mg/ml tRNA, 1x Denhardt's, with 20 ng/ml cRNA probe(s). Following hybridizations, slides were washed twice at 65ºC and once at RT with 1x SSC, 50% formamide and 0.1% Tween20. Slides were preincubated in 1x MABT, 2% blocking reagent for 20 min followed by 1 h incubation with alkaline phosphatase-ntidigoxigenin antibody (1:1000) or/and peroxidase-anti-fluorescein antibody (1:100). Peroxidase activity was detected by washing slides three times with TNT (Tris 150 mM, NaCl 150 mM, Tween20 0.05 %, pH 7.5), incubation for 30 min with a biotinyl-tyramide solution, 3 washes with TNT and incubation for 30 min with streptavidin-Alexa488. Alkaline phosphatase activity was detected by incubating slides with Fast Red substrate for 30 min. Sections were mounted in DABCO mounting medium.

2.14 Expression profiling

Oligonucleotide microarray analyses were performed for eight individual RNA samples (4 arrays from RNA of pheromone-stimulated mice (experimental group), 4 arrays of RNA from stimulus-deprived animals (control group)), each containing pooled vomeronasal RNA of five male mice (Hagendorf *et al.,* 2009). Total RNA was isolated from VNO preparations using Trizol Reagent and RNeasy Mini Kit according to the manufacturer's instructions. The quality (2100 bioanalyzer, RNA 6000 Pico LabChip) and quantity (NanoDrop® ND-1000 UV-Vis Spectrophotometer) of the starting RNA were analyzed. Samples were only processed if the quality was satisfactory as indicated by the absence of degradation of ribosomal RNA (28S/18S rRNA ratios ~2). Synthesis of double-stranded cDNA, generation of biotinylated cRNA, hybridization to Mouse Genome430_2.0 arrays, washing (GeneChip Fluidics Station 400), staining and scanning of the arrays (GeneChip Scanner3000) were done as recommended in the Affymetrix Expression_s2_manual (www.affymetrix.com) (Hagendorf *et*

al., 2009). Additionally, RNA quality was controlled by hybridization to Affymetrix Test 3 chips. Signal intensities, detection calls (present, absent, and marginal), and pairwise analyses of expression changes between experimental and control arrays were determined from processed array images using the GCOS1.4 software (Affymetrix). Data were exported as Microsoft Excel sheets, and analyzed using the Significance Analysis of Microarrays (SAM) software tool (available at: http://wwwstat.stanford.edu/~tibs/SAM). GCOS1.4 software was used to calculate the average noise (2.55 ± 0.1), the average background signal level (54.62 ± 0.84), the average percentages of 'present' and 'absent' calls ('present' = 54.96 ± 0.72%; 'absent' = 43.28 ± 0.75%), the average signal level for all probe sets (1364.98 ± 17), the average actin 3'/5' signal ratio (1.41 ± 0.03), and the average GAPDH 3'/5' signal ratio (0.98 ± 0.04) (Hagendorf *et al.,* 2009). One array from stimulus deprived controls was eliminated from further analysis, because it did not meet general quality standards. A scaling across all probe sets of a given array to a target intensity of 1000 was included to compensate for variations in the amount and quality of the cRNA samples and other experimental variables. Transcripts were defined as differentially expressed between the stimulated mice and the odor deprived controls. Signal intensities have to met the following criteria: 1) the gene had to be detected in at least 100% of the samples of either group, 2) either pairwise statistical analyses of expression changes using a Mann-Whitney test for independent samples showed a *p*-value of $p < 0.05$, or random overlap matrix analysis of multiple pairwise comparisons (exp/contr *versus* contr/contr; under both conditions each transcript is compared twelve times) showed regulated expression only in exp/contr comparisons (Hagendorf *et al.,* 2009).

2.15 Animal preparation

All animal procedures were in compliance with local and European Union legislation on the protection of animals used for experimental purposes (Directive 86/609/EEC) and with recommendations put forward by the Federation of European Laboratory Animal Science Associations. Mice were housed in groups of both sexes at RT on a 12 h light/dark cycle with food and water available *ad libitum*. If not stated otherwise, experiments used young adults of either sex. We did not observe any obvious differences between males and females in Ca^{2+} imaging recordings.

2.15.1 Dissociation of vomeronasal sensory neurons

Male and female C57BL/6 mice were decapitated. The vomer bone capsule surrounding the VNO was dissected and opened to gain access to the epithelium. The vomeronasal epithelium was dissected from the cartilage and placed in divalent cation-free papain solution. The vomeronasal epithelium was incubated in the enzyme solution for 15 min at 37 °C and transferred to $E_{regular}$ solution for gentle trituration with fire-polished Pasteur pipettes. Dissociated cells were subsequently filtered through a 70 µm nylon mesh cell strainer into fresh $E_{regular}$ solution in Concanavalin A-coated 35 mm Petri dishes and allowed to settle and attach. The $E_{regular}$ solution was carefully removed and replaced with the Ca^{2+} - sensitive dye fura-2/AM (2µM) (Molecular Probes) in $E_{regular}$ solution. Cells were allowed to load for 20 min at RT before being washed with fura-2/AM-free $E_{regular}$ solution for another 15 min.

2.15.2 Dissociation of olfactory sensory neurons

Male and female Photina mice were decapitated. The skull was cut sagitally and the septum was removed to gain access to the main olfactory epithelium. The olfactory epithelium was dissected from the cartilage and placed in divalent cation-free papain solution. The olfactory epithelium was incubated in the enzyme solution for 15 min at 37 °C and transferred to $E_{regular}$ solution for gentle trituration with fire-polished Pasteur pipettes. Dissociated cells were subsequently filtered through a 70 µm nylon mesh cell strainer into fresh $E_{regular}$ solution in Concanavalin A-coated 35 mm Petri dishes and allowed to settle and attach. The $E_{regular}$ solution was carefully drawn off the attached cells and replaced with the Ca^{2+}-sensitive dye fura-2/AM (2µM) (Molecular Probes) in $E_{regular}$ solution. Cells were allowed to load for 30 min at RT before being washed with fura-2/AM -free $E_{regular}$ solution for another 15 min.

2.15.3 MOE coronal vibratome slices

c-Photina® pups (P0-P5) were sacrificed by decapitation. The skin, lower jaw, the teeth and the palate were gently removed. The nose of the pups was dissected in oxygenated, ice-cold

solution. For preparation of acute slices, the intact nose was embedded in 4% low-gelling-temperature agarose and coronal slices (150 µm) were cut on a vibratome in ice-cold oxygenated solution (E_{oxy}). Slices were transferred to a submerged, chilled, and oxygenated storage chamber until use.

2.15.4 *En face* preparation of the VNO sensory epithelium

Inspired by a main olfactory epithelial preparation originally developed by Ma *et al.* and later modified for dendritic knob Ca^{2+} imaging, we adopted and modified a previously published technique for electro-vomeronasogram (EVG) recordings (Leinders-Zufall *et al*., 2000) to record Ca^{2+} transients from intact vomeronasal sensory epithelia. The fur, lower jaw, and palate of a mouse head were removed and a sagittal hemisection was performed ~1 mm lateral to midline. The hemisected head was transferred to a 35 mm culture dish, embedded in agar (4%) and superfused continuously with $E_{regular}$ solution at RT. The cartilaginous capsule surrounding the vomeronasal organ was opened laterally and the cavernous tissue was gently removed to gain access to the luminal surface of the VNO sensory epithelium.

2.16 Ca^{2+} imaging

2.16.1 Ratiometric Ca^{2+} imaging in HEK293 cells

48 h post transfection, Ca^{2+} imaging assays were performed on the stage of an inverted microscope equipped for ratiometric Ca^{2+} imaging. HEK293 cells were incubated with the Ca^{2+}-sensitive reporter dye fura-2/AM (4 µM) for 30 min, washed in $E_{regular}$ solution and briefly exposed to various stimuli (10 s) using a custom-built multi-barrell perfusion system. At 400 x magnification, fluorescence intensity images at 340 nm / 380 nm excitation wavelengths were captured by a cooled CCD camera (640 × 480 pixels) at 1 Hz frame rate and stored on a PC. Fields of view were randomly chosen. In order to avoid false-negative results caused by potential receptor adaptation, only two experiments were performed per culture dish. Offline analysis of time-lapse experiments was performed using TILLVision software. All cells in a given field of view were marked as individual regions of interest (ROIs), and the integrated fluorescence ratio f_{340}/f_{380} for each ROI was calculated and processed as a function of time. For FPR experiments fMLF (9µM), Lipoxin A (0.9µM), uPAR (1µM), and CRAMP (5µM) were sequentially applied in random order. Each compound was tested in at least four different transfections and several different experiments ($n \geq 62$). For V1RD3 experiments male urine (1:100), soiled bedding (1:100), fresh bedding (1:100) were applied and geranylaceton, 2-heptanone, 3-methyl-2-buten-1ol, 2,4-di-tert-butylphenol, 3-penten-2-one, 2-butyl-1-octanol, 3-amino-1,2,4-triazole, 3-methylcyclopentanone, 2,5-

dimethylpyrazine, 3-cyclohexene-1-methanol, phenol, p-xylol, 1-iodoundecane, 2-ethylphenol, cis-4-ethylcyclohexanol, 3-ethylphenol, 4-ethylphenol, ethylbenzene, ethylcyclohexane were applied in random order using 160 µM, respectively. To test for response specificity and to control for mechanical perfusion artifacts, two types negative control experiments were routinely performed: a) untransfected HEK293 cells were sequentially exposed to all test molecules; and b) cells were briefly exposed to standard $E_{regular}$ solution (without addition of a potential ligand). General excitability of HEK293 cells was monitored by ATP-dependent activation of endogenous purinergic receptors.

2.16.2 Ca^{2+} imaging in isolated vomeronasal neurons

Vomeronasal organ dissection and isolation of single vomeronasal neurons was performed as described under 2.15.1. The vomeronasal organ was cut into small pieces and incubated in E_{lowCa} containing 50 µg/ml papain and 20 U/ml DNAse for 15 min at 37°C. The tissue was then transferred to $E_{regular}$ and triturated using fire-polished Pasteur pipettes. Single vomeronasal neurons were separated from non-dissociated cells using 70 µm cell strainer nylon meshes and transferred onto Concanavalin A-coated glass-bottom dishes. During dye loading (fura-2/AM; 3 µM; 40 min), cells adhered to the bottom of the dish. After washing with $E_{regular}$, dishes were transferred to the stage of an inverted microscope equipped for ratio metric live-cell imaging with a 150 W xenon arc lamp, a motorized fast-change filter wheel illumination system for multi-wavelength excitation, a 12-bit 1376 x 1032 pixel charge-coupled device camera, and cell^R imaging software. Cells were viewed at 600x magnification using an oil-immersion objective and illuminated sequentially at 340 nm and 380 nm at variable frame rates (5 to 0.5 Hz). The average pixel intensity within user-selected regions of interest was digitized. Ca^{2+}-dependent fluorescence signals at 510 nm were calculated as the f_{340}/f_{380} intensity ratio. Stimuli were applied using a custom-made pressure-driven focal perfusion system as described above. In all Ca^{2+} imaging experiments (except experiments intended to test for repetitive responses or dose-response relationship), no neuron was stimulated with the same compound twice. Vice versa, no cell was investigated in more than one distinct experiment.

2.16.3 Calcium imaging MOE slices

MOE slices were incubated with the Ca^{2+}-sensitive reporter dye fluo4 AM (2 µM; Molecular Probes) for 30 min at 4 °C, washed in $E_{regular}$ and briefly exposed to Henkel 100 (1:10,000) (10s) using a custom-built multi-barell perfusion system. The MOE slices were transferred to an upright confocal Leica Microsystems microscope CFS SP5 equipped with a 20x (water immersion, HCX Apo, high numerical aperture) objective. Fluo-4 was excited using the 488 nm line of an argon laser and emitted fluorescence was captured using a 500–550 nm filter. Changes in cytosolic Ca^{2+} were monitored over time at 1 Hz frame rate. Offline analysis of time-lapse experiments was performed using LAS-AF software. All cells in a given field of view were marked as individual regions of interest (ROIs), and the relative fluorescence intensity for each ROI was calculated and processed as a function of time.

2.16.4 Bioluminescence imaging MOE slices

MOE slices were incubated with coelenterazine (10µM) for 3 h at 4 °C. Coelenterazine is the substrate for many luciferases and photoproteins including *Renilla reniformis* luciferase and aequorin. After loading, MOE slices were briefly exposed to various stimuli. Measurements were done with 20x, 60x, and 100x magnification at variable frame rates (1Hz and 25 Hz). Offline analysis of time-lapse experiments was performed using cell^M software. All responding cells in a given field of view were marked as individual regions of interest (ROIs), and the relative bioluminescence intensity for each ROI was calculated and processed as a function of time.



Fig. 2.2: Olympus LV200 bioluminescence microscope. Adapted from Olympus

2.16.5 *En face* confocal Ca^{2+} imaging at the luminal surface of the vomeronasal organ sensory epithelium

For Ca^{2+}-sensitive dye loading, the vomeronasal organ was incubated (30 min; 37°C) in $E_{regular}$ containing fluo-4/AM (3 µM). The dye loading was negligible in sustentacular cells, but

robust in vomeronasal neurons. After washing twice, the culture dish was mounted on the stage of an upright scanning confocal microscope equipped with a 10x (water immersion, numerical aperture 0.30) and 40x (water immersion, numerical aperture 0.80) objective. Fluo-4 was excited using the 488 nm line of an argon laser and emitted fluorescence was captured using a bandpass filter (500–550 nm). Changes in dendritic knob cytosolic Ca^{2+} were monitored over time at 0.3 Hz frame rate. An increase in cytosolic Ca^{2+} (as indicated by an increase in fluorescence intensity) was judged as a stimulus-dependent neuronal response if the following two criteria were both fulfilled: a) the peak intensity value exceeded a given threshold that was calculated as the average baseline intensity before stimulation plus an intensity value corresponding to twice the baseline intensity standard deviation ($I_{resp} > I_{baseline} + 2 \times SD(I_{baseline})$) ; b) the increase in fluorescence intensity was observed within 5 s after application of a given stimulus. Original traces were analyzed by a different individual than the one who performed the experiments. This individual was blind to stimulus identity. Stimulus application as well as solution exchange during inter-stimulus intervals was achieved by a custom-made, pressure-driven focal application device consisting of a software-controlled valve bank connected to a 7-in-1 'perfusion pencil'. Rhodamine application controlled for uniform flow and even stimulus application throughout the vomeronasal organ sensory surface.

2.17 Labeling of Mitochondria in OSNs using MitoTracker®

The cell-permeant MitoTracker® probes contain a mildly thiol-reactive chloromethyl moiety for labeling mitochondria in living cells. To label mitochondria cells are incubated with 25 nM MitoTracker® and incubated for 30 min at RT. The MitoTracker® probes passively diffuse across the plasma membrane and accumulate in active mitochondria. The properties of the two different MitoTracker® probes are listed.

Product	Ex (nm) *	Em (nm) *	Oxidation State	Retained after Fixation
MitoTracker® Deep Red FM	490	516	NA	No
MitoTracker® Green FM	644	665	NA	Yes

2.18 Statistical Analysis

If not stated otherwise, results are presented as means +/- SEM and statistical analyses were performed using paired or unpaired t-tests (as dictated by data distribution and experimental design).

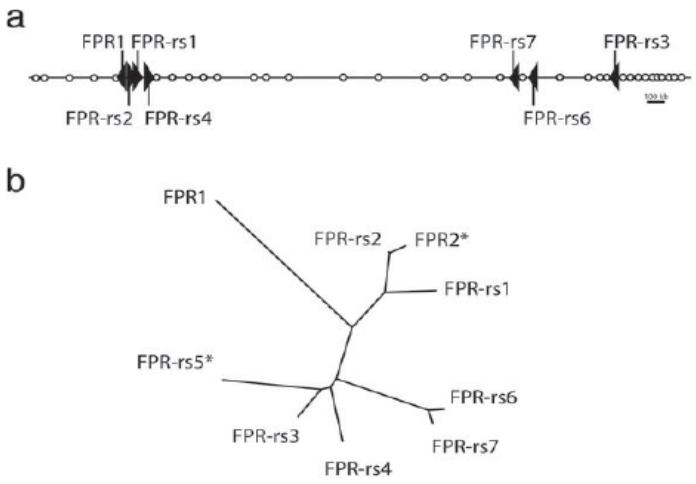
3 Results

3.1 Formyl peptide receptor-like proteins are a novel family of vomeronasal chemosensors

At least two different systems mediate the detection of olfactory cues: the main olfactory and the vomeronasal system; the first being largely specialized in the identification of general odorants while the second appears mainly responsible for pheromone detection (Zufall and Munger, 2001; Breer *et al.*, 2006). While thousands of compounds are known to be odorous for mammals, a surprisingly limited number of vomeronasal ligands have been identified (Leinders-Zufall *et al.*, 2000; 2004; Chamero *et al*., 2007; Kimoto *et al*., 2005; 2007; Nodari *et al*., 2008; Boschat *et al.,* 2002). At the core of our current understanding of olfactory coding is the expression by each sensory neuron of a single chemoreceptor gene, chosen among a large repertoire pertaining to the OR, TAAR, V1R or V2R olfactory chemoreceptor families. In an attempt to better understand the molecular tools used by mammals to socially interact, we searched for potentially still unidentified mouse vomeronasal chemoreceptors. These putative receptors were expected to possess the characteristics shared by all known olfactory chemoreceptors, i.e. 1) to be seven-transmembrane proteins, 2) to be expressed in a punctate fashion in the neuroepithelium, 3) to exclude the coexpression of other olfactory chemoreceptor groups, 4) to exclude cotranscription of members of their own group, 5) to be located at the dendritic endings of sensory neurons and 6) to trigger cellular responses to agonists possibly encountered by the animals.

3.1.1 FPR-like receptors in olfactory sensory neurons

We performed an RT-PCR screen on mouse vomeronasal sensory tissue using primers corresponding to known and putative heptahelical receptor transcripts; we identified 5 non-V1R and non-V2R GPCR genes, all members of the formyl peptide receptor (FPR) gene family. FPRs are found in all mammals and are encoded in humans by 3 and 7 genes in mice, respectively (Fig. 3.1a, b). FPR genes are located on chromosome 17, all of them found in a region encompassing 2.7 Mb (Fig. 3.1a). Intrafamily sequence identities between FPRs range from 67% to 96%.



c

% identity	FPR1	FPR-rs1	FPR-rs2	FPR-rs3	FPR-rs4	FPR-rs6	FPR-rs7
FPR1		73	76	70	69	68	67
FPR-rs1			88	77	80	74	74
FPR-rs2				78	80	75	76
FPR-rs3					91	86	85
FPR-rs4						84	83
FPR-rs6							96
FPR-rs7							

Fig. 3.1: The mouse FPR family. (a) Genomic organization of FPR genes (black triangles). Orientation of the triangles indicates direction of transcription. Empty circles correspond to non- FPR genes, which include V1R and V2R genes, *Riok2, Lix1, Lnpep, Has1, Snrpa, Ppp2r1a* and *Zfp160.* (b) Unrooted tree corresponding to the 7 potentially functional mouse FPRs. Two peptides identified by asterisks represent the translated products of two FPR pseudogenes in C57BL/6. (c) Amino acid identities between mouse FPRs

Two mouse FPR genes not transcribed in vomeronasal neurons, FPR1 and FPR-rs2, have been shown to play a role in immunity and to be expressed in immune cells and other cell types. We evaluated by RT-qPCR the expression of all mouse FPR genes in a broad range of tissues and organs. Presence of FPR-rs1, rs3, rs4, rs6 and rs7 transcripts was exclusively observed in vomeronasal tissue extracts (Fig. 3.2, Fig. 3.3i).

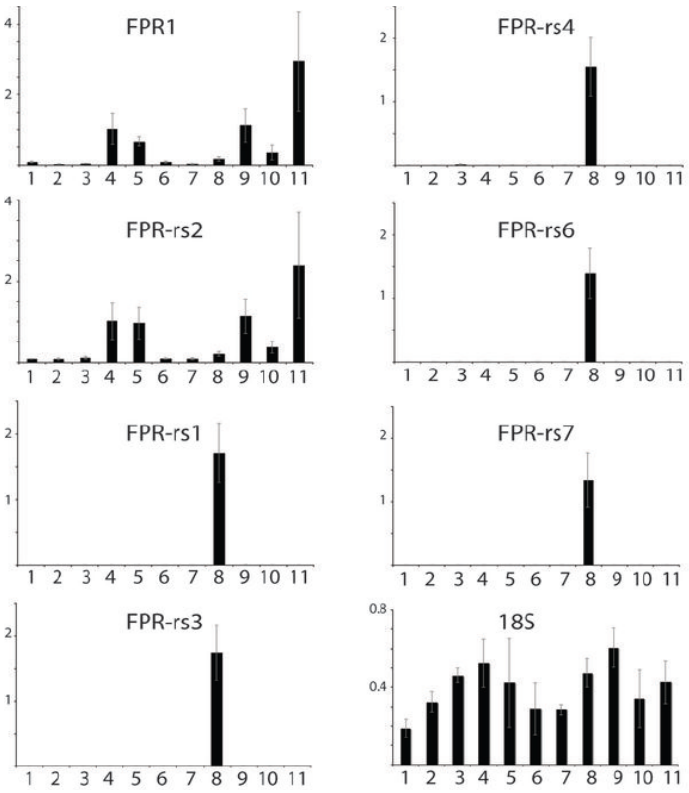


Fig. 3.2: Expression of FPR-rs1, rs3, rs4, rs6 and rs7 in vomeronasal tissue.
RT qPCRs were performed on kidney, lung, intestine, thymus, spleen, skeletal muscle, tongue, main olfactory epithelium and vomeronasal tissues. Lanes correspond respectively to muscle (1), kidney (2), intestine (3), lung (4), spleen (5), thymus (6), cerebellum (7), VNO (8), MOE (9), tongue (10) and blood (11). FPR-rs1, rs3, rs4, rs6 and rs7 transcription was exclusively observed in vomeronasal tissue. FPR1 and FPR-rs2 are expressed, in agreement with previously published data, in multiple organs. Transcripts of these two genes are also found in vomeronasal and main olfactory epithelium tissue, but *in situ* hybridizations indicate a glandular (i.e. not neuronal) location of these transcripts. Expression levels of 18S RNA are shown as controls. Mean values are indicated +/- SD, each corresponding to three independent pools of two animals.

In situ analysis of FPR-rs1, rs3, rs4, rs6 and rs7 transcription showed strong and punctate expression in the vomeronasal neuroepithelium (Fig. 3.3b-f), similar to patterns observed for V1R and V2R genes. FPR-rs1, rs3, rs4, rs6 and rs7-expressing neurons represented 0.7%, 0.8%, 0.6%, 1.2% and 0.8% of vomeronasal neurons, respectively, which corresponds to a total of 4.1%. To further investigate FPR-rs expression, we raised a rabbit antiserum against FPR-rs3. Immunohistochemical localization of FPR-rs3 on vomeronasal sections showed a punctate expression pattern corresponding to the staining of single sensory neurons, similar to the one obtained by *in situ* hybridization. The FPR-rs3 receptor was present in sensory neuron somata as well as dendritic endings (Fig. 3.3g). We evaluated the potential expression of FPR-rs3 in rat vomeronasal slices and found punctate mRNA and protein expression (Fig. 3.3h) similar to what was observed in mice. Comparable results were obtained on gerbil vomeronasal sensory tissue. The vomeronasal neuroepithelium is divided into two molecularly and possibly functionally distinct zones, one referred to as apical, expressing V1Rs and $G\alpha_{i2}$, the other basal and expressing V2Rs and $G\alpha_{o}$. Neurons transcribing FPR-rs3, FPR-rs4, FPR-rs6 and FPR-rs7 were localized in the apical $G\alpha_{i2}$-expressing layer of the neuroepithelium (Fig. 3.4).

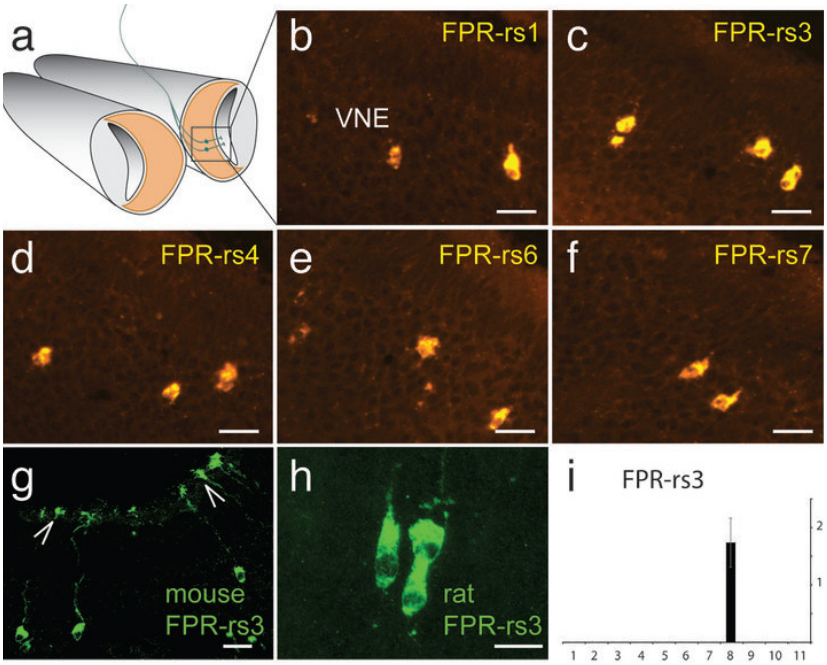


Fig. 3.3: FPR genes are expressed by vomeronasal sensory neurons. (a) Schematic of a VNO sectioned coronally. (b-f) DIG-labeled antisense probes of FPR-rs1, rs3, rs4, rs6 and rs7 hybridized to coronal sections of mouse VNO neuroepithelium show punctate expression. (g) Immunohistochemical localization of FPR-rs3 in mouse VSN somata and dendritic endings (arrows). (h) Expression of FPR-rs3 in rat VNO neuroepithelium. (i) RT-qPCRs with primers specific for mouse FPR-rs3 performed on muscle (1), kidney (2), intestine (3), lung (4), spleen (5), thymus (6), cerebellum (7), VNO (8), MOE (9), tongue (10) and blood (11) extracts. FPR-rs3 transcripts are only found in VNO tissue. Scale bar 40 µm.

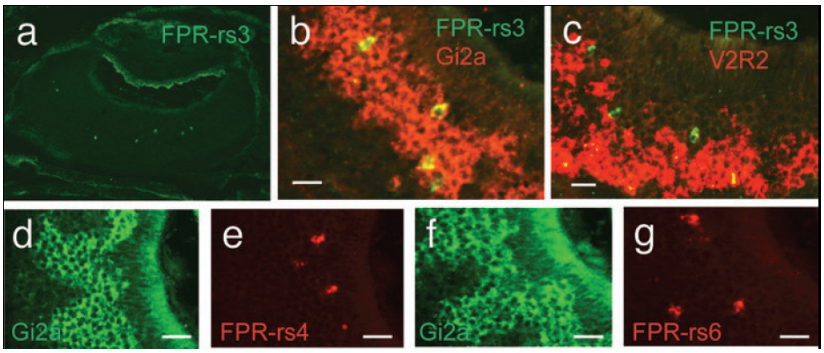


Fig. 3.4: Distribution of FPR-expressing sensory neurons. FPR-rs3 transcripts are present in vomeronasal sensory neurons located along the dorso-ventral area of the sensory epithelium (a). These neurons coexpress $G\alpha_{i2}$ (b), but not V2R2 transcripts (c). (d-g) FPR-rs4 and FPR-rs6 expressing neurons coexpress $G\alpha_{i2}$. Scale bar 40 µm.

Members of a given olfactory receptor gene family are not coexpressed with members of another family. To evaluate whether this characteristic was shared by FPR genes, we took an approach based on double *in situ* hybridizations, using a large panel of probes recognizing most chemoreceptors expressed by vomeronasal sensory neurons. A total of 2293 vomeronasal neurons expressing FPR-rs3 were examined; none showed colabeling with any of the probes (Fig. 3.5a-k), strongly suggesting a transcription mechanism excluding the coexpression of vomeronasal chemoreceptors pertaining to other families. A second peculiar hallmark shared by most olfactory chemoreceptor genes is monogenic expression, i.e. the transcription of a single chemoreceptor gene, from a given family, per sensory neuron. We investigated the potential cotranscription of different members of the FPR family. Vomeronasal sections were cohybridized with a FPR-rs3-specific probe and probes recognizing FPR-rs1, rs4, rs6 or rs7. 911 FPR-rs3-expressing vomeronasal neurons were visualized; none did exhibit coexpression Fig. 3.5l-o), indicating a monogenic transcription similar to the one observed for odorant or V1R receptor genes.

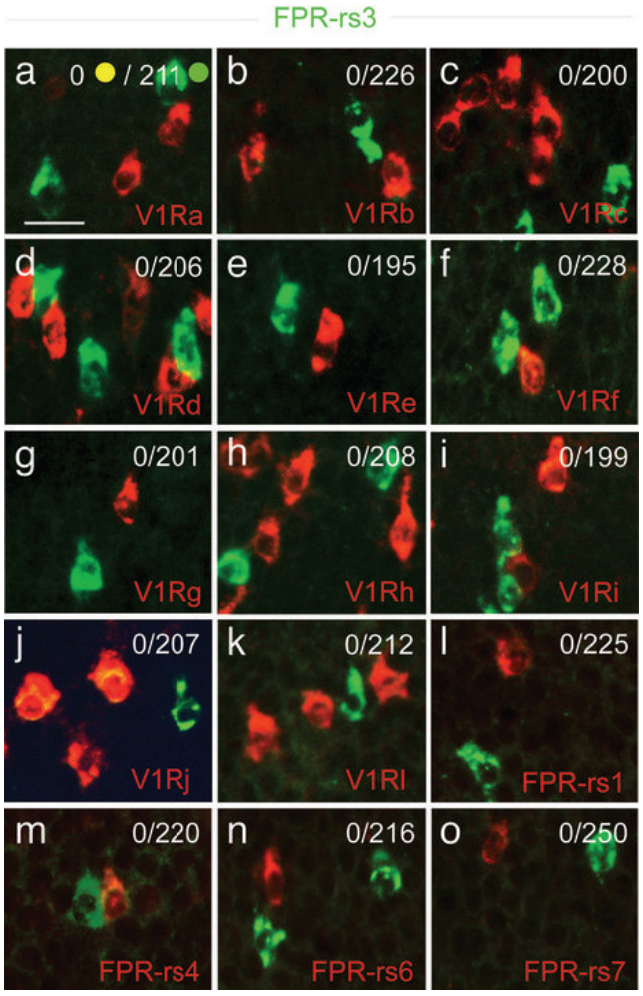


Fig. 3.5: Exclusive expression of FPR genes in vomeronasal neurons. (a-k) Double *in situ* hybridizations with probes covering the whole V1R repertoire (red) and FPR-rs3 (green) show the absence of coexpression between FPR-rs3 and V1R genes. Intrafamily monogenic expression, which is observed for V1Rs, also characterizes FPR-rs3 (l-o), whose transcripts do not colocalize with FPR-rs1, rs4, rs6 and rs7 transcripts. The X/Y ratio indicates the number (X) of neurons coexpressing FPR-rs3 and a member of the tested FPR family, among Y FPR-rs3- positive neurons. Scale bar 20 µm.

3.1.2 *In vitro* agonists of FPR-rs receptors

FPR1 and FPR-rs2 are expressed by granulocytes, monocytes, or macrophages and recognize multiple agonists. These include molecules associated with inflammation or disease, such as formyl peptides which are released by gram negative bacteria, HIV-derived peptides, the antimicrobial peptide CRAMP, lipoxin A4, uPAR and the acute phase protein SAA. No ligands are known for mouse FPR-rs3, rs4, rs6 or rs7 receptors. To explore their agonist characteristics, HEK293 cells were transiently transfected with FPR-rs1 as well as FPR-rs3, FPR-rs4, FPR-rs6 and FPR-rs7. We hypothesized FPR-rs1, 3, 4, 6 and 7 could respond to FPR1 or FPR-rs2 agonists; these potential ligands were evaluated by measuring agonist-induced Ca^{2+} transients in HEK293 cells loaded with the ratiometric Ca^{2+}-sensitive reporter dye fura- 2/AM. Ca^{2+} transients were recorded after addition of 9 µM fMLF, 0.9 µM lipoxin A4, 5 µM CRAMP and 1 µM uPAR (Fig. 3.6a-d). Every transfected FPR-rs did provide responsiveness to at least one ligand. Adaptation was observed after exposure to a single agonist. FPR-rs did respond to varying degrees to most stimuli (Fig. 3.6d), an observation consistent with the very widely tuned agonist characteristics of FPRs expressed in the immune system, such as FPR1 and FPR-rs2.

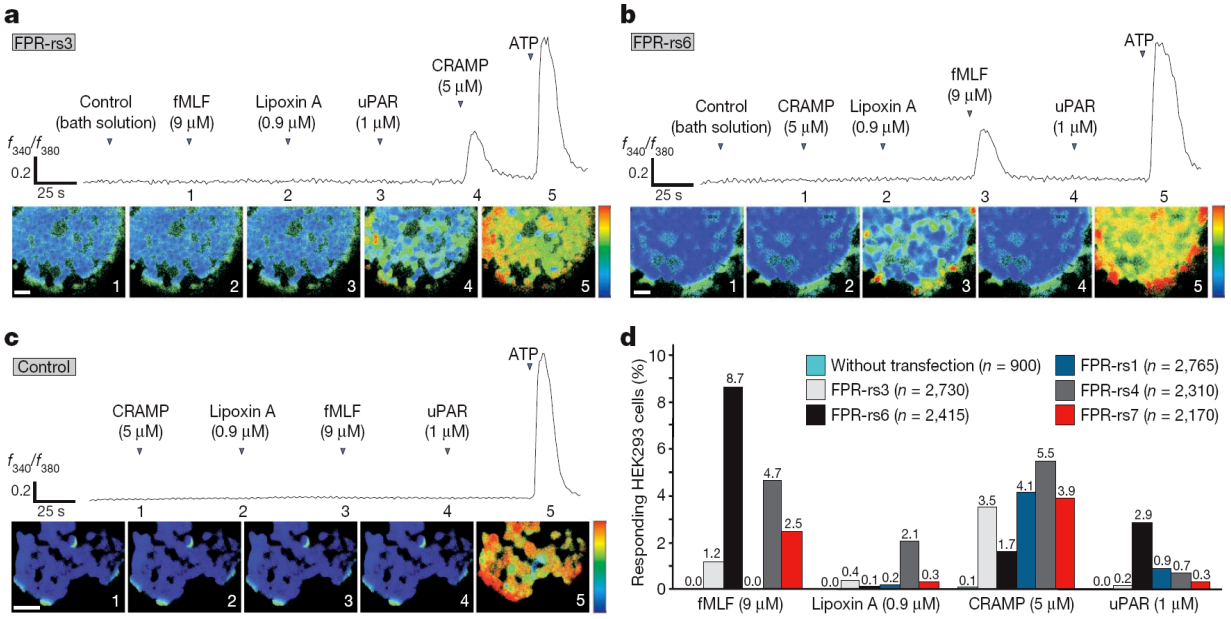


Fig. 3.6: Recognition by FPRs of pathogen/inflammation-related compounds. (a-c) Representative original recordings of Ca^{2+} signals in either HEK293 cells expressing FPR-rs3 (a) or FPR-rs6 (b) or untransfected controls (c). Relative cytosolic Ca^{2+} concentrations are depicted in pseudocolor (rainbow spectra: low Ca^{2+} (blue) / high Ca^{2+} (red)). The integrated fluorescence ratio (f_{340}/f_{380}) in a user-defined region of interest is depicted as a function of time. Numbered images correspond to individual frames at indicated time points (1-5). FPR-rs3-transfected cells respond to CRAMP (5 µM), whereas FPR-rs6- expressing cells respond to fMLF (9 µM). Untransfected HEK293 cells did not respond to any of the stimuli. (d) Semi-quantitative bar chart illustrating the ligand-receptor interactions as measured by Ca^{2+} assays in FPR-expressing HEK293 cells. The response 'probability' is plotted in percent as a function of 8 both stimulus and receptor identity. Recordings (n ≥ 50) from at least three independent transfections were repeated multiple times for each possible receptor-ligand combination. Scale bar 50 µm.

3.1.3 Vomeronasal responses to FPR-rs agonists

Since our findings suggested a capacity of the vomeronasal organ to perceive compounds related to bacteria and inflammation, potential Ca^{2+} transients elicited on vomeronasal neurons by the addition of these compounds were measured. Two independent approaches were used: a) we measured cytosolic Ca^{2+} signals in dissociated vomeronasal sensory neurons and b), we established an intact whole-mount preparation allowing confocal Ca^{2+}-imaging in individual dendritic knobs without disrupting the integrity of the sensory epithelium or axonal projections. First, acutely dissociated vomeronasal sensory neurons, loaded with fura-2/AM, were stimulated by application of the formyl peptide fMLF (0.9 µM / 9 µM), CRAMP (0.9 µM), lipoxin A4 (0.9 µM), diluted urine (1:100) and an elevated extracellular K^+ solution (40 mM) (Fig. 3.7 b,c). The integrated fluorescence ratio (f_{340}/f_{380}) in defined regions of interest covering large areas of individual cell somata was monitored as a function of time. From a total of 598 K^+-sensitive vomeronasal neurons investigated in 105 independent experiments (14 animals), 143 neurons (23.9%) responded to diluted urine. At a concentration of 0.9 µM, 5.5%, 4.6% and 11.6% of the recorded vomeronasal neurons responded to fMLF, lipoxin A4 and CRAMP application, respectively. A higher concentration of fMLF (9 µM) triggered responses in 9.9% of neurons (Fig. 3.7 b). Next, the response profiles of ligand-sensitive vomeronasal neurons were tested. When fMLF, CRAMP and lipoxin A4 (0.9 µM each) were applied sequentially (in random order), response profiles were not homogenous: 23 out of 28 CRAMP-sensitive VSNs (82.1%), 7 out of 11 lipoxin A4-sensitive neurons (63.6%) and 8 out of 11 fMLF-sensitive cells (72.7%) responded exclusively to CRAMP, lipoxin A4 and fMLF, respectively. The remaining neurons were sensitive to 2 out of the 3 peptides (2 VSNs responded to CRAMP and fMLF; 3 VSNs responded to CRAMP and lipoxin A4; 1 VSN responded to lipoxin A4 and fMLF), whereas no vomeronasal neuron (n = 50) responded to all 3 ligands (Fig. 3.7c). These data are consistent with the expression of different FPR-rs (and therefore non-identical agonist profiles) in randomly chosen vomeronasal neurons.

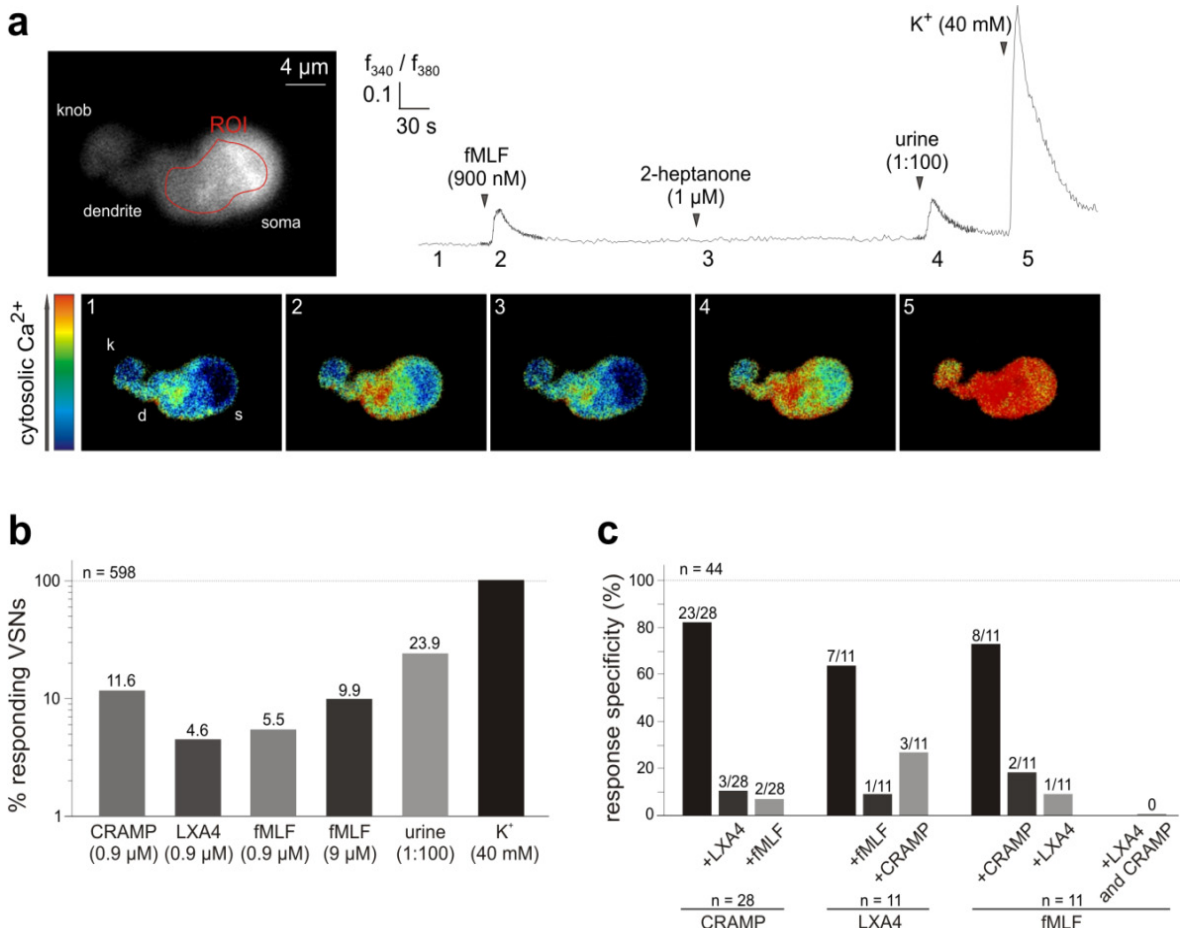


Fig. 3.7: Isolated vomeronasal sensory neurons respond to fMLF.
(a) Representative original recording of cytosolic Ca^{2+} signals in response to fMLF (0.9 µM), diluted urine (1:100) and elevated K^+ (40 mM). The integrated fluorescence ratio (f_{340}/f_{380}) in a user-defined region of interest (ROI: red area, inset) is viewed as a function of time. Relative Ca^{2+} concentrations are depicted in pseudocolor. Numbered images correspond to individual frames at indicated time points (1-5). (b) Semilogarithmic bar chart illustrating the stimulus-dependent response rate in K^+-sensitive vomeronasal neurons. (c) Tuning profile of agonist-sensitive vomeronasal neurons (n = 50) sequentially exposed to fMLF, CRAMP and lipoxin A4 (LXA4) in random order.

The second strategy was based on the analysis of single neuron sensitivity to FPR-rs agonists in the intact vomeronasal sensory neuroepithelium. We established a vomeronasal organ whole mount imaging assay based on Ca^{2+} transients, termed *en face* Ca^{2+}-imaging and recorded responses from individual dendritic knobs of fluo-4/AM-loaded vomeronasal neurons (Fig 3.9 a,b). This approach presents several advantages: a) dendritic tips are kept covered by mucus, b) neurons stay surrounded by sustentacular cells and c) axonal projections to the accessory olfactory bulb are kept intact. 15 - 25 individual knobs were typically visualized per experiment (Fig. 3.8b), among which 95% responded to K^+-dependent membrane depolarization with a transient increase in cytosolic Ca^{2+} (Fig. 3.9 d). The remaining K^+-insensitive neurons (5%) were discarded from further analysis. Application of known vomeronasal stimuli including urine, soiled bedding, 2-heptanone, 2, 5- DMP and the SYFPEITHI peptide induced repeated Ca^{2+} transients in vomeronasal dendrites (Fig. 3.8 a,b,c).

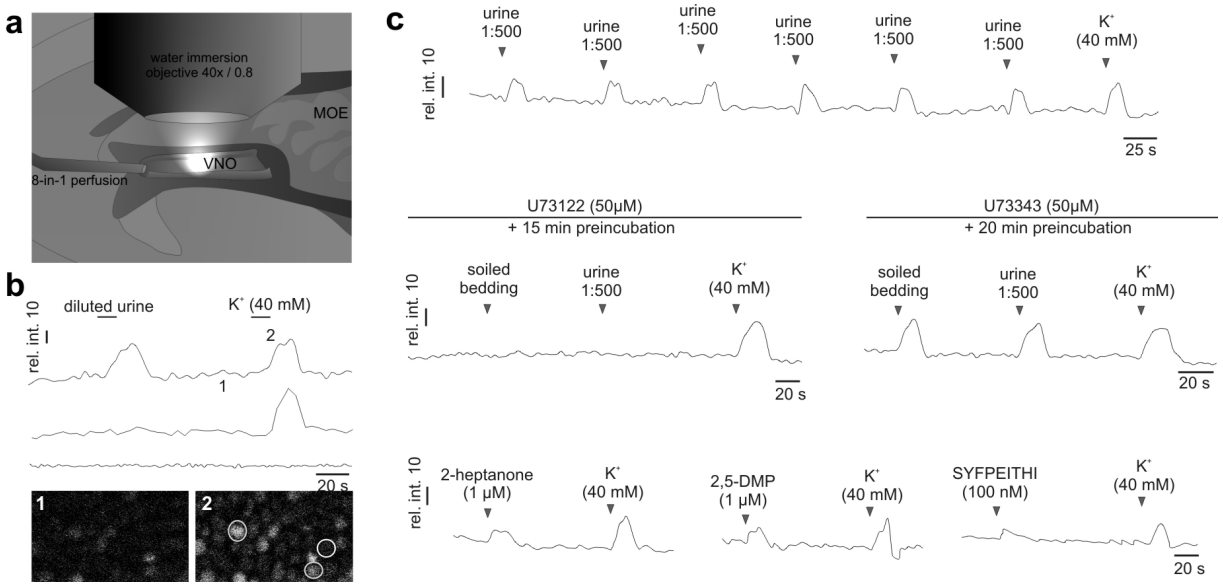


Fig. 3.8: *En face* confocal Ca^{2+}-imaging allows for live-cell recording of vomeronasal neuron activity at the site of primary signal transduction.
(a) Schematic diagram illustrating the experimental setup for *en face* confocal Ca^{2+}-imaging. (b) Representative original recording of cytosolic Ca^{2+} signals in response to diluted urine (1:500) and elevated K^+ (40 mM). Relative Ca^{2+} concentration changes are reflected by shifts in grey-scale fluorescence intensities in user-defined ROIs (white circles), displayed in arbitrary units and viewed as a function of time. Numbered images correspond to individual frames at indicated time points (1, 2). (c) Representative original traces illustrating the suitability of *en face* confocal Ca^{2+}-imaging for physiological analysis of single vomeronasal neuron response profiles. Urine stimulation induces robust and repetitive Ca^{2+} signals (n = 20). Responses to complex natural stimuli (soiled bedding extracts / diluted urine) are strongly inhibited by pre-incubation with a specific blocker of phospholipase C (U73122, n = 28), whereas its inactive analog (U73343, n = 20) shows no effect. In addition, single knob Ca^{2+} transients are detected in response to different previously identified pheromonal stimuli (2-heptanone, n = 9 ;2,5-dimethylpyrazine (DMP), n = 11 ; SYFPEITHI, n = 19).

In 25 independent control experiments, repeated focal application of standard bath solution never elicited a response. In a total of 221 different experiments (21 animals), the vomeronasal surface was sequentially exposed to brief pulses (10 s) of the formyl peptide fMLF, SMUPAR-HIS (uPAR), or lipoxin A4 (LXA4) (Fig. 3.9 c). Similar to observations in isolated vomeronasal neurons (Fig. 3.7), we recorded responses in 4.8%, 4.1% and 5.9% of vomeronasal neurons after perfusion with fMLF, LXA4 and uPAR, respectively (Fig. 3.9 e). As expected from previously reported data, Ca^{2+} transients in response to described vomeronasal stimuli were observed less frequently: 1.2% for 2-heptanone and 1.1% for 2,5-dimethylpyrazine. When increasing concentrations of fMLF were sequentially applied over a five orders of magnitude concentration range (0.9 nM to 9 µM; n = 1641 VSNs / 82 experiments, Fig. 3.9f), initial Ca^{2+} signals could be detected at 90 nM fMLF (Fig. 3.9 f). Neurons responding to a given concentration of fMLF did invariably respond to higher concentrations of fMLF (Fig. 3.10). Similar to data obtained from dissociated neurons, vomeronasal neurons in the intact epithelium displayed some variability in their individual ligand profile when tested for their responses to fMLF, LXA4 and uPAR (Fig. 3.9g).

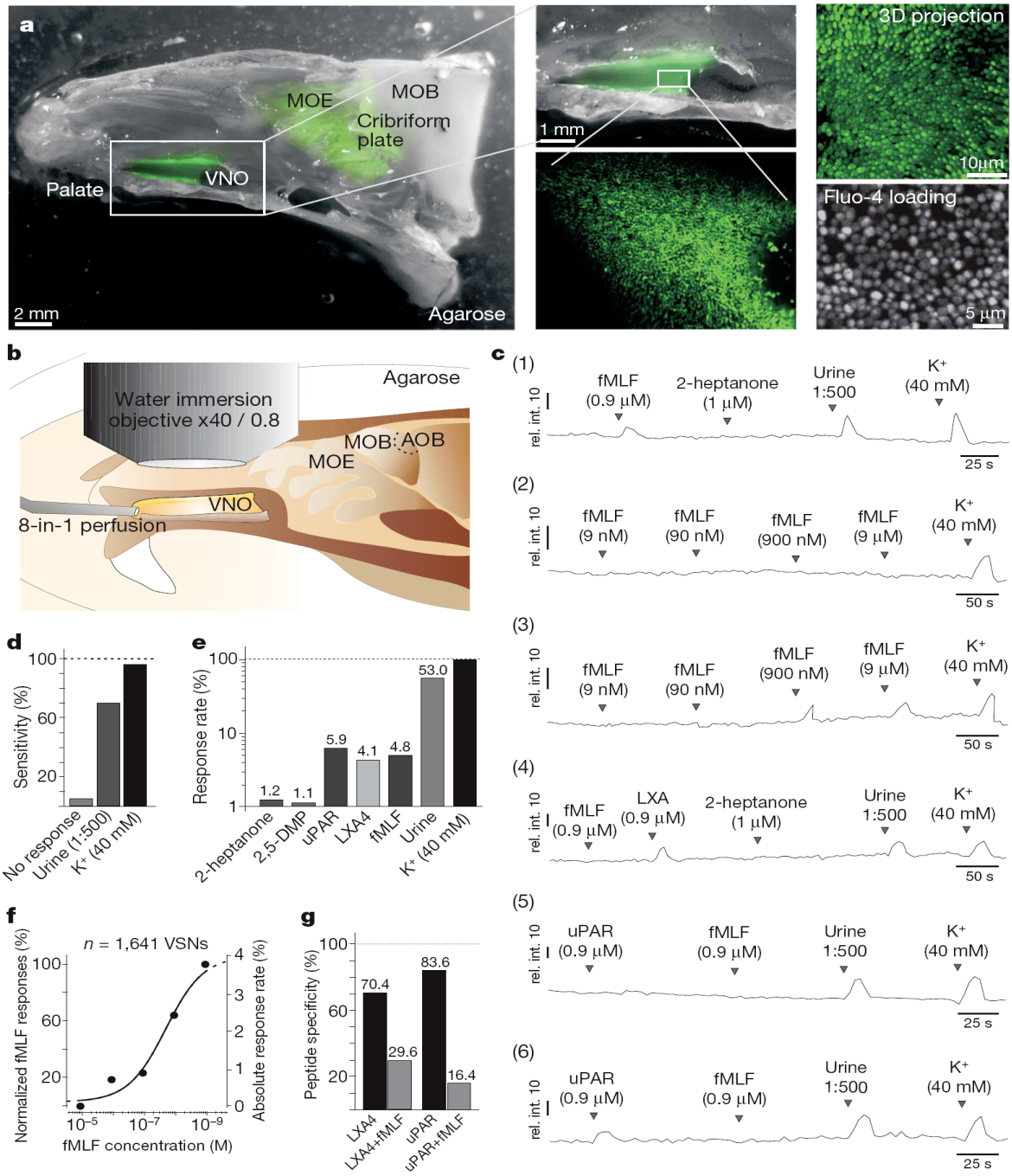


Fig. 3.9: Formyl-peptide-evoked Ca^{2+} signals in the intact vomeronasal epithelium. (a) Bright field, fluorescence and confocal images illustrating the *en face* confocal Ca^{2+}-imaging approach established in this study. Left: merged macroscopic bright field and fluorescence images of the hemisected rostral head of an OMP-GFP mouse. The vomeronasal organ was opened laterally and the cavernous tissue was removed, see inset at higher magnification (middle panel, top). Middle panel, bottom: low magnification *en face* confocal scan of the dendritic surface of the vomeronasal organ sensory epithelium area shown above. Right panel, top: 3D transparency projection of a high magnification confocal z-stack through the apical part of the sensory epithelium. Right panel, bottom: high magnification confocal section of fluo-4/AM-loaded vomeronasal neurons. (b) Schematic diagram showing the experimental setup used for *en face* confocal Ca^{2+}-imaging. (ci-vi) Representative original recordings of cytosolic Ca^{2+} signals in single dendritic vomeronasal neurons knobs in response to fMLF (9 nM - 9 µM), LXA4 (0.9 µM), uPAR (0.9 µM), 2-heptanone (1 µM), diluted urine (1:500) and elevated K^+ (40 mM). The integrated fluorescence intensities in user-defined ROIs are displayed in arbitrary units and viewed as a function of time. (d) Bar graph showing general vomeronasal neuron viability as 95% of all neurons investigated is sensitive to membrane depolarization. (e) Semi logarithmic bar chart illustrating the stimulus-dependent response rate in K^+-sensitive vomeronasal neurons. (f) *Quasi* dose-response curve depicting the concentration dependence of fMLF sensitivity. The percentage of responding vomeronasal neurons was normalized to the number of

neurons activated by 9 µM fMLF. Data points are fit to a Hill equation. (g) Tuning profile of formyl peptide-sensitive vomeronasal neurons sequentially exposed to uPAR, LXA4 or fMLF (0.9 µM each).

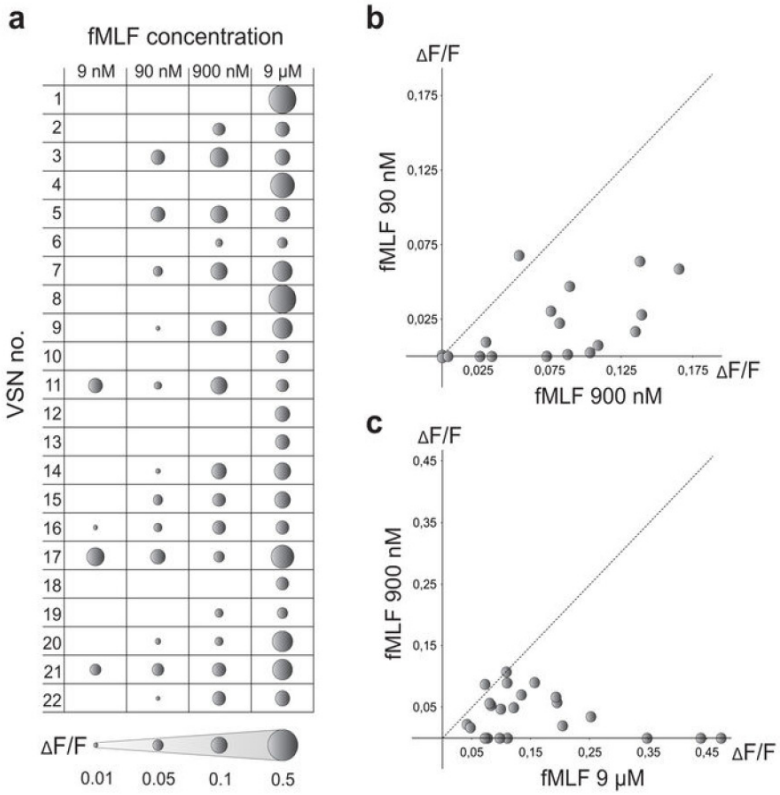


Fig. 3.10: Dose response relationship of single fMLF-sensitive VSNs. a) Dot plot response profiles from 22 individual VSNs sequentially stimulated with increasing fMLF concentrations. Cells responding to a given peptide concentration invariably respond to higher concentrations. In the majority of neurons, an increase in stimulus concentration correlates with an increased Ca^{2+} signal. The absence of a dot indicates that the stimulus was tested, but did not induce a response. The scale shows the dot size corresponding to selected response amplitudes. (b,c) Scatter plots comparing single neuron Ca^{2+} response amplitudes (ΔF/F) induced by two different fMLF concentrations (90 nM *versus* 900 nM (b); 900 nM *versus* 9 µM (c)). The accumulation of dots below the angular dotted lines indicates an overall hierarchical correlation between stimulus concentration and response magnitude.

3.2 Functional characterization of vomeronasal receptor V1RD3

Two distinct populations of vomeronasal sensory neurons have been identified, each expressing either V1R (Dulac and Axel, 1995; Rodriguez *et al.,* 2002) or V2R receptor proteins (Herrada and Dulac, 1997; Matsunami and Buck, 1997; Ryba and Tirindelli, 1997). So far, only one V1R has been deorphanized (Boschat *et al.,* 2002). To gain insight into the coding logic underlying VNO-dependent social communication, we searched for potentially still unidentified mouse vomeronasal receptor-ligand pairs, combining recombinant receptor expression in a heterologous cell system and physiological *in-situ* recording methods. To determine whether transcription of vomeronasal receptor genes is actively regulated in the mouse VNO, we surveyed expression profiles of adult male C57BL/6 mice that had been singly housed either in an essentially odor-free environment (deprived group) or exposed to rich sources of pheromonal cues (stimulated group) (Hagendorf *et al*., 2009). Stimulation cycles (7 d) were composed of 6 h exposure to fresh male urine (2:00 – 8:00 P.M.), 12 h exposure to female-soiled bedding (8:00 P.M. to 8:00 A.M.) and additional 6 h without stimulation (8:00 A.M. to 2:00 P.M.) to allow for relief from potential sensory adaptation (Fig. 3.11).

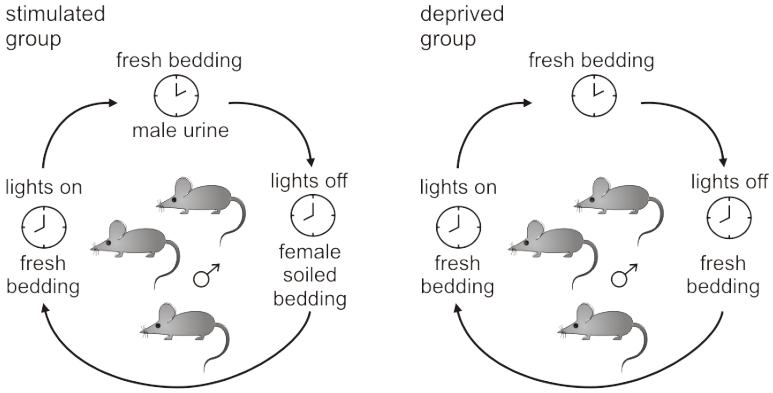


Fig. 3.11: Schematic diagram illustrating the experimental strategy used for pheromone exposure (left) and stimulus deprivation (right) of singly housed C57BL/6 mice.

Vomeronasal receptor transcription levels were compared between stimulated and deprived tissue using a total of seven Affymetrix microarrays (four experiments and three control replicates), each microarray chip probing pooled mRNA from five animals (Hagendorf *et al*., 2009). From a total of 34,000 mouse genes, the most pronounced changes for a chemosensory receptor were observed for the vomeronasal receptor *V1rd3* (upregulation). This receptor was cloned and recombinantly expressed in a heterologous cell system in which effective plasma membrane translocation could be monitored using biarsenical dyes (Fig. 3.12). About 2% of HEK293 cells were successfully transfected with a V1R / tetracysteine construct and exhibited green fluorescence upon FlAsH/Lumio Green™

superfusion. Approximately 1% of transfected HEK293 cells showed membrane-bound staining (Fig. 3.12).

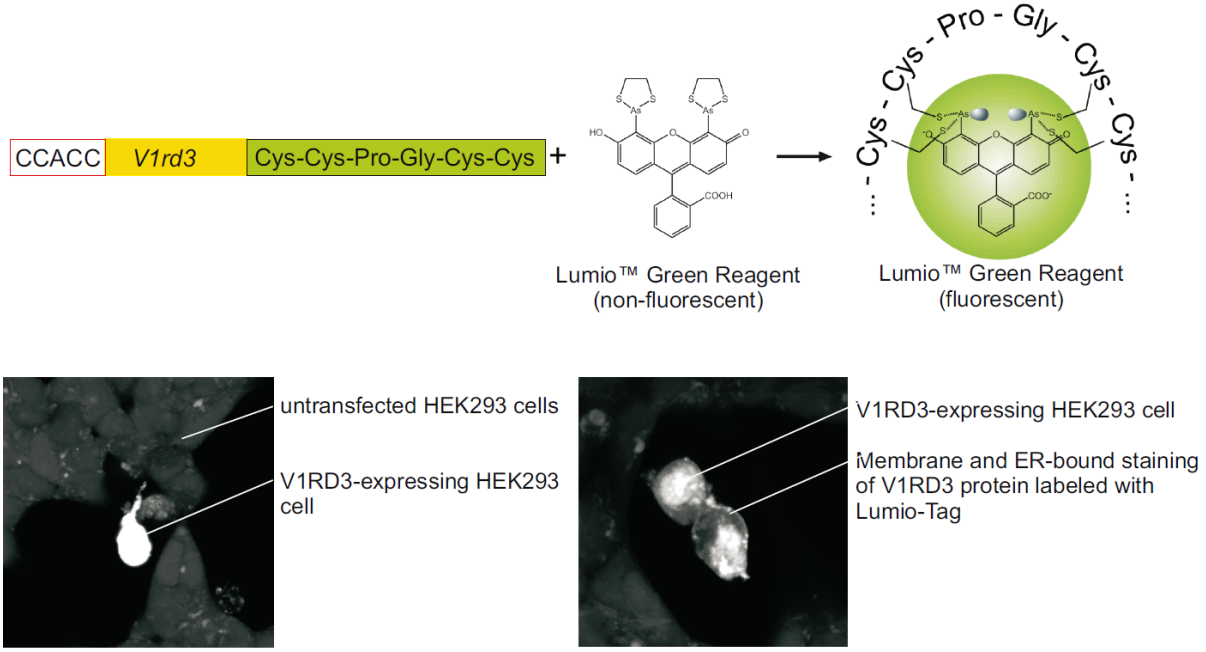


Fig. 3.12: Generation of the *V1rd3* / tetracysteine motif fusion construct. Representative images show recombinant expression of FlAsH/Lumio Green™-labeled receptor in HEK293 cells.

3.2.1 Functional characterization of the vomeronasal receptor V1RD3

No ligands are known for the mouse V1RD3 receptor. To explore its agonist characteristics, HEK293 cells were transiently transfected with *V1rd3*. Since complex stimulus mixtures such as soiled bedding or male urine were used for stimulation in expression profiling experiments, we hypothesized that V1RD3 responds to at least one of these stimulus mixtures. Potential ligands were evaluated by measuring agonist-induced Ca^{2+} transients in V1RD3-expressing cells loaded with the ratiometric Ca^{2+}-sensitive reporter dye fura-2/AM. In an initial series of experiments, cells were exposed to the following stimulus / control mixtures: fresh bedding extracts (diluted 1:100), soiled bedding extracts (diluted 1:100) and male urine (diluted 1:100) (Fig. 3.13 a). The integrated fluorescence ratios (f_{340}/f_{380}) in user-defined regions of interest (ROIs) were viewed as a function of time. As reported for OR expression in HEK293 cells (Spehr *et al*., 2003), strong response adaptation was observed once a given cell had been activated. Untransfected HEK293 cells were routinely tested in parallel as negative controls. HEK293 cells expressing V1RD3 responded to diluted male urine but not to diluted fresh or soiled bedding extracts. 1.25% of V1RD3-expressing cells responded to diluted male urine (n = 25 / ~2000) (Fig. 3.13 a). Untransfected HEK293 cells never showed responses (n = 0 / ~2500).

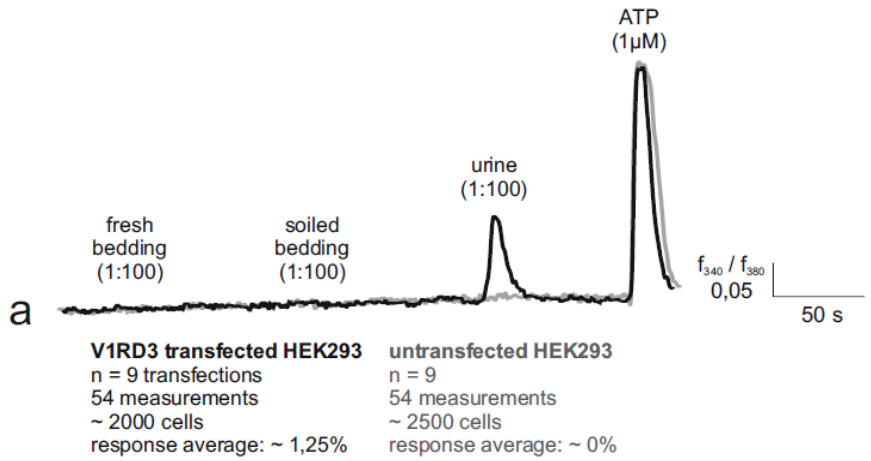


Fig. 3.13 a: Investigation of activity-dependent cytosolic Ca^{2+} variation in V1RD3-transfected HEK293 cells loaded with fura-2/AM. Cells were stimulated with fresh bedding extracts, soiled bedding extracts and male urine. Stimuli were applied for 10 s. The integrated fluorescence ratio (f_{340}/f_{380}) in a user-defined ROI was viewed as a function of time. ATP served as a positive control for cell viability.

Next, we searched for individual substances present in urine of male mice that could function as V1RD3 agonists. Data mining revealed 13 different urinary constituents that were commercially available (Table. 3.1). Until now, a cognate vomeronasal receptor was only identified for one of these compounds (2-heptanone / V1RB2, Boschat *et al.,* 2002). The substances were divided into three different mixtures (classified as A, B, and C). The activity of each mixture was assessed in Ca^{2+}-imaging experiments in V1RD3 transfected HEK293 cells (Fig. 3.13 b). Individual stimulus concentrations within mixtures were adjusted to 160 µM.

A	4-ethylphenol	→	Achiraman *et al.*, 2002
	2,4-ditert-butylphenol	→	Yamamoto *et al.*, 1991
	3-amino -1,2,4-triazole	→	Archer *et al.*, 1984
	geranylacetone		
B	2-butyl-1-octanol	→	Cavaggioni *et al.*, 2006
	2,5-dimethylpyrazine	→	Novotny *et al.*, 1986; Leinders-Zufall *et al.*, 2000
	2-heptanone	V1RB2 →	Leinders-Zufall *et al.*, 2000; Boschat *et al.*, 2002
	3-cyclohexene -1-methanol	→	Achiraman et al., 2002
C	3-methyl-2-buten-1-ol	→	Röck *et al.*, 2006
	p-xylol	→	Tsujimoto *et al.*, 1998
	3-penten-2-one	→	Röck *et al.*, 2006
	3-methyl-cyclopentanone	→	Röck *et al.*, 2006
	1-iodoundecane	→	Achiraman *et al.*, 2002

Table 3.1: Table of commercially available urinary compounds. These 13 different compounds are described as constituents of male mouse urine. We classified the substances into three different mixtures (A, B, C).

From a total of ~1500 cells investigated in 53 independent experiments (10 transfections), 15 cells (1%) responded to mixture A, 3 cells (0.2%) responded to mixture B and 2 cells (0.13%) responded to mixture C (Fig. 3.13). The results indicate that one of the four constituents of mixture A (4-ethylphenol, 2,4-ditert-butylphenol, 3-amino-1,2,4-triazole, geranylacetone) could be a ligand for V1RD3. Untransfected cells never elicited a response to mixture A.

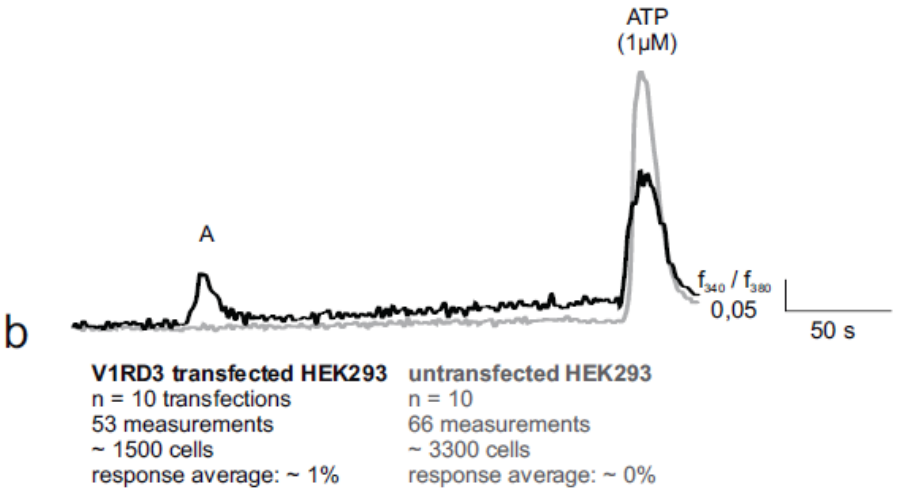


Fig. 3.13 b: Investigation of activity-dependent Ca^{2+} variation in V1RD3-transfected HEK293 cells loaded with fura-2/AM and stimulated with mixture A. The integrated fluorescence ratio (f_{340}/f_{380}) in a user-defined ROI was viewed as a function of time. Stimuli were applied for 10 s. ATP served as positive control. Untransfected HEK293 cells showed no responses.

Next, we tested individual mixture A substances for their potential agonistic properties when applied to V1RD3 transfected HEK293 cells. Our results showed that 4-ethylphenol exclusively elicited Ca^{2+} transients in 37 out of ~3000 cells corresponding to a response average of ~1.2% (Fig. 3.13 c). 2,4-ditert-butylphenol, 3-amino-1,2,4-triazole, and geranylacetone were inactive. Untransfected HEK293 cells showed no responses.

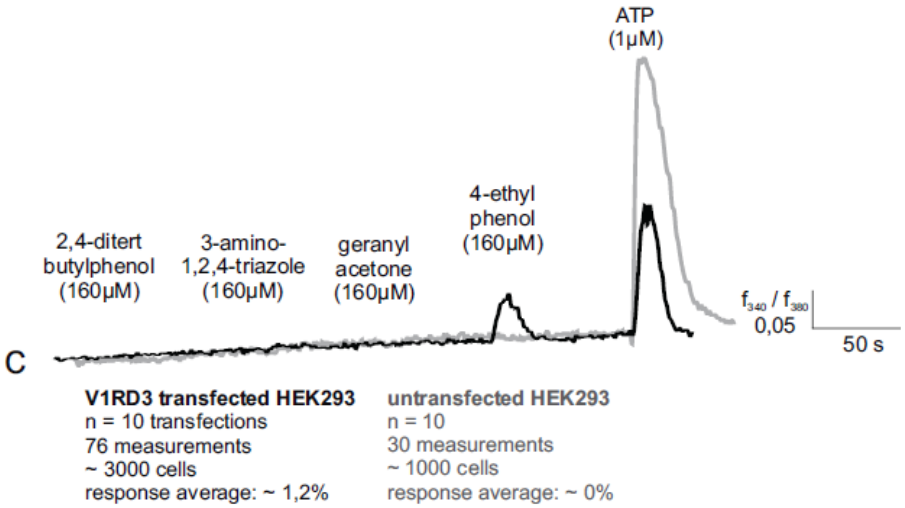


Fig. 3.13 c: Investigation of activity-dependent Ca^{2+} variation in V1RD3-transfected HEK293 cells loaded with fura-2/AM and stimulated with 2,4-ditertbutylphenol, 3-amino1,2,4-triazole, geranylacetone, 4-ethylphenol. The integrated fluorescence ratio (f_{340}/f_{380}) in a user-defined ROI was viewed as a function of time. Stimuli were applied for 10 s. ATP served as positive control. Untransfected HEK293 cells showed no responses.

Next, we examined structural analogs to 4-ethylphenol. 3-ethylphenol and 2-ethylphenol differ in the site of the ethyl group, respectively. We applied 3-ethylphenol and 2-ethylphenol to V1RD3 transfected cells. 3-ethylphenol activated HEK293 cells with a response average of ~1% (n = 19 / ~2000) (Fig. 3.13 d). 2-ethylphenol activated V1RD3-expressing cells with a response average of ~0.8% (n = 14 / ~2000) (Fig. 3.13 e).

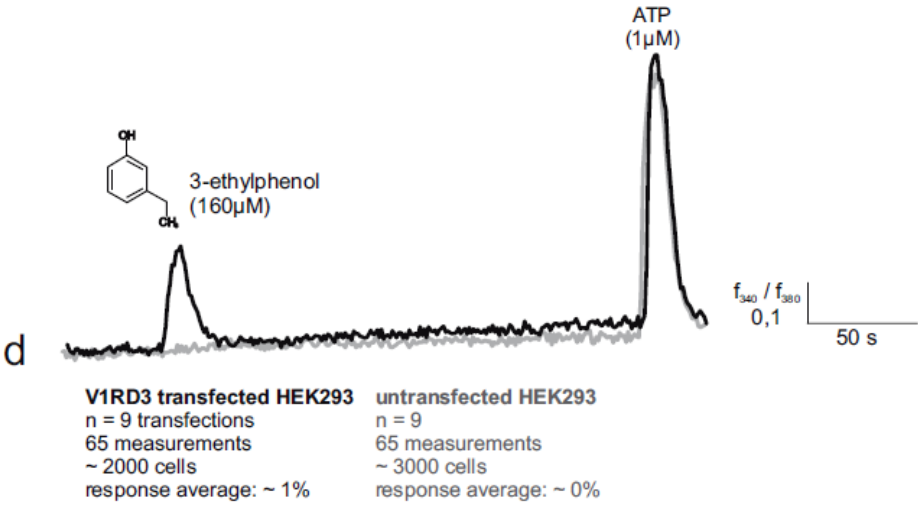


Fig. 3.13 d: Investigation of activity-dependent Ca^{2+} variation in V1RD3-transfected HEK293 cells loaded with fura-2/AM and stimulated with 3-ethylphenol. The integrated fluorescence ratio (f_{340}/f_{380}) in a user-defined ROI was viewed as a function of time. Stimuli were applied for 10 s. ATP served as positive control. Untransfected HEK293 cells showed no responses.

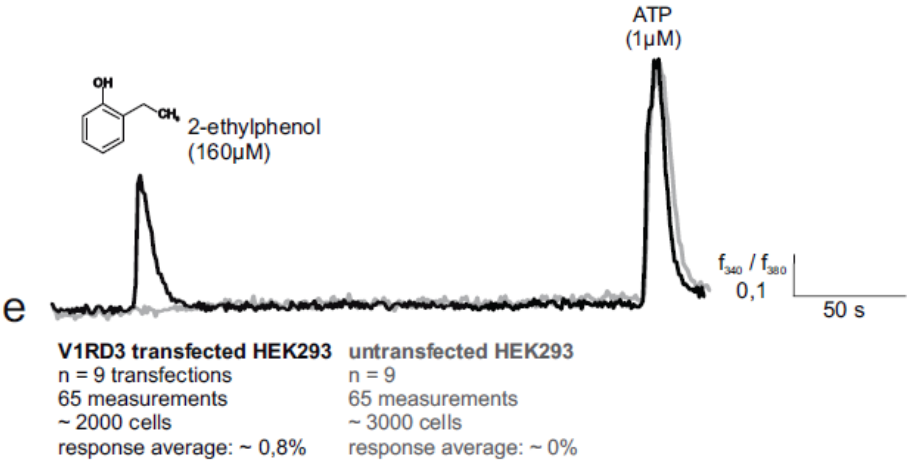


Fig. 3.13 e: Investigation of activity-dependent Ca^{2+} variation in V1RD3- transfected HEK293 cells loaded with fura-2/AM and stimulated with 2-ethylphenol. The integrated fluorescence ratio (f_{340}/f_{380}) in a user-defined ROI was viewed as a function of time. Stimuli were applied for 10 s. ATP served as positive control. Untransfected HEK293 cells showed no responses.

Subsequently, we tested substances which do not possess an alcohol group or an aromatic ring, respectively. We applied ethylbenzene and ethylcyclohexane to V1RD3 transfected cells. Our results showed that ethylbenzene and ethylcyclohexane were both able to activate V1RD3-expressing cells with identical response averages of ~1.3% (38 / ~2800), respectively (Fig.3.13 f and Fig. 3.13 g).

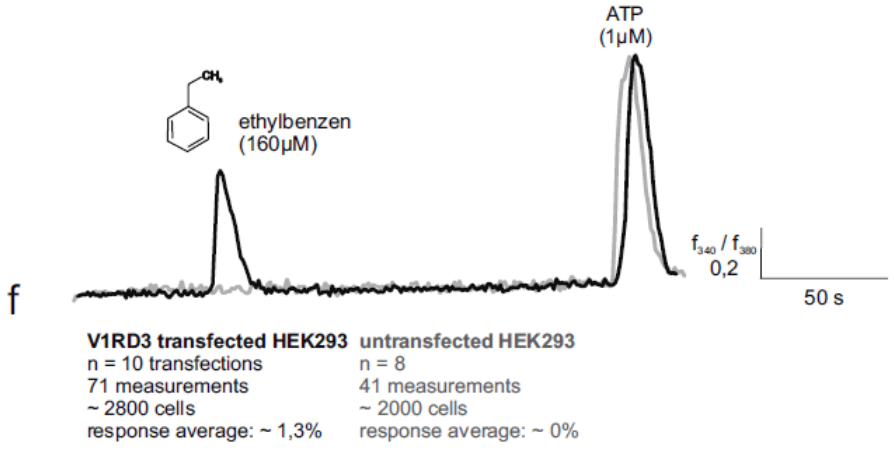


Fig. 3.13 f: Investigation of activity-dependent Ca^{2+} variation in V1RD3-transfected HEK293 cells loaded with fura-2/AM and stimulated with ethylbenzene. The integrated fluorescence ratio (f_{340}/f_{380}) in a user-defined ROI was viewed as a function of time. Stimuli were applied for 10 s. ATP served as positive control. Untransfected HEK293 cells showed no responses.

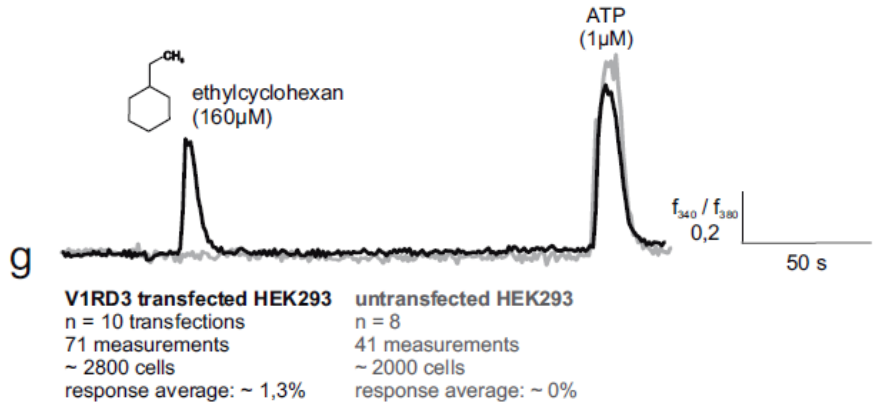


Fig. 3.13 g: Investigation of activity-dependent Ca^{2+} variation in V1RD3-transfected HEK293 cells loaded with fura-2/AM and stimulated with ethylcyclohexane. The integrated fluorescence ratios (f_{340}/f_{380}) in a user-defined ROI were viewed as a function of time. Stimuli were applied for 10 s. ATP served as positive control. Untransfected HEK293 cells showed no response.

Furthermore, we tested cis-4-ethylcyclohexanol on V1RD3-expressing cells. Cis-4-ethylcyclohexanol possesses an alcohol group but lacks an aromatic ring. From a total of ~2300 cells, 20 cells were able to respond to cis-4-ethylcyclohexanol with a response average of ~0.9% (Fig. 3.13 h).

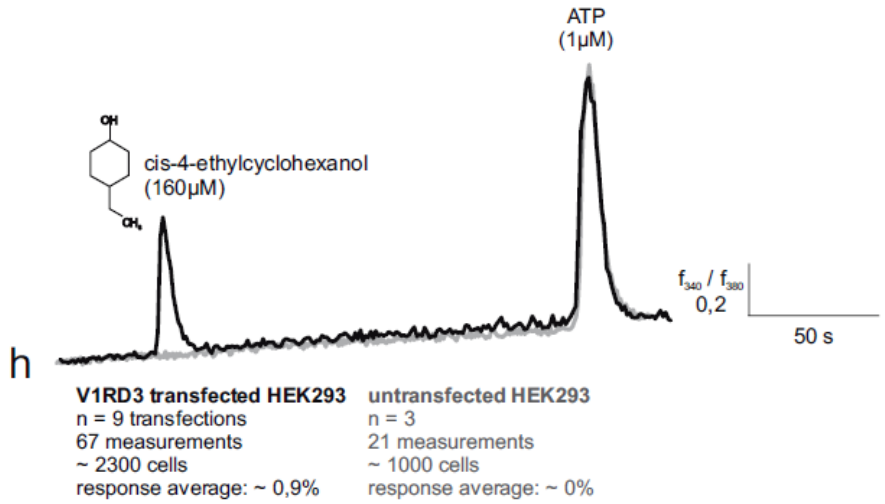


Fig. 3.13 h: Investigation of activity-dependent Ca^{2+} variation in V1RD3-transfected HEK293 cells loaded with fura-2/AM and stimulated with cis-4-ethylcyclohexanol. The integrated fluorescence ratio (f_{340}/f_{380}) in a user-defined ROI was viewed as a function of time. Stimuli were applied for 10 s. ATP served as positive control. Untransfected HEK293 cells showed no responses.

In total, we identified six different substances that elicited intracellular Ca^{2+} transients in V1RD3-expressing cells. Thus, we can describe a V1RD3-specific receptive field that includes six active and structurally similar compounds (4-ethylphenol, 3-ethylphenol, 2-ethylphenol, ethylbenzene, ethylcyclohexane and cis-4-ethylcyclohexanol). By contrast, thirteen inactive substances that show less or essentially no structural similarities were also identified. Fig. 3.14 summarizes the results obtained from heterologous expression in a schematic diagram. The substances shown in the inner circle (light grey) were able to activate V1RD3-expressing cells, whereas substances depicted in the outer circle (dark grey) remained inactive. The three substances which are not located within either circle elicited

unspecific responses in untransfected cells and have therefore not been tested in V1RD3-expressing cells.

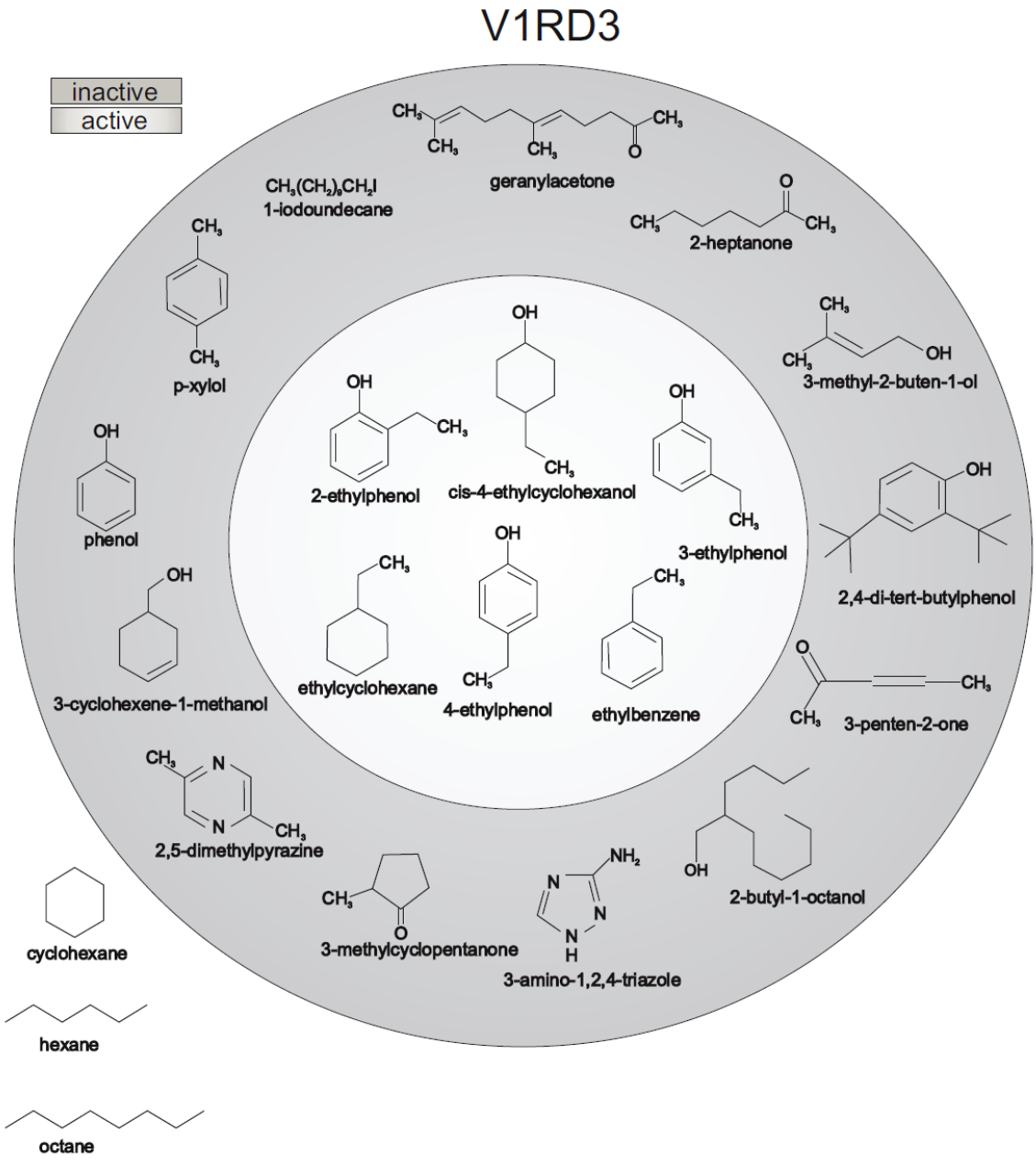


Fig. 3.14: Receptive field of V1RD3. Substances located in the inner ring activate HEK293 cells expressing V1RD3 receptor and substances located in the outer ring do not show any activation. Cyclohexane, hexane and octane generated unspecific responses in untransfected HEK293 cells.

3.2.2 4-ethylphenol evoked Ca^{2+} signals and firing of action potentials in intact VSNs

4-ethylphenol was identified as a potential ligand for V1RD3 in heterologous cells. To validate whether 4-ethylphenol is able to activate vomeronasal sensory neurons *in situ*, we used two different approaches. On the one hand, we used Ca^{2+}-imaging recordings in the VNO whole-mount preparation and, on the other hand, whole-cell patch clamp recordings in an acute VNO slice preparation (Fig. 3.15). In the whole organ preparation, we observed that

4-ethylphenol induced Ca^{2+} transients in single knobs of vomeronasal sensory neurons. VSNs responded to 4-ethylphenol with a response average of ~1.3% (n = 3 / 230). 4-ethylphenol analogs, such as 3-ethylphenol and 2-ethylphenol, induced Ca^{2+} transients in the same dendritic knobs that were activated by 4-ethylphenol (n = 4 / 350, 1.1%) (Fig.3.15). Whole-cell current clamp recordings also showed that 4-ethylphenol elicited repetitive action potential firing after 10 s application in 6 / 119 cells (5%). Fig. 3.15 shows a representative recording from a VSN that repetitively responded to 4-ethylphenol.

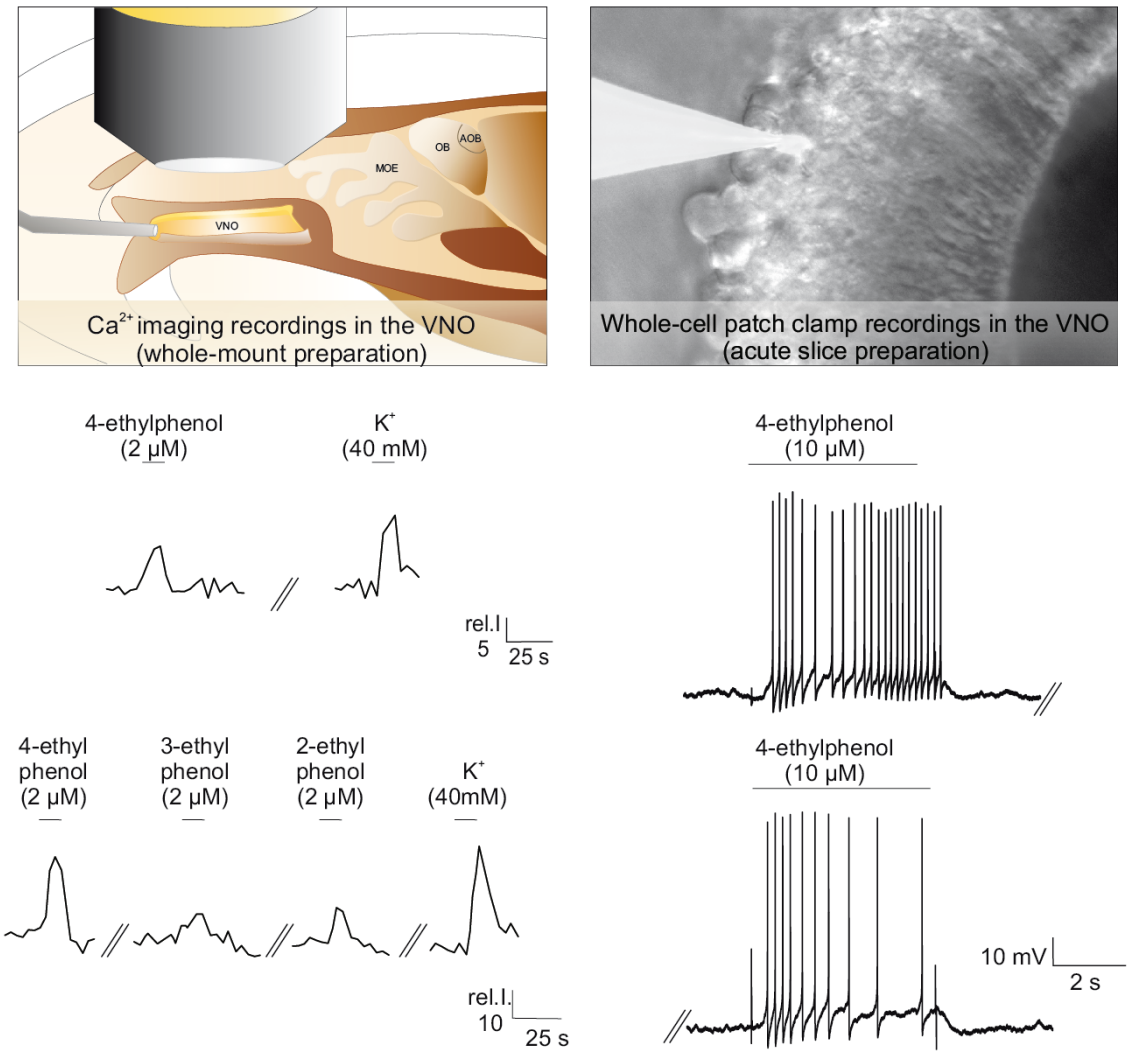


Fig. 3.15: 4-ethylphenol activates vomeronasal sensory neurons. Left side: Ca^{2+}-imaging recordings in vomeronasal dendritic knobs using the whole-mount preparation. The relative fluorescence intensities (rel.I) in user-defined ROIs were viewed as a function of time. 4-ethylphenol (2 µM) activates single knobs of VSNs with a response average about 1.3%. 4-ethylphenol, 3-ethylphenol and 2-ethylphenol are able to elicit Ca^{2+} transients in the same VSNs (n = 4 / 350, 1.1%). Right side: whole-cell current clamp recordings in one VSN. VSN is able to respond repetitively to 4-ethylphenol (10 µM) for 10 s, by firing action potentials (n = 6 / 119; 5%).

3.2.3 4-ethylphenol is actively synthesized and added to urine before secretion

In a collaborative approach, we used gas chromatography and mass spectroscopy to identify and quantify constituents of complex stimulus sources such as urine. We compared the amount of 4-ethylphenol in pooled male mouse urine (n ≥ 40 different animals; 5 independent experiments) and pooled female mouse urine (n ≥ 40 different animals; 4 independent experiments). The results showed that the amount of 4-ethylphenol in urine of male mice (136.3 µg/L) is significantly increased ($p < 0.01$; 360.6%) as compared to female mouse urine (37.8 µg/L). This indicates gender-specific synthesis of 4-ethylphenol and suggests a gender-dependent effect elicited by the secreted substance (Fig. 3.16a). Next, we investigated if 4-ethylphenol is a systemic degradation product and, thus, found in bladder urine, or if 4-ethylphenol is actively added to urine e.g. by the preputial gland. We compared secreted male urine with male urine directly extracted from the bladder. Our results show that bladder urine did not contain significant amounts of 4-ethylphenol, indicating that 4-ethylphenol is not a systemic degradation product. 4-ethylphenol, however, could be actively synthesized and added to urine by glands. As shown by chemical screening, the preputial glands appear not to play a role in 4-ethylphenol secretion (Fig. 3.16 b). On-going analyses of male-specific gland homogenates, e.g. from the seminal vesicles, the coagulation gland and the prostate, aim to reveal the source of 4-ethylphenol in the body. Furthermore, we started pilot behavioral assays to describe the role of 4-ethylphenol in social communication of mice.

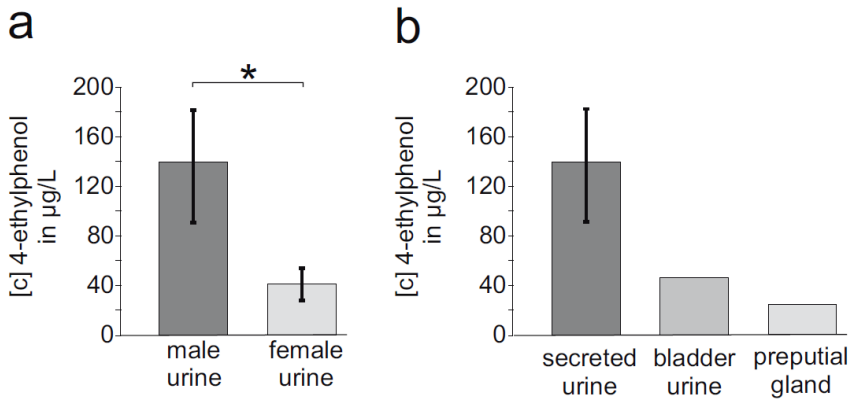


Fig. 3.16: 4-ethylphenol is secreted to urine. a) The amount of 4-ethylphenol in pooled urine of male mice (n = 5 experiments) was significantly increased ($p < 0.01$; 360.6%) compared to pooled urine of female mice (n = 4 experiments). b) Comparison of the amount of 4-ethylphenol in male mice bladder urine and preputial glands. 4-ethylphenol is neither a degradation product of the body nor it is secreted by preputial glands. Mean values are indicated +/- s.e.m.

3.3 The role of mitochondrial Ca^{2+} in mouse olfactory sensory neurons

Ionized Calcium is an important messenger in OSN signal transduction. Upon odor binding, Ca^{2+} enters the cilia of OSNs via cyclic nucleotide-gated channel opening. Subsequent signaling pathways trigger a secondary increase of intracellular Ca^{2+} in the soma (Leinders-Zufall and Zufall, 1995; Zufall *et al*., 2000). In many cells, resting cytosolic Ca^{2+} levels are re-established via both rapid compartmentalization by the endoplasmic reticulum and / or mitochondria and Ca^{2+} removal by plasma membrane Ca^{2+} ATPases (PMCA) and Ca^{2+} exchangers. Here, we investigated the function of mitochondria during OSN activity in the main olfactory epithelium. Using bioluminescence imaging in MOE tissue slices from dedicated transgenic mice, we established a novel imaging approach to record Ca^{2+} signals in OSN mitochondria at high temporal resolution. Transgenic *PhotoTopo*® mice stably express the Ca^{2+}-sensitive photoprotein *photina*® targeted to the inner mitochondrial membrane. Ca^{2+} ions entering mitochondria via mitochondrial Ca^{2+} channels (MiCa) activate the photoprotein. This activation induces a conformational change of the photoprotein and leads to the generation of bioluminescence (Fig. 3.17).

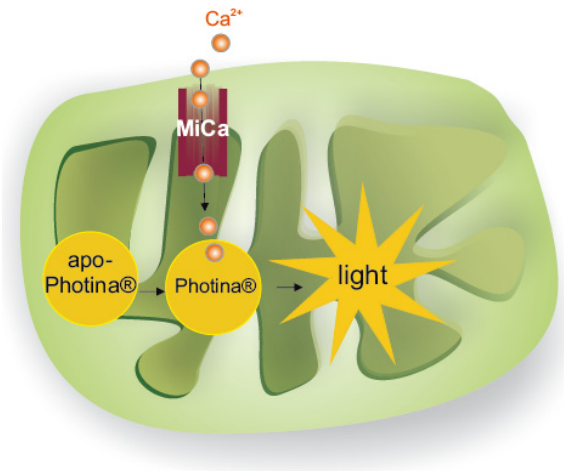


Fig. 3.17: Schematic diagram of a mitochondrion of *PhotoTopo* ® mice labeled with *photina*® protein at the inner site of the mitochondrial membrane. Ca^{2+} influx into mitochondrion via Ca^{2+} channels (MiCa) leads to an activation of the apo-photoprotein *photina*® and to the generation of bioluminescence.

Three independent approaches were used in parallel to target OSN Ca^{2+} signaling from different but complementary experimental angles: a) we measured cytosolic Ca^{2+} signals in dissociated olfactory sensory neurons at high temporal resolution b) we measured cytosolic Ca^{2+} signals in individual OSNs in intact MOE slices using confocal Ca^{2+}-imaging at high spatial resolution and c) we established monitoring of mitochondrial Ca^{2+} in MOE slices using bioluminescence imaging at high temporal resolution. To investigate odor-dependent Ca^{2+} responses, we stimulated OSNs with an odor mixture of 103 different odor molecules (1:10,000 dilution, ~50 µM each). Application of 40 mM K^+ Ringer's solution, resultant membrane depolarization and opening of voltage-dependent Ca^{2+} channels served as a positive control for neuronal viability. We investigated odor-dependent Ca^{2+} responses in both mitochondrial and cytosolic compartments. We used a variety of pharmacological tools

to modify the activity of different signaling enzymes and ion channels (Fig. 3.18). Fig. 3.18 shows a schematic drawing of an OSN (not drawn to scale). Depicted are the nucleus, endoplasmic reticulum, cytoplasm, mitochondrion and all enzymes, receptors, and ion channels we targeted in different experiments. We used *MDL12, 330A,* an adenylate cyclase inhibitor, to disrupt olfactory signal transduction in canonical OSNs. We removed extracellular Ca^{2+} (*0 Ca^{2+}*) to differentiate Ca^{2+} release from internal stores and extracellular Ca^{2+} influx. *Thapsigargin* raises cytosolic Ca^{2+} concentrations by blocking the SERCA pumps at the ER, which causes the gradual depletion of Ca^{2+} stored in the ER. To directly affect mitochondrial activity, we used three different drugs. *FCCP* is a protonophore that destroys the electrochemical gradient across the inner mitochondrial membrane. This leads to indirect inhibition of MiCa, resulting in the disruption of Ca^{2+} influx into mitochondria. *CGP37157* is a selective inhibitor of the mitochondrial Na^{+}/Ca^{2+} exchanger, causing an accumulation of Ca^{2+} ions in mitochondria. *Oligomycin* inhibits the ATP synthase, thus preventing ATP degradation in the absence of a proton gradient.

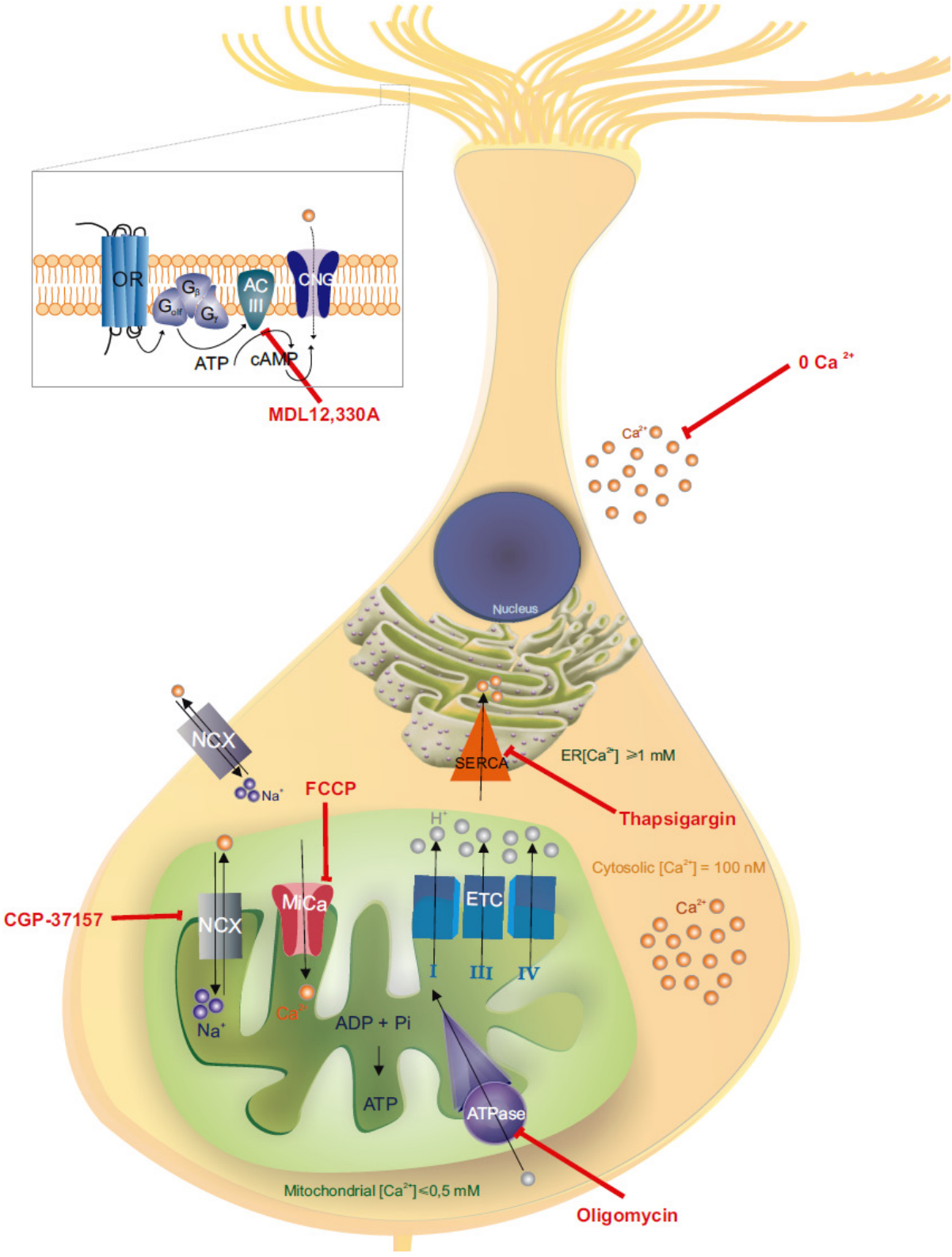


Fig. 3.18: Pharmacological tools to investigate the role of Ca^{2+} in OSNs Schematic diagram of an OSN depicting its nucleus, endoplasmic reticulum (ER), cytoplasm and mitochondria (not drawn to scale). The drugs (red) affect different enzymes, receptors and ion channels of the cell. MDL12, 330A inhibits the adenylate cyclase III of the olfactory signal transduction cascade. We removed extracellular Ca^{2+} (0 Ca^{2+}) to verify if Ca^{2+} is released from internal stores or arise from extracellular sources. Thapsigargin raises cytosolic Ca^{2+} concentration by blocking the SERCA pumps, which causes the depletion of intracellular Ca^{2+} stores. FCCP is a protonophore that disrupts the Ca^{2+} influx into the mitochondria via the MiCa. CGP37157 is a selective inhibitor of the mitochondrial Na^{+}/Ca^{2+} exchanger. Oligomycin inhibits the ATP synthase, thus preventing ATP degradation in the absence of a proton gradient.

3.3.1 Odor responses are mediated by canonical OSNs

We measured Ca^{2+} transients elicited in OSNs by odor stimulation. The relative fluorescence / bioluminescence intensities (rel.I) in user-defined ROIs were viewed as a function of time. First, acutely dissociated OSNs, loaded with fura-2/AM, were stimulated with an odor mixture eliciting cytosolic Ca^{2+} transients in 28.14% of K^+-responsive cells (n = 148 / 526). Next, we performed confocal cytosolic Ca^{2+}-imaging in individual fluo-4/AM-loaded OSNs in acute MOE slices. OSNs stimulation with an odor mixture elicited cytosolic Ca^{2+} transients in 37.1% of K^+-responsive cells (n = 164 / 442). Furthermore, we investigated mitochondrial Ca^{2+} transients in coelenterazine-loaded MOE slices using bioluminescence imaging. Our results showed that OSNs display an odor-dependent increase in mitochondrial Ca^{2+} in 46% of K^+-responsive regions (n = 169 /536) (Fig. 3.19). To investigate if Ca^{2+} influx into mitochondria and cytoplasm is mediated by canonical OSNs, we inhibited the adenylate cyclase III (ACIII) using MDL12,330A. The inhibition of the ACIII dramatically reduced the response index of OSNs to 6.7% in single cell cytosolic Ca^{2+}-imaging experiments (n = 20 / 298). The response average in cytosolic slice Ca^{2+}-imaging experiments decreased to 3.65% (n = 27 / 740) and to 4.1% (n = 2 / 50) in mitochondrial bioluminescence imaging (Fig. 3.19). These findings evidence that cytosolic and mitochondrial odor responses were mediated by canonical OSNs.

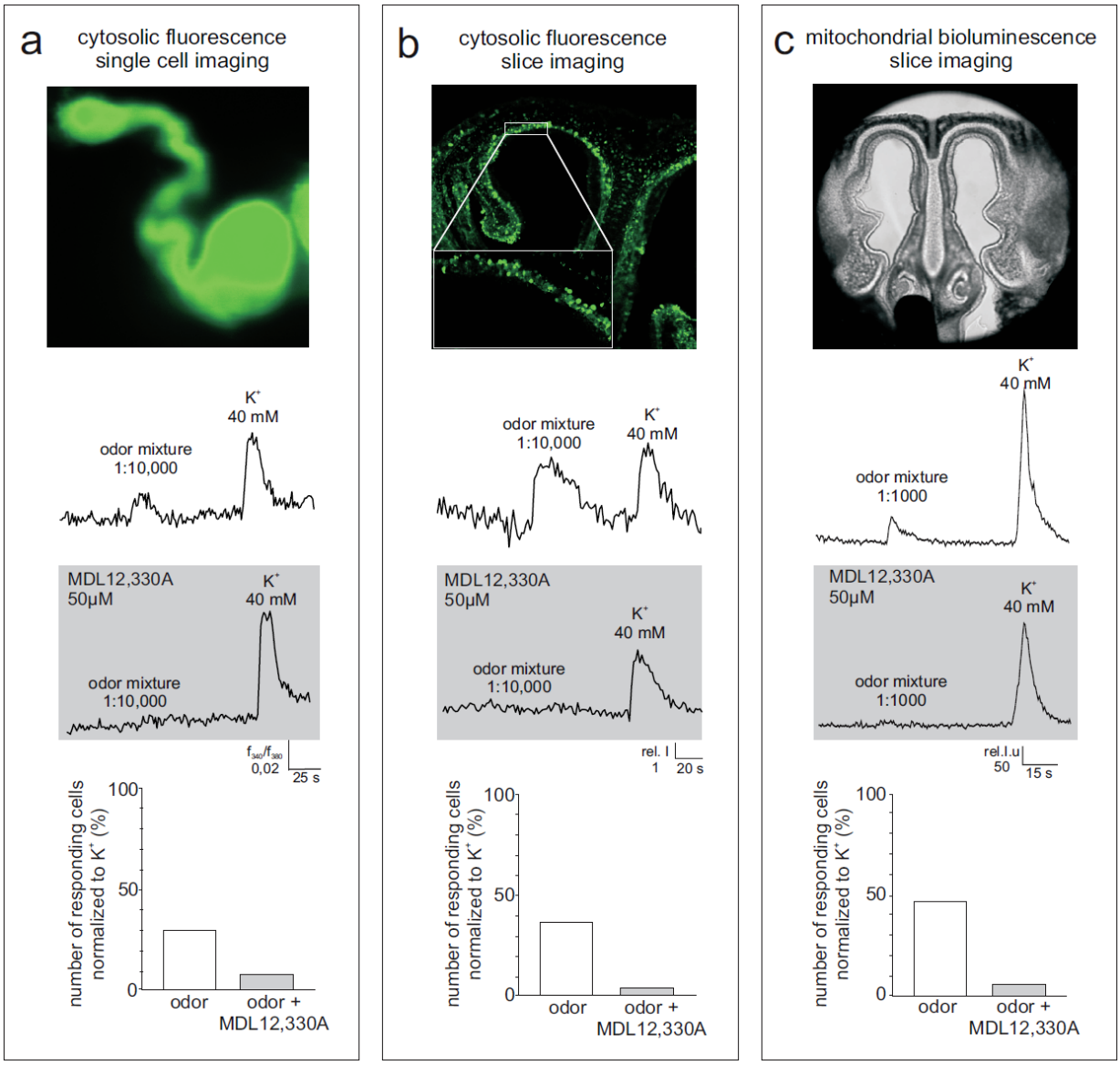


Fig. 3.19: Investigation of activity-dependent Ca^{2+} dynamics in OSN cytoplasm and mitochondria. OSNs were stimulated with odors under control condition *versus* ACIII inhibition (MDL12,330A). a) Cytosolic fluorescence single cell imaging. Top: Fluorescence image of a representative fura-2/AM-loaded dissociated OSN. Middle: Representative original recording of cytosolic Ca^{2+} signals in response to odors (1:10,000) and elevated K^+ (40 mM). The integrated fluorescence ratio (f_{340}/f_{380}) in a user-defined ROI is viewed as a function of time. Middle grey: Representative original recording of cytosolic Ca^{2+} signals under ACIII inhibition, showing odor responses are blocked. Bottom: Bar diagram showing the number of responding cells under control conditions *versus* ACIII inhibition. b) Cytosolic fluorescence MOE slice imaging. Top: Fluorescence image of an acute MOE slice loaded with fluo-4/AM. Middle: Representative original recording of cytosolic Ca^{2+} signals in response to odors (1:10,000) and elevated K^+ (40 mM). The relative fluorescence intensity (rel.I) in a user-defined ROI is viewed as a function of time. Middle grey: Representative original recording of cytosolic Ca^{2+} signals under ACIII inhibition, showing odor responses are blocked. Bottom: Bar diagram showing the number of responding cells comparing control conditions with ACIII inhibition. c) Mitochondrial bioluminescence slice imaging. Top: Brightfield image of an acute MOE slice of *PhotoTopo*® mice loaded with the substrate coelenterazine. Middle: Representative original recording of mitochondrial Ca^{2+} signals in response to odors (1:10,000) and elevated K^+ (40 mM). The relative bioluminescence intensities (rel.I.u) in a user-defined ROI were viewed as a function of time. Middle grey: Representative original recording of mitochondrial Ca^{2+} signals under ACIII inhibition, showing odor responses are blocked in mitochondria. Bottom: Bar diagram showing the number of responding regions comparing control conditions with ACIII inhibition. Stimuli were applied for 10s.

3.3.2 Odor responses depend on extracellular Ca^{2+}

Next, we removed extracellular Ca^{2+} to evaluate whether the observed secondary Ca^{2+} signals depend on extracellular sources or release from internal stores. Fig. 3.20 shows representative original recordings of cytosolic (Fig. 3.20 ab) and mitochondrial Ca^{2+} signals (Fig. 3.20 c) under control conditions and in Ca^{2+} free solution. Odor responses are abolished in Ca^{2+} free medium. We recorded odor responses in 1.4% (n = 3 / 212) of OSNs in single cell Ca^{2+}-imaging (Fig. 3.19 a) when extracellular Ca^{2+} was removed. In cytosolic slice Ca^{2+}-imaging, 0.4% (n = 2 /460) of OSNs responded to odors when extracellular Ca^{2+} was removed (Fig. 3.19b). Accordingly, 5.2% (n = 4 / 77) of OSNs responded to odors in Ca^{2+} free media in mitochondrial Ca^{2+}-imaging experiments (Fig. 3.19c). Upon addition of Ca^{2+}, odor responses recovered and stimulation induced robust Ca^{2+} signals in both cytosolic and mitochondrial Ca^{2+} imaging experiments. The results show that odor-mediated Ca^{2+} accumulation in both the cytoplasm and mitochondria is dependent on extracellular sources.

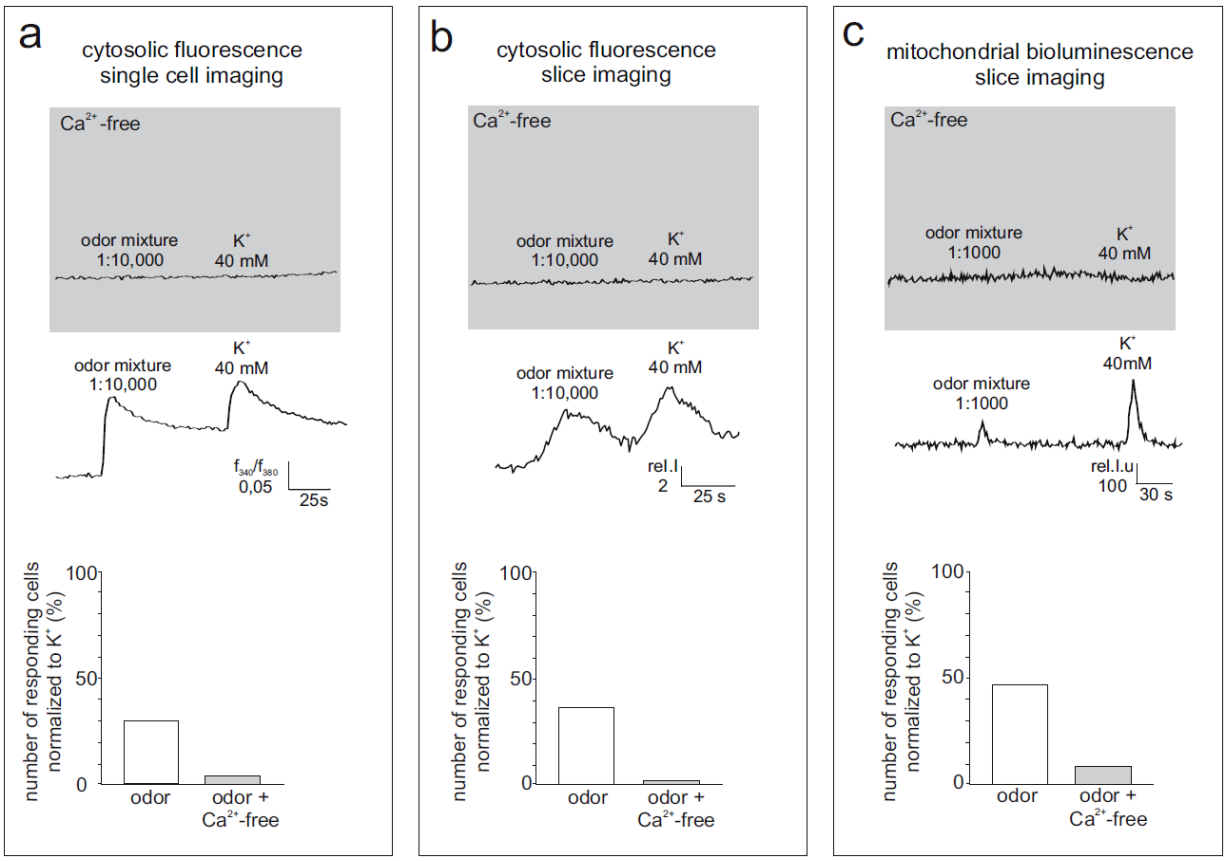


Fig. 3.20: Investigation of activity-dependent Ca^{2+} dynamics in OSN cytoplasm and mitochondria. OSNs were stimulated with a complex odor mixture under control condition *versus* Ca^{2+} free medium. Representative original recordings correspond to one cell. a) Cytosolic fluorescence single cell imaging. The integrated fluorescence ratios (f_{340}/f_{380}) in user-defined ROIs were viewed as a function of time. Grey: Representative original recording of cytosolic Ca^{2+} signals in Ca^{2+} free medium, showing odor responses are blocked. Middle: Upon addition of Ca^{2+}, odor and K^+ responses recovered. Bottom: Bar diagram showing the number of responding cells under control conditions (28.14%) *versus* Ca^{2+} free conditions (1.4%). b) Cytosolic fluorescence slice imaging. The relative fluorescence intensities (rel.I) in user-defined ROIs were viewed as a function of time. Grey: Representative original recording of cytosolic Ca^{2+} signals in Ca^{2+} free medium, showing odor responses are blocked. Middle: Upon addition of Ca^{2+}, odor and K^+ responses recovered. Bottom: Bar diagram showing the number of responding cells comparing control conditions (37.1%) *versus* Ca^{2+} free conditions (0.4%). c) Mitochondrial bioluminescence slice imaging. The relative bioluminescence intensities (rel.I.u) in user-defined ROIs were viewed as a function of

time. Grey: Representative original recording of mitochondrial Ca^{2+} signals in Ca^{2+} free medium, showing odor responses are blocked in mitochondria. Middle: Upon addition of Ca^{2+}, odor and K^+ responses recovered. Bottom: Bar diagram showing the number of responding regions comparing control conditions (46%) *versus* Ca^{2+} free conditions (5.2%). Stimuli were applied for 10s.

3.3.3 Inhibition of SERCA prolongs odor response duration

To characterize the effect of Ca^{2+} sequestration in the ER on cytosolic Ca^{2+} levels, we irreversibly inhibited SERCA pumps to block ER Ca^{2+} sequestration using 10 µM thapsigargin. We investigated odor-mediated Ca^{2+} responses in OSNs under control condition *versus* thapsigargin treatment. 34.8% (n = 49 / 141) and 20% (n = 35 / 218) of K^+-responsive cells responded to odors after thapsigargin treatment in cytosolic single cell and cytosolic slice Ca^{2+}-imaging experiments, respectively. Here, we analyzed the half-maximal width of odor responses. The half-width describes the odor response duration and, thus, serves as a quantitative description of odor response kinetics. Under control conditions, the half-width was 14.9 s and 18.4 s in cytosolic single cell and cytosolic slice Ca^{2+}-imaging, respectively. Inhibition of SERCA pumps led to depletion of Ca^{2+} from internal stores and significantly prolonged the half-width of odor responses to 21.9 s ($p = 0.02$) and 33.4 s ($p < 0.0001$), respectively (Fig. 3.21). These results show that SERCA pumps are involved in cytosolic Ca^{2+} buffering during odor-mediated activation of OSNs.

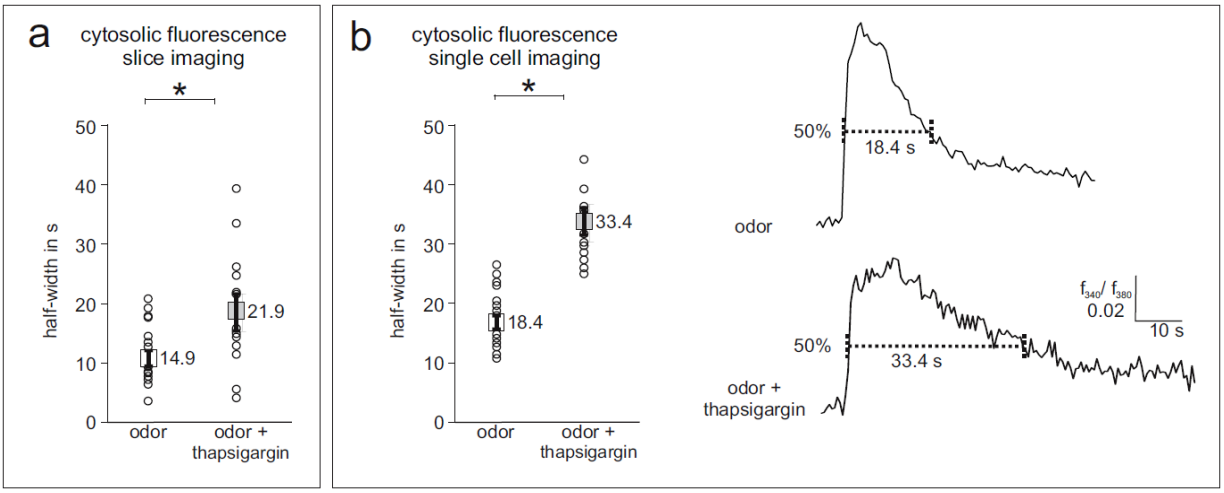


Fig. 3.21: Investigation of odor-dependent cytoplasmic Ca^{2+} dynamics when ER Ca^{2+} sequestration is inhibited by thapsigargin (10 µM), an inhibitor for SERCA pumps. We investigated the half-width of odor-mediated Ca^{2+} responses in OSNs. a) Investigation of the half-width in cytosolic slice imaging showed a significant prolongation of odor response duration from 14.9 s to 21.9 s ($p = 0.02$) b) Left: Investigation of the half-width of cytosolic single cell Ca^{2+} responses showed a significant prolongation of odor response duration from 18.4 s to 33.4 s ($p < 0.0001$) Right: Representative original traces of odor responses under control *versus* thapsigargin conditions. The integrated fluorescence ratios (f_{340}/f_{380}) in user-defined ROIs were viewed as a function of time. Mean values are indicated +/- s.e.m.

3.3.4 Inhibition of mitochondrial NCX prolongs odor response duration

Does mitochondrial Ca^{2+} release influence the characteristics of cytosolic Ca^{2+} transients? We used 10 µM CGP-37157 as a potent and specific inhibitor for the mitochondrial NCX. Our results show that inhibition of mitochondrial NCX induced a significant prolongation of odor response duration in mitochondrial Ca^{2+}-imaging from 6.4 s to 10.2 s ($p < 0.002$, $n = 40$) (Fig. 3.22 a). These data validate the inhibitory function of the drug. Next, we tested the effect of NCX inhibition in cytosolic single cell Ca^{2+}-imaging experiments. We observed that cytosolic odor response duration was significantly prolonged from 18.4 s to 25.5 s ($p = 0.02$, $n = 51$) (Fig. 3.22 b). When Ca^{2+} release from mitochondria is inhibited, Ca^{2+} influx into mitochondria is impeded due to absence of a concentration gradient. Thus, Ca^{2+} that accumulates in the cytoplasm during odor stimulation remains in the cytoplasm for a longer time period. Our data, therefore, show that inhibition of mitochondrial Ca^{2+} release changes odor-dependent cytosolic Ca^{2+} transients in OSNs.

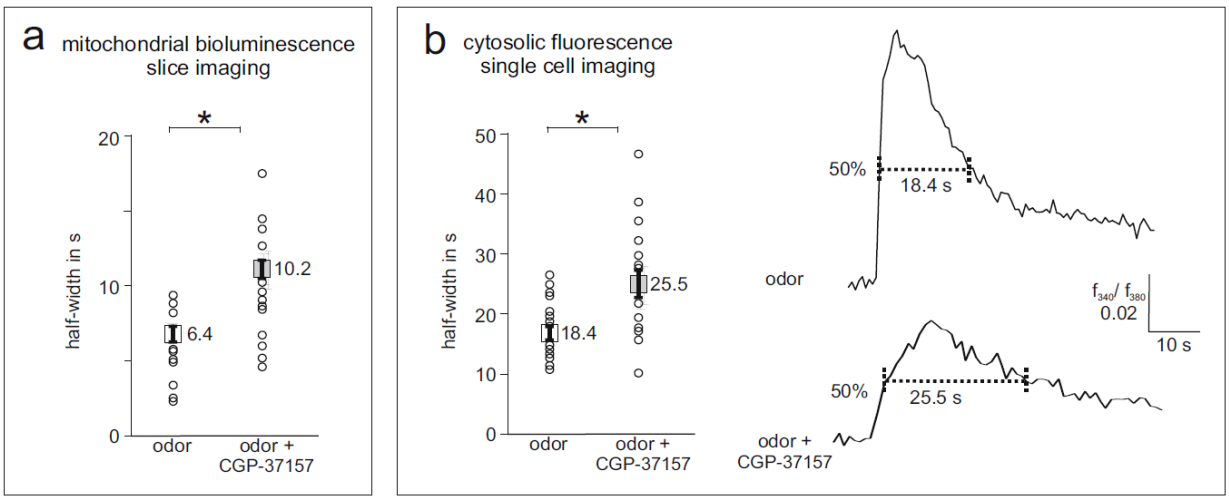


Fig. 3.22: Investigation of odor-dependent Ca^{2+} dynamics in mitochondria and cytoplasm when mitochondrial Ca^{2+} release was inhibited by 10 µM CGP-37157, an inhibitor for the mitochondrial NCX. We investigated the half-width of odor-mediated Ca^{2+} response in OSNs. a) Investigation of the half-width in mitochondrial Ca^{2+}-imaging showed a significant prolongation of odor response duration from 6.4 s to 10.2 s ($p < 0.002$) upon inhibition of mitochondrial Ca^{2+} release. b) Left: Investigation of the half-width in cytosolic single cell Ca^{2+}-imaging showed a significant prolongation of odor response duration from 18.4 s to 25.5 s ($p = 0.02$) upon inhibition of mitochondrial Ca^{2+} release. Right: Representative original traces of odor responses under control *versus* CGP-37157 conditions. The integrated fluorescence ratios (f_{340}/f_{380}) in user-defined ROIs were viewed as a function of time. Mean values are indicated +/- s.e.m.

3.3.5 Inhibition of mitochondrial Ca^{2+} sequestration extends odor response duration

Mitochondrial Ca^{2+} sequestration has profound consequences for specific characteristics of cytosolic Ca^{2+} transients. To investigate the mitochondrial role in Ca^{2+} homeostasis and odor-dependent Ca^{2+} signaling in OSNs, we searched for a substance that completely blocks mitochondrial Ca^{2+} sequestration. Chemical uncouplers (protonophores) such as 4-(trifluoromethoxyl) s-phenyl-hydrazone (FCCP) mediate a rapid and reversible disruption of the proton gradient and, therefore, strongly reduce Ca^{2+} sequestration into mitochondria. We used FCCP in combination with Oligomycin which prevents the 'reverse-mode' degradation of ATP to ADP by the ATP synthase in the absence of a proton gradient. 169 out of 536 K^+-responsive regions (46%) showed odor-dependent Ca^{2+} transients in mitochondria. When MOE slices were preincubated with 5 µM FCCP for 2 min, we never observed odor-dependent Ca^{2+} transients in OSN mitochondria. After 2 min wash out of the drug, odor responses and K^+ responses recovered (n = 22) (Fig. 3.23 a).

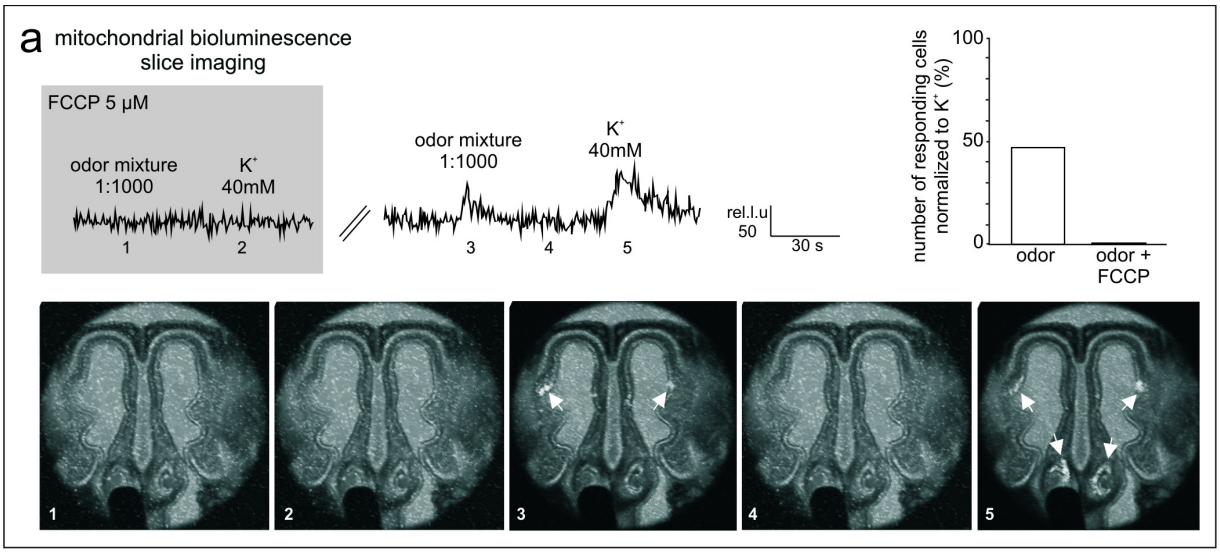


Fig. 3.23 a: Investigation of odor-dependent Ca^{2+} dynamics in mitochondria when Ca^{2+} sequestration was inhibited by 5 µM FCCP. FCCP is a protonophore that destroys the proton gradient across the inner mitochondrial membrane. FCCP blocks mitochondrial Ca^{2+} sequestration in OSNs. Representative original traces show that odor responses are completely blocked during FCCP treatment. After wash out (2 min) odor responses recovered (n = 22). The relative bioluminescence intensities (rel.I.u) in a user-defined ROI were viewed as a function of time. Under control conditions, 46% of all K^+-responsive regions responded to odors (n = 169 / 536). We never observed odor responses during FCCP treatment. Numbered images correspond to individual frames at indicated time points (1-5). Arrows illustrate mitochondrial Ca^{2+} transients in OSNs. Stimuli were applied for 10 s.

By contrast, occurrence of cytosolic Ca^{2+} transients in presence of FCCP was essentially unaltered. 33.3% (n = 53 / 159) and 14.1% (n = 22 / 151) of K^+-responsive cells responded to odors in cytosolic single cell and slice Ca^{2+}-imaging, respectively (Fig. 3.23 b, c). Investigation of the half-width of odor-mediated cytoplasmic Ca^{2+} responses showed that response duration was significantly prolonged when Ca^{2+} sequestration into mitochondria was blocked. Odor responses were prolonged from 14.9 s to 18.1 s and 18.4 s to 33.0 s in cytosolic slice and single cell Ca^{2+}-imaging, respectively (Fig. 3.23 b, c). Thus, odor-mediated cytosolic Ca^{2+} signals were significantly changed when mitochondrial Ca^{2+} sequestration was inhibited, indicating that mitochondria play a crucial role in Ca^{2+} buffering of OSNs during neuronal activity.

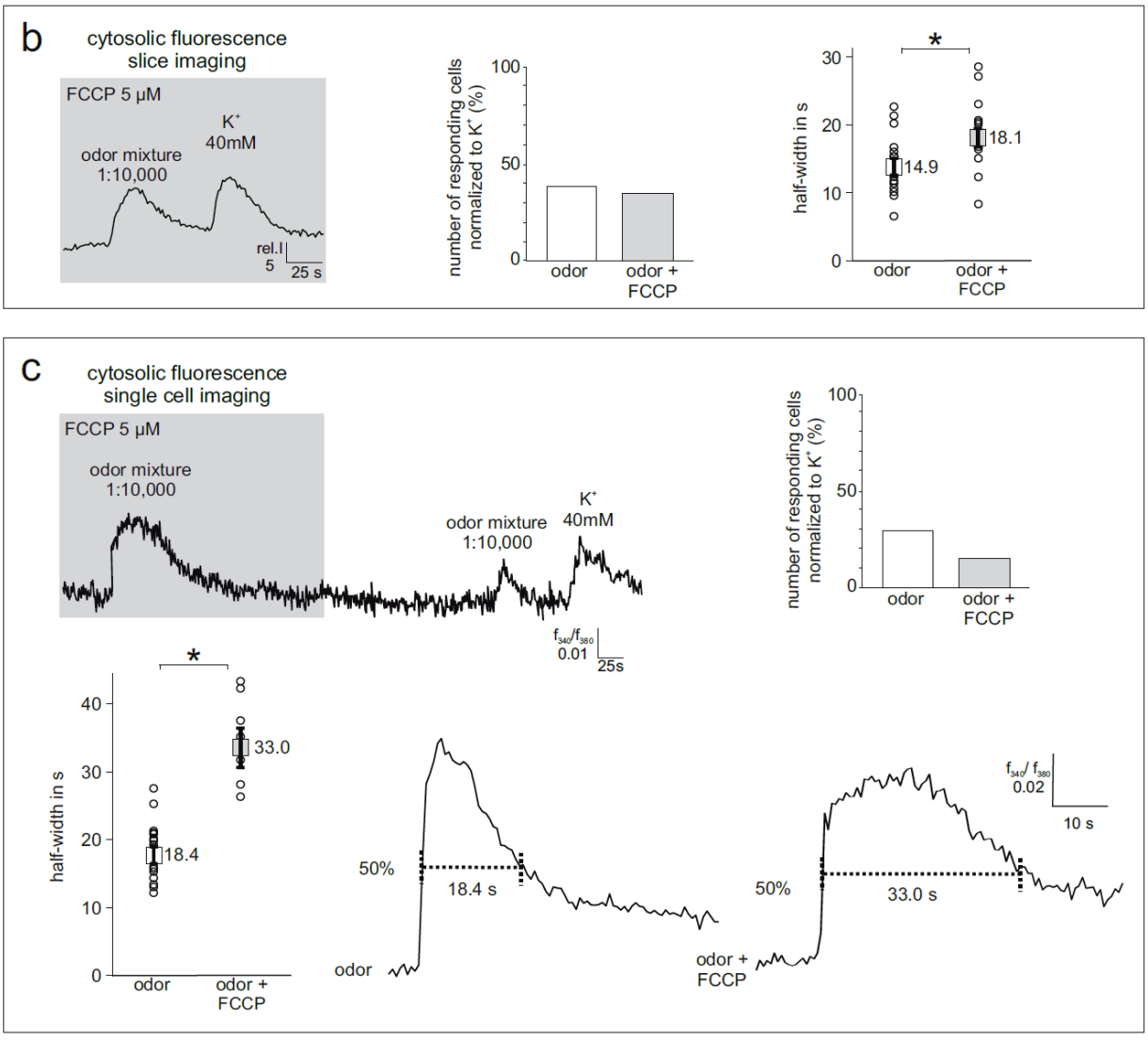


Fig. 3.23 b, c: Investigation of odor-dependent Ca^{2+} dynamics in the cytoplasm when mitochondrial Ca^{2+} sequestration was inhibited by 5 µM FCCP. b) Representative original trace showing odor and elevated K^+ responses during FCCP treatment. The relative fluorescence intensities (rel.I) in user-defined ROIs were viewed as a function of time. Middle: Diagram shows that response average does not differ between control (37%, n = 164 / 442) and FCCP (33.3%, n = 53 / 159) conditions. Right: Investigation of the half-width shows significant prolongation (from 14.9 s to 18.1 s) of odor response (p = 0.004). c) Left, top: Representative original trace showing odor responses under FCCP conditions and responses to odors and elevated K^+ after wash out (2 min). The integrated fluorescence ratios (f_{340}/f_{380}) in a user-defined ROI were viewed as a function of time. Right, top:

Bar diagram showing the response average of OSNs under control (28.14%, n = 148 / 526) *versus* FCCP (14.1%, n = 22 / 151) conditions. Left, bottom: Investigation of the half-width shows significant prolongation (from 18.4 s to 33.0 s) of odor response when mitochondrial Ca^{2+} sequestration was inhibited by FCCP ($p < 0.0001$). Right, bottom: Representative original traces showing prolongation of odor response duration under control and under FCCP conditions. Stimuli were applied for 10 s. Mean values are indicated +/- s.e.m.

3.3.6 Both ER and mitochondria function synergistically as Ca^{2+} buffer systems in OSNs

Next, we compared the half-width of odor responses in cytosolic slice Ca^{2+}-imaging under control condition and during three different pharmacological treatments. We inhibited mitochondrial Ca^{2+} sequestration using FCCP, we blocked ER Ca^{2+} sequestration by thapsigargin preincubation, and we concurrently inhibited both Ca^{2+} buffer systems, ER and mitochondria, applying FCCP and thapsigargin simultaneously. We analyzed 164 K^+-responsive cells under control conditions. 53 K^+-responsive cells were analyzed during FCCP treatment. 35 K^+-responsive cells were analyzed after thapsigargin treatment and 54 K^+-responsive cells were analyzed after simultaneous treatment with both FCCP and thapsigargin. The results show that inhibition of mitochondrial Ca^{2+} sequestration leads to a significant increase of the Ca^{2+} response half-width from 14.3 s to 18.1 s ($p = 0.03$). The inhibition of SERCA pumps also results in a significant half-width increase to 21.9 s ($p = 0.02$) (Fig. 3.24). The concurrent inhibition of both buffer systems (ER and mitochondria) induces a half-width increase to 55.2 s ($p < 0.0001$) (Fig. 3.24). Furthermore, the odor response duration of cells treated with both FCCP and thapsigargin was significantly increased compared to cells treated with either of the two inhibitors alone ($p < 0.0001$). These results demonstrate that impairment of either buffer system in OSNs significantly prolongs odor response duration. Consequently, these results indicate that, in case both storage organelles are lack functionality, resting conditions in OSNs are exclusively established by the activity of PMCAs and plasma membrane NCXs.

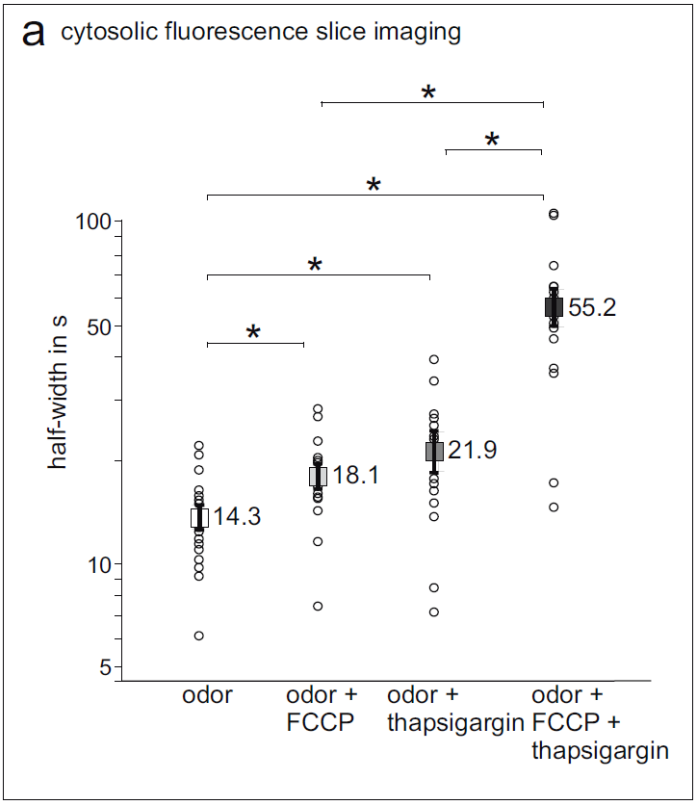


Fig. 3.24: Investigation of half-width in cytosolic fluorescence slice imaging. Logarithmic diagram illustrating odor responses under control (n = 164), FCCP (5 µM; n = 53), thapsigargin (10 µM; n = 35), and FCCP (5 µM) plus thapsigargin (10 µM) conditions (n = 54). Odor responses are significantly prolonged by FCCP, thapsigargin, and FCCP plus thapsigargin, respectively ($p = 0.03$; 0.02; < 0.0001). Odor response duration of cells treated with both FCCP and thapsigargin is significantly increased compared to control cells or cells treated with

either of the two inhibitors alone ($p < 0.0001$; < 0.0001; for odor with FCCP and odor with thapsigargin, respectively). Mean values are indicated +/- s.e.m.

3.3.7 Mitochondria modulate odor-dependent Ca^{2+} rise time

Since our findings suggest a role of mitochondria in regulation of odor-dependent cytosolic Ca^{2+} kinetics, we investigated Ca^{2+} rise times under different pharmacological conditions. Two independent analytical approaches were used. We measured a) Ca^{2+} rise times from 10% to 70% (t_{10-70}; early and rapid phase) of the odor response amplitude and b) Ca^{2+} rise times from 70% to 90% (t_{70-90}; late and rather slow phase) of the odor response amplitude. Average t_{10-70} was 3.8 s; 3.0 s and 2.1 s under control conditions, FCCP (5 µM), and thapsigargin (10 µM) treatment, respectively (Fig. 3.25). We, thus, observed a significantly increased Ca^{2+} rise time from 10% to 70% in odor responses when cells were treated with thapsigargin ($p = 0.02$). The results show that the ER is able to buffer Ca^{2+} during the early and fast response phase. Average t_{70-90} was 2.0 s; 5.5 s and 2.6 s under control, FCCP, and thapsigargin conditions, respectively, showing a significant increase of Ca^{2+} rise time when mitochondrial Ca^{2+} sequestration is inhibited ($p < 0.0001$). By contrast, inhibition of mitochondrial Ca^{2+} uptake did not affect t_{10-70}.These results indicate that mitochondrial buffer function is most relevant when local cytoplasmic Ca^{2+} concentrations are high.

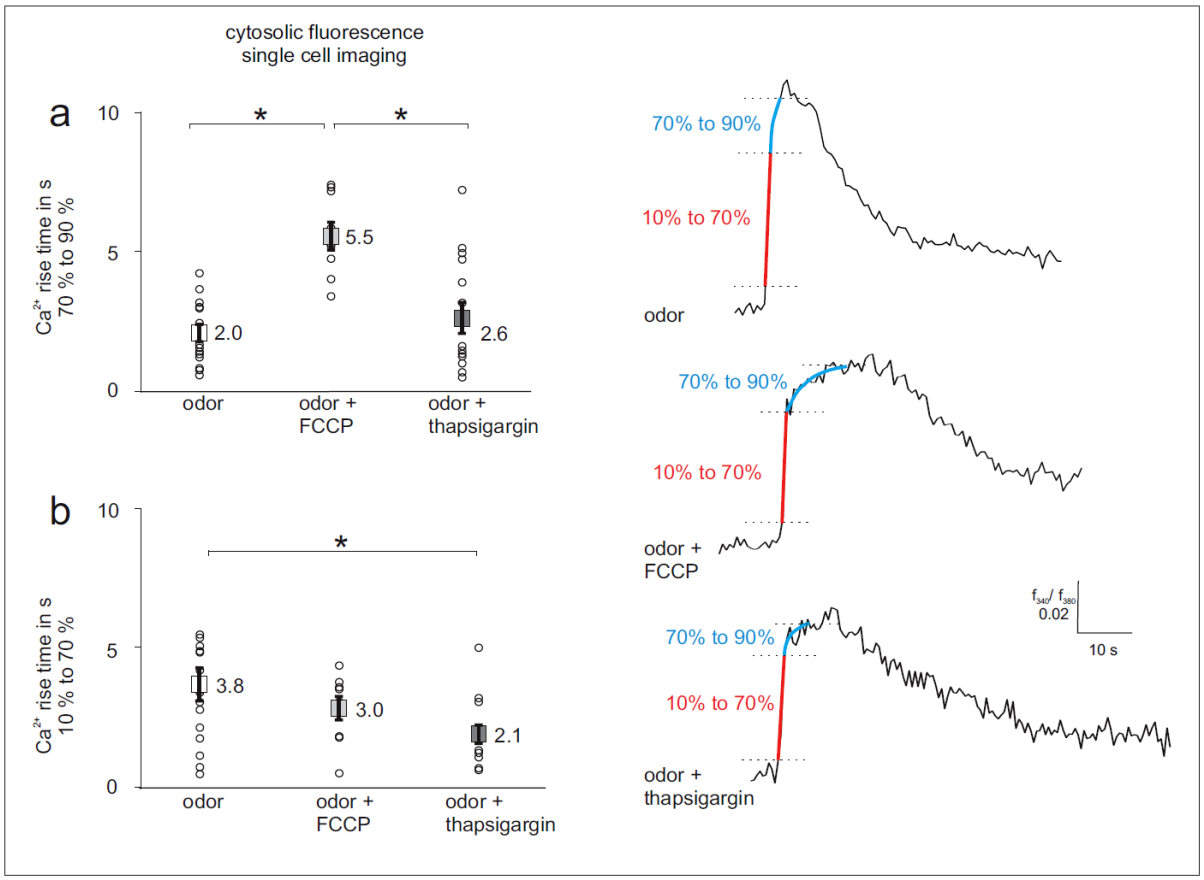


Fig. 3.25: Investigation of odor-dependent Ca^{2+} rise times in cytosolic fluorescence single cell Ca^{2+}-imaging under different pharmacological conditions. a) Ca^{2+} rise times were measured from 70% to 90% under control conditions, FCCP (5 µM), and thapsigargin (10 µM) treatment. Ca^{2+} rise time is significantly prolonged when mitochondrial Ca^{2+} sequestration is inhibited (FCCP). Results show an increase from 2.0 s to 5.5 s ($p < 0.0001$).

b) Ca^{2+} rise times were measured from 10% to 70% under different conditions. Ca^{2+} rise time is significantly reduced when ER Ca^{2+} sequestration is inhibited (thapsigargin). Results show a reduction from 3.8 s to 2.1 s (p = 0.02). Right: Representative original traces of odor responses measured under control, FCCP and thapsigargin conditions. The integrated fluorescence ratios (f_{340}/f_{380}) in user-defined ROIs were viewed as a function of time. Mean values are indicated +/- s.e.m.

3.3.8 Mitochondria modulate Ca^{2+} signaling during primary signal transduction

Our findings reveal a crucial role of mitochondria in Ca^{2+} regulation in OSN somata. Therefore, we next investigated a potential mitochondrial function in odor-mediated Ca^{2+} signals that occur within the dendritic tips, close to the site of primary signal transduction in OSNs. We investigated 25 knobs under control conditions and 30 knobs during FCCP treatment (5 µM). We observed a significant increase from 11.0 s to 22.3 s of the Ca^{2+} response half-width in FCCP treated cells (p = 0.0015). These data suggest that mitochondria are not only involved in regulation of cytosolic Ca^{2+} in somata, but also in dendritic knob endings of OSNs (Fig. 3.26), thus, potentially regulating Ca^{2+} transients that result from primary signal transduction events.

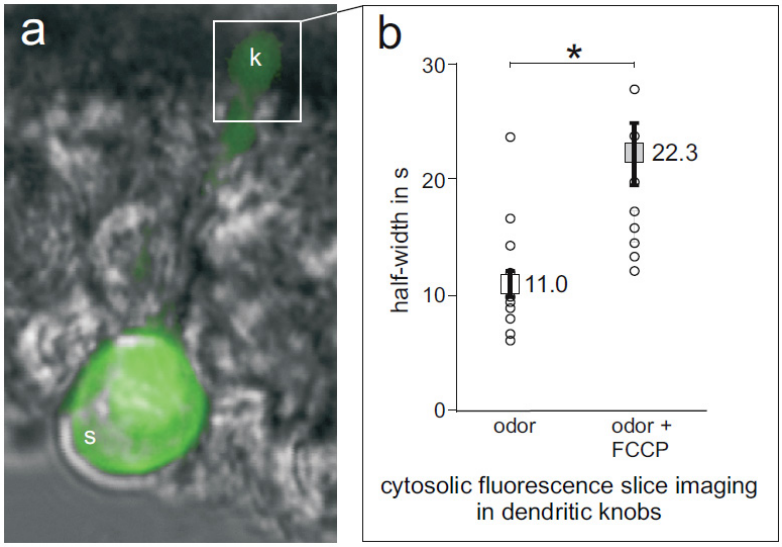


Fig. 3.26: Investigation of odor response duration in OSN dendritic knob endings under control condition *versus* FCCP treatment (5 µM). a) Merged bright field and fluorescence image of an area within the sensory epithelium of a mOR-EG mouse. OSNs which express the mOR-EG receptor coexpress GFP (green). b) Half-width of odor responses in dendritic knob endings is shown under control *versus* FCCP conditions. Half-width increased significantly in FCCP treated cells from 11.0 s to 22.3 s (p = 0.0015). k = knob, s = soma. Mean values are indicated +/- s.e.m.

3.3.9 Mitochondria show odor-dependent translocation to dendritic compartments

Next, we investigated odor-dependent mitochondrial translocation. Therefore, we loaded a) dissociated OSNs from OMP-GFP mice and b) dissociated OSNs from mOR-EG mice with a specific fluorescent mitochondrial marker (MitoTracker® Red FM) and measured relative fluorescence intensities upon odor stimulation in different parts of the neurons. Dissociated OSNs from OMP-GFP mice were stimulated with an odor mixture of 103 odors (1:10,000; ~50 µM each). OSNs of mOR-EG mice were stimulated with 100 µM vanillin, a specific ligand for the mOR-EG receptor. Relative fluorescence intensities were measured before odor application (pre-stimulus), during odor application (stimulation) and after odor application (post-stimulus) in different OSN regions. In unstimulated OSNs, mitochondria did

not show movement directionality. We investigated 5, 7 and 6 OSNs of OMP-GFP neurons in somatic and dendritic regions as well as dendritic knobs, respectively. The results show that, upon odor stimulation, the relative fluorescence intensities of mitochondrial staining significantly decrease in the soma (p = 0.015). By contrast, relative fluorescence intensity significantly increases in both dendrites (p = 0.037) and dendritic knob endings (p = 0.038) (Fig. 3.27 abc). When analyzing all cells that showed any directional mitochondrial movements, we never observed mitochondrial movement in an opposite direction in stimulated cells.

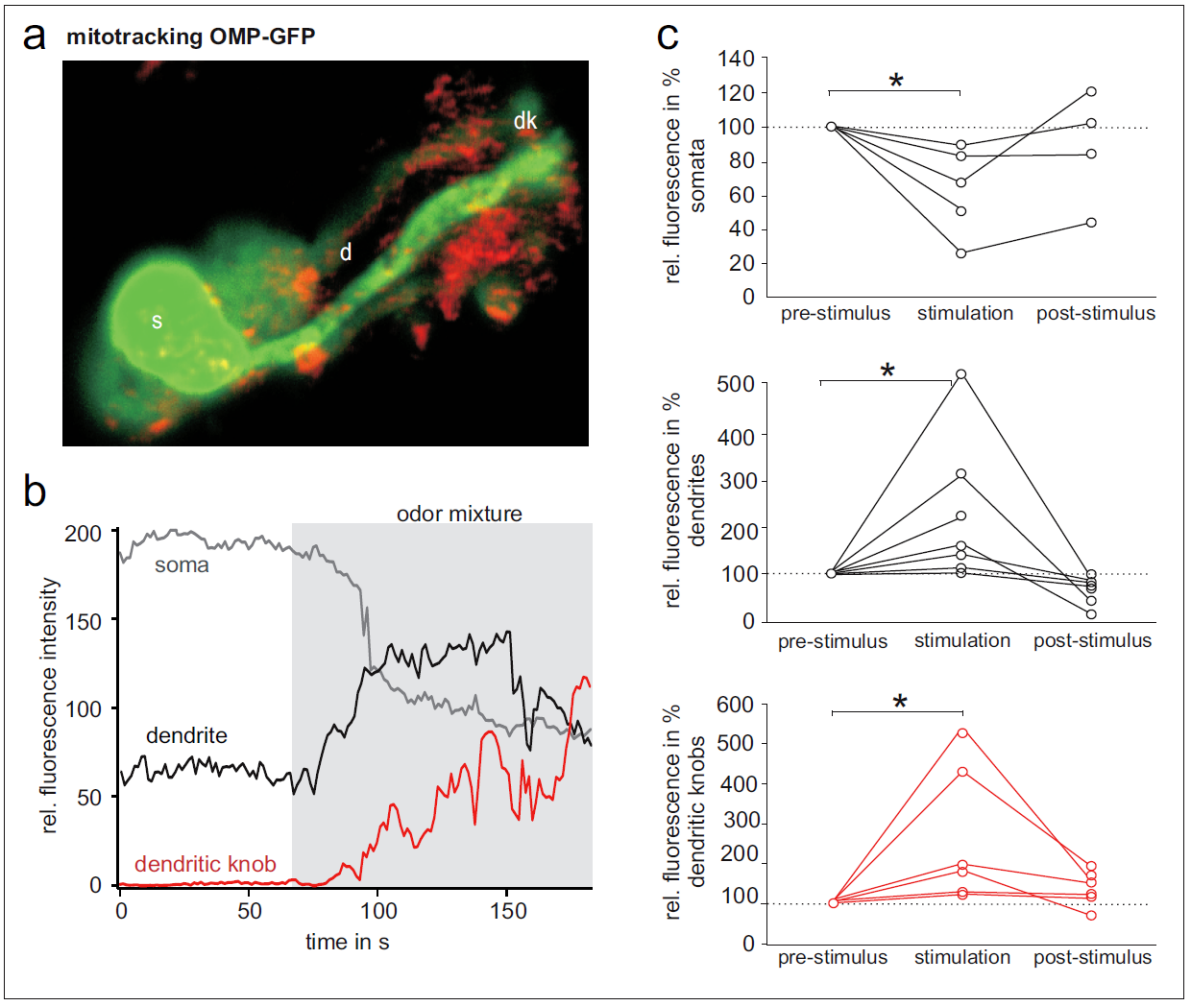


Fig. 3.27: Investigation of odor-dependent mitochondrial translocation in dissociated OSNs of OMP-GFP mice. a) Merged fluorescence image of three dissociated OSNs (green) and MitoTracker® Red FM labeled mitochondria (red). Mitochondria are redistributed all over the cell. b) Representative original trace of odor responses. The relative fluorescence intensity (rel.I) in a user-defined ROI is viewed as a function of time. Different parts of OSNs (soma, dendrite and dendritic knob) were investigated. Relative fluorescence intensities were measured before odor application (pre), during odor application (stimulus) and after odor application (post). Upon odor stimulation, relative fluorescence intensity significantly decreased in the soma and increased in the dendrite and dendritic knobs. s = soma, d = dendrite, dk = dendritic knob

Analog results were observed in dissociated OSNs from mOR-EG mice. We analyzed 4 isolated mOR-EG neurons in somatic and dendritic areas, respectively. Vanillin stimulation led to a significant decrease of relative fluorescence intensities in the soma (n = 4; p = 0.025) and a significant increase in dendrites and dendritic knob endings (n = 4; p = 0.015) (Fig. 3.28). After stimulation, relative fluorescence intensity slowly recovered to base levels, indicating that mitochondria also translocate retrogradely as activity declines. These findings demonstrate an odor-dependent translocation of mitochondria from the soma to dendrite and dendritic knob endings.

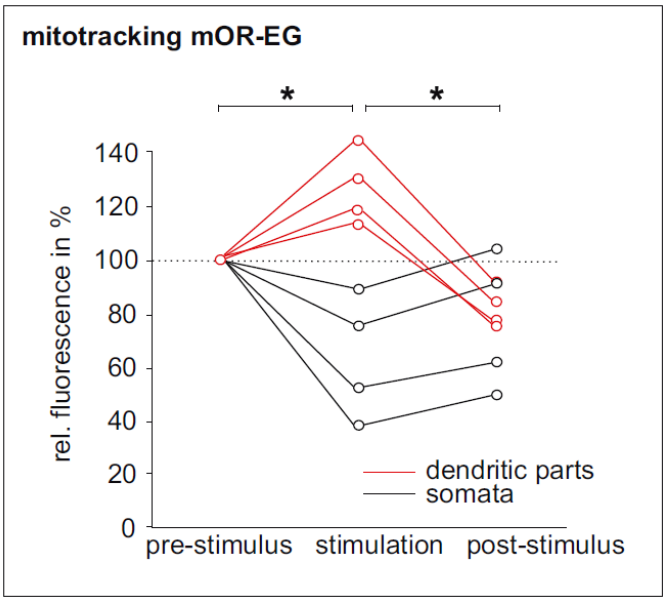


Fig. 3.28: Investigation of odor-dependent mitochondrial translocation in dissociated OSNs of mOR-EG mice. Relative fluorescence intensities were measured before vanillin application (pre), during vanillin application (stimulus) and after vanillin application (post). Upon vanillin stimulation, relative fluorescence intensities significantly decreased in the soma (p = 0.025) and significantly increased after wash-out (p = 0.026). Observation of dendrites and dendritic knobs showed that upon vanillin stimulation relative fluorescence intensities significantly increased (p = 0.015) and significantly decreased after wash-out (p = 0.0006).

4 Discussion

In most vertebrates, the olfactory system plays a critical role in discriminating thousands of different odors and regulating social and reproductive behaviors. However, many physiological mechanisms underlying olfactory sensory signaling still remain unclear. Therefore, the overall aim of my thesis was to gain a deeper understanding of sensory signaling mechanisms in the mouse olfactory system. Specifically, my research concentrated on three important aspects of olfactory signaling. Two research projects focused on the molecular and cellular basis of social communication mediated by sensory neurons in the vomeronasal organ, whereas a third project targeted the mitochondrial role during neuronal activity in olfactory sensory neurons. To address these questions, I used physiological recording methods (Ca^{2+} imaging) as well as molecular and biochemical techniques.

In a collaborative approach with colleagues from Prof. Ivan Rodriguez' laboratory at the University of Geneva, we could identify a new receptor class in the VNO, the formyl-peptide-receptor-like (FPRs) family. We identified agonists for these receptors and showed vomeronasal activation upon stimulation with those agonists by establishing a new intact *in situ* preparation of the VNO suited for *en face* confocal Ca^{2+} imaging in VSN dendritic tips.

Moreover, I identified a cognate V1R receptor-ligand pair. I functionally characterized recombinant V1RD3, which we found upregulated in VNO expression profiling assays, and showed that its ligand (4-ethylphenol) is able to activate native VSNs by evoking both dendritic Ca^{2+} transients and action potential firing. In a collaborative effort with colleagues from the Fraunhofer Institute for Process Engineering and Packaging IVV in Freising, we used gas chromatography and mass spectroscopy to quantitatively investigate 4-ethylphenol content in different mouse bodily secretions and tissues that could metabolize and secrete 4-ethylphenol.

In my third project, my experiments revealed a crucial role for mitochondria in odor-dependent OSN activation. I showed that mitochondria are critical mediators of olfactory cytosolic Ca^{2+} signaling in both OSN somata and knobs. Furthermore, mitochondria are translocated to the dendritic tips upon odor stimulation.

4.1 Formyl peptide receptor-like proteins are a novel family of vomeronasal chemosensors

We report the transcription of a novel class of chemoreceptor genes by vomeronasal sensory neurons, whose expression follows the unique transcriptional characteristics shared by the four known olfactory chemoreceptor gene families (Buck and Axel, 1991; Liberles *et al*., 2006; Dulac and Axel, 1995; Herrada and Dulac, 1997, Matsunami and Buck, 1997; Ryba and Tirindelli, 1997). Resulting from this initial finding, our data shed light on novel

vomeronasal agonists. They include fMLF, the prototypical formylated peptide from *E. coli* (Le *et al.*, 2001), Lipoxin A4, a lipid mediator generated at sites of inflammation (Takano *et al,* 1997), and CRAMP, a member of the cathelicidin family of antimicrobial peptides (Kurosaka *et al.*, 2005). These compounds are not part of a group defined by chemical composition or structure, but rather by a link to pathogens, or with inflammation, which may result from an immune response to germs. Since these FPR-rs agonists are mostly produced in tissues and serum following inflammation processes, what could be their physiological link to the olfactory system?

It turns out that these molecules are also present in bodily fluids such as urine, in which CRAMP, uPAR and SAA can be found in situations associated with various diseases (Takata *et al*., 2008; Chromek *et al*., 2006; Casella *et al.,* 2002) (a situation somehow reminiscent of the vomeronasal response to sulfated glucocorticoids, molecules whose concentrations in urine depend on the stress level of the animals (Nodari *et al*., 2008)). Although the functional role played by FPR-rs1, 3, 4, 6 and 7 receptors in olfactory sensory neurons remains to be determined, their agonist characteristics suggest that they may allow the detection of various contaminated compounds such as spoiled food, or alternatively, enable the identification of unhealthy conspecifics via the evaluation of bodily secretions, a job at which mice excel (Kavaliers *et al*., 2005; 2006).

4.1.1 Body odors and immune system

When two animals first meet, they usually undergo an initial period of olfactory investigation before engaging in social interaction (Brown, 1979). Most animals gain information about conspecifics, through body odors, emitted from urine, feces, scent gland, saliva, etc. (Brown, 1979). Mammals can identify conspecifics by their individual odors or ‘olfactory fingerprints’. Accordingly, urine and other odor cues are critically important e.g. in rodent mate selection (Huck and Banks, 1982). Yamazaki *et al.* showed in 1979 that the immune system plays a crucial role in generating a unique body odor that mice can discern from urine. The authors found that males from two strains of mice, which were genetically identical except for the major histocompatibility complex (MHC) genes, preferred to mate with females of the opposite strain. Mice were, thus, able to discriminate genetic individuality based on differences in urine odor signature (Yamaguchi *et al.,* 1981).

Several hypotheses have been proposed that aim to explain how the MHC influences social recognition. One hypothesis postulates that MHC molecule fragments and the degradation products of their peptide ligands can serve as potential odorants (Beauchamp and Yamazaki, 2003). It has been also proposed that MHC peptide ligands are precursors of volatile odorants (Singer *et al.,* 1997). In 1987, Singh and coworkers showed in rats that classical MHC class I peptide ligands could be excreted in urine. Since transmembrane MHC proteins

are proteolytically cleaved at the cell surface and then secreted to bodily fluids (Singh *et al.,* 1987), MHC peptide ligands potentially become available to conspecifics as constituents of bodily secretions. The authors hypothesized that these peptides could provide the molecular basis for the unique MHC-dependent body / urine odor (Singh *et al.,* 1987) and, thus, serve as the most likely candidates for individuality signals.

In 2004, experiments for the first time revealed a role for MHC class I peptides as chemosensory stimuli. Leinders-Zufall *et al.* showed that MHC class I peptides function as sensory stimuli for V2R-expressing VSNs and that they serve as individuality signals underlying mate recognition (Leinders-Zufall *et al.,* 2004). To show that MHC peptides alone cause crucial social behavior, dissimilar MHC peptides were synthesized and added to urine of a familiar male. In contrast to cognate peptides that had no effect on social behavior, dissimilar MHC peptides caused pregnancy block (Leinders-Zufall *et al.,* 2004). In 2009, Leinders-Zufall *et al*. additionally showed that VSNs expressing one specific receptor, V2R1b, detect MHC peptides and distinguish peptides differing in their amino-acid residue (Leinders-Zufall *et al*., 2009). These results clearly demonstrate that MHC peptides influence social behavior and provided an unexpected link between the immune system and the sense of smell.

A parallel line of research revealed a role of bacteria, the main target of the immune system, in the generation of unique urine odors. Bacteria alter the odor production of different gland secretions in mammals (Brown, 1979). Gastrointestinal bacteria are essential for the production of the maternal odor in the feces of lactating female rats and mice. Antibiotics, which inhibit gastrointestinal bacteria, prevent development of such maternal odors (Leon, 1974; Lee, 1981; Skeen and Thiessen, 1977). Furthermore, it was shown that urine of germ-free rats differs from that of conventionally housed rats in various volatile components (Holland *et al.,* 1983), postulating that individual differences in urine odors of rats and mice are due to differences in urinary volatiles produced by bacteria. Studies with a number of vertebrate species showed that parasitic infections influence female mate choice, i.e. females prefer parasite-free males (Hamilton and Zuk, 1982). Such an olfactory ‘screening’ of a conspecific’s health status is based on the chemical signature of bodily fluids (Kavaliers *et al*., 2005). An additional role of the immune system may, thus, also be to ensure a healthy body odor by eliminating parasites and bacteria, which would alter the olfactory fingerprints of the animal.

In 1989, Williams and Pembroke postulated that dogs are able to detect malignant tumors on the basis of body odor. Their hypothesis derived from a patient reporting that her dog constantly sniffed at a specific body area. Subsequent histological examination confirmed a malignant tumor at this site. Although these events remain unsupported by experimental evidence, the idea that ‘dogs can smell cancer’ is not entirely unreasonable (Willis *et al.,*

2004). Tumors produce volatile compounds, which are released through breath and sweat (Phillips *et al.,* 1999). Willis *et al*. (2004) demonstrated that dogs can detect cancer by olfactory means more successfully than would be expected by chance alone, suggesting a potential diagnostic role for dogs in oncology (Willis *et al*., 2004).

Here, we showed that FPRs are expressed in a unique subpopulation of VSNs and that they respond to a new class of chemosensory stimuli. However, the role of FPRs in social behavior remains to be evaluated. It will be essential to show that behavioral responses to bacterial degradation products depend on FPRs. Therefore, behavioral assays, e.g. a two bottle choice test, could possibly demonstrate if mice avoid water when bacterial degradation products such as fMLF, CRAMP and lipoxin A are added. A next step could be to cause an inflammatory response in a mouse, e.g. by Lipopolysaccharide (LPS) injection (Rowley and Turner*,* 1964), and assess if conspecifics avoid the infected animal and, using a genetic approach, if this aversion depends on FPR-expressing VSNs.

Furthermore, there is evidence that some FPRs could play different chemosensory roles. Four of the five FPR receptors are expressed in VSNs of the apical zone, whereas one FPR (FPR-rs1) is expressed in VSNs of the basal zone. The spatial segregation of the vomeronasal sensory epithelium in general suggests that apical and basal VSNs encode different chemosensory information (Brennan and Zufall, 2006). Hence, stimuli that activate FPR-expressing VSNs in the apical and basal zone may evoke different physiological changes or behavioral responses.

The discovery of FPRs in the VNO strengthens and extends the concept of a link between the immune and nervous system. MHC class I peptide ligands are classical mediators of immune responses that, at the same time, act as crucial determinants for mate selection (Leinders-Zufall *et al.,* 2004; 2009; Kelliher *et al*., 2006). On the other hand, FPRs are prototypical chemokine receptors of immune cells that turn out to also play a role in olfaction. FPRs might enable an individual to assess the health status of a conspecific, due to the body odor and, therefore, could influence mate choice too.

Do FPRs influence olfaction in human? There is evidence that human FPRs are also expressed in other tissue than immune cells, e.g. brain, heart, liver, stomach, ovary, uterus, placenta, testis (Migeotte *et al.,* 2006). So far, however, a potential expression of FPRs in the human olfactory epithelium has not been investigated.

4.2 Functional characterization of vomeronasal receptor V1RD3

Two distinct populations of vomeronasal sensory neurons have been identified each expressing either V1R (Dulac and Axel, 1997) or V2R (Herrada and Dulac, 1997; Matsunami and Buck, 197; Ryba and Tirindelli, 1997) receptor proteins. Each VSN expresses a single member of the vomeronasal receptor gene repertoire. *V1r* and *V2r* genes are proposed to encode candidate chemosensory receptors. Mice lacking an entire gene cluster comprising 16 *V1r* genes are impaired in their ability to respond to pheromonal cues (Del Punta *et al.*, 2002). These observations suggest that V1Rs may be directly involved in detection of pheromones.

One vomeronasal receptor ligand pair has been described. Ca^{2+} imaging and patch clamp recordings from GFP-tagged V1Rb2-expressing cells identified 2-heptanone as an *in situ* ligand for V1Rb2 (Boschat *et al.,* 2002). The discovery of this first receptor agonist pair in the VNO was expected to provide a valuable tool for studies aiming to understand the signal transduction cascade in the VNO. However, no such follow-up studies on the transduction cascade induced by this receptor-ligand pair have been published so far. Moreover, other ligands for specific V1R receptors have not been identified and, thus, there is no direct functional evidence implicating these proteins as pheromone receptors. In an attempt to better understand the molecular tools used by mammals to socially interact, we searched for still unidentified mouse vomeronasal receptor-ligand pairs, combining recombinant receptor expression in a heterologous cell system and physiological recording methods in the mouse model. Here, we functionally characterized the vomeronasal receptor V1RD3 which we found upregulated in expression profiling assays in C57Bl/6 mice stimulated with urine (Hagendorf *et al.*, 2009). We identified six putative ligands for V1RD3 in a heterologous cell system and showed that one ligand (4-ethylphenol) evoked action potential firing and Ca^{2+} entry in intact VSNs. Furthermore, we demonstrated that 4-ethylphenol is secreted in urine and we found that the amount of 4-ethylphenol in male urine is approximately four times higher compared to female urine.

Which tissue metabolizes and secretes 4-ethylphenol and what role does 4-ethylphenol play in pheromonal communication? We investigated secreted urine, bladder urine and preputial gland homogenate of male mice to evaluate whether 4-ethylphenol is a ‘conventional’ metabolic degradation product or if it is 'intentionally' secreted to urine by glands. Preputial glands are important for secreting some pheromones such as α-farnesene and β-farnesene. These are able to accelerate puberty in mice (Novotny *et al.,* 1999). We show that the high male specific concentration of 4-ethylphenol present in secreted urine is neither found in bladder urine nor in preputial glands, indicating that 4-ethylphenol is added to urine after glomerular filtration from a yet unidentified source. Hence, we are currently investigating other male-specific glands e.g. prostate, seminal vesicle and coagulation glands. Moreover,

we aim to determine if 4-ethylphenol secretion is modulated by the testosterone level and, therefore, we additionally investigate urine from castrated male mice. If the production of 4-ethylphenol is testosterone-dependent, its secretion could signal sexual fitness or sexual maturity. Furthermore, male mice could use 4-ethylphenol to mark their territory and avoid rivalry. Alternatively, testosterone-dependent 4-ethylphenol could serve as an attractant for females.

In 2002, Achiraman and Archunan showed that Swiss mice secret male-specific compounds such as 4-ethylphenol in urine. They postulated that 4-ethylphenol acts as an attractant for females and creates aversion in males (Achiraman and Archunan, 2002). Furthermore, the authors claimed that 4-ethylphenol is present in male urine and absent in urine of castrated males. The production of 4-ethylphenol was not rescued in castrated males when treated with testosterone (Achiraman and Archunan, 2002). However, a major caveat of the study by Achiraman and Archunan is the design of the behavioral tests. The authors performed an odor preference test instead of a social behavior assay. They applied the 4-ethylphenol diluted in DMSO as stimulus and the solvent alone as control. Afterwards, they counted the number of 'visits' made by male and female mice, respectively. The authors observed that both female and male mice display some interest in 4-ethylphenol as compared to the solvent. Male mice, however, showed less interest than females. These results could simply be interpreted as indicating that both female and male mice detect the odorous compound 4-ethylphenol with some gender dependence. Accordingly, Achiraman and Archunan overinterpret their results. A functional role for 4-ethylphenol as a male attractant remains to be shown.

In 2008, Zhang and coworkers investigated sex pheromones in rats (Zhang *et al.*, 2008). They characterized volatile constituents of rat preputial gland and rat urine using GC-MS. The authors found that 4-ethylphenol is present in male and female rat urine, but not in preputial glands. The concentration of 4-ethylphenol was higher in male than in female rats and the production of 4-ethylphenol was suppressed by castration. Furthermore, behavioral analysis validated pheromonal activity of 4-ethylphenol by testing its chemosensory attractiveness to female rats. The results demonstrate that adding 4-ethylphenol to castrated male urine increased the attractiveness of castrated male urine to sexually naïve females. The authors used the same behavioral assay as described by Achiraman and Archunan. However, there is an important difference. Zhang and coworkers applied 4-ethylphenol in a castrated urine background. Urinary background information is essential for VNO-mediated behaviors. Mice gain much more information about the emittent, e.g. about gender or hierarchical status, from a stimulus blend than from a single compound (Laing *et al.,* 1989; Carlsson *et al.*, 2007). Hence, this strategy allows smelling a test substance in a context. Possibly, presentation of the substance alone could render the information useless. In

rodents, the vomeronasal pump is important for stimulus access. VSNs are isolated from the nasal cavity and therefore isolated from the air stream of normal respiration. Therefore, a vomeronasal stimulus requires arousal and activation of the vascular pump to gain access to the VNO sensory epithelium (Meredith and O'Connell, 1979; Pankevich *et al.*, 2003). In contrast to single substances, urine could contain various stimuli that activate the vascular pump mechanism of the VNO. In the MOE, however, trimethyl-thiazoline (TMT), a compound that is secreted from the fox anal gland (Vernet-Maury *et al.*, 1984), activates dorsal OSNs and elicits innate fear behavior even when applied solely (Hebb *et al.*, 2004; Kobayakawa *et al.*, 2007).

Given that 4-ethylphenol is thought to serve as a pheromone for rats, could it also act as a pheromone for mice? The classical definition of the term 'pheromone' disallows this hypothesis. A pheromone is a secreted molecule used for social communication between conspecifics by changing the recipient's behavior or endocrine status (Karlson and Lüscher, 1995; Wyatt *et al.*, 2003). The definition avoids the terms odor because a pheromone does not have to be odorous or volatile as long as the signal is a chemical substance that is transferred between conspecifics. In some cases, the distinctions between general odorants and pheromones are blurred (Touhara and Vosshall, 2009). A pheromone can be an odorous compound, and an odorant can be a pheromone. A pheromone released and utilized by one species can be produced as a general odorant for a second species but might also be informative for a third species, e.g. for predators (Touhara and Vosshall, 2009). General odors can also induce behavioral or physiological changes. It has been shown, that vomeronasal neurons also detect non pheromonal odorants (Sam *et al.,* 2001), implying that V1R-expressing neurons may not be restricted to the detection of pheromones, but may also perceive non-species-related signals that could identify e.g. prey, predators, and the physical environment (Touhara and Vosshall, 2009).

In conclusion, the exact role of 4-ethylphenol in murine social communication has to be revealed using appropriate behavioral assays. First, a urinary background for substance exposure is essential. Second, a designated social communication assay in which two mice freely interact with each other (e.g. in an open field arena) is mandatory. Marking one mouse (female, male or castrated male) with 4-ethylphenol and observing how other male or female mice interact, will help to understand the role of 4-ethylphenol in social communication. These experiments are currently on-going and will allow to draw conclusions about a potential function of 4-ethylphenol with respect to sexual aversion and / or attraction.

4.2.1 The receptive field of V1RD3

As described above, an important project of this thesis was the characterization of V1RD3 in a heterologous cell system. So far, ligands for V1Rs had not been unequivocally identified. The expression of chemosensory receptors, including vomeronasal receptors in heterologous cells is complicated because these proteins are often inefficiently translocated to the plasma membrane. To improve functional recombinant expression, several groups have searched for cofactors such as chaperones and other proteins to facilitate and stabilize cell-surface expression of olfactory receptors. The one-transmembrane-domain protein RTP1 (receptor transporter protein 1), expressed in olfactory neurons, enhances cell-surface expression of ORs (Saito *et al.,* 2004).

To gain information about the structure of ligands that are able to activate V1RD3, we cloned and heterologously expressed *V1rd3* in HEK293 cells. When we cotransfected plasmids encoding for *RTP1* and *V1rd3,* we observed a higher percentage of V1RD3 transfected cells, indicating that RTP1 also serves as cell-surface enhancer for vomeronasal receptors. To confirm efficient plasma membrane localization of the receptor we fused *V1rd3* to a tetracysteine motif (FlAsH-tag) (Tsien, 1989). The FlAsH-tag enables site-specific fluorescent labeling of proteins in live cells and provides a method for *in vivo* detection and subcellular localization of proteins using fluorescence microscopy (Adams and Tsien, 2008). The small size of the FlAsH-tag (6 amino acids, 585 Da) is less likely to interfere with the structure of the protein compared to frequently used GFP derivatives (26.9 kDa). Furthermore, FlAsH labeling reagents are membrane-permeable and bind the FlAsH-tag with high specificity and high affinity (Tsien, 1989). Using this approach, we confirmed membrane expression of V1RD3 in ~1 % of HEK 293 cells and we found six active ligands (4-ethylphenol, 3-ethylphenol, 2-ethylphenol, ethylbenzene, ethylcyclohexane and cis-4-ethylcyclohexanol) as well as thirteen inactive substances. The results demonstrate that the binding site of V1RD3 shows a preference for a six carbon ring structure backbone with an attached ethyl group. All active ligands are characterized by this structural motif. Substances that lack the ethyl group, as observed e.g. in phenol, were not able to activate V1RD3. Four of the six active ligands possess an alcohol group that apparently is dispensable for receptor-ligand interaction. Ethylcyclohexane and ethylbenzene for example do not possess an alcohol group but are able to activate V1RD3. Whether the six carbon ring structure consists of conjugated double bonds or single bonds does not affect receptor-ligand interaction, as apparent for ethylcyclohexane and ethylbenzene. Double bonds render the carbon ring highly inflexible compared to single bond rings which are extremely flexible due to free bond rotation. Interestingly, both structures can bind to V1RD3 with similar affinity, indicating that the binding pocket of the receptor accommodates different carbon ring structures, but is rather

selective for the ethyl group. In summary, we demonstrate the first, admittedly incomplete receptive field for a recombinant vomeronasal receptor.

In 2000, Leinders-Zufall *et al.* tested six structurally different pheromones (2,5-dimethylpyrazine, 2-sec-butyl-4,5-dihydrothiazole, 2,3-dehydro-exo-brevcomin, α-farnesene, β-farnesene, 2-heptanone, 6-hydroxy-6-methyl-3-heptanone) for vomeronasal activity using confocal Ca^{2+} imaging and electro-vomeronasogram (EVG) recordings. These pheromones evoke excitatory responses in single VSNs, leading to action potential generation and elevated Ca^{2+} entry. In no case did a given VSN respond to more than one of the six pheromones, showing that each pheromone activated a unique, non-overlapping subset of VSNs. (Leinders-Zufall *et al.*, 2000). Here, we could confirm these results, illustrating that vomeronasal receptors are remarkably sensitive and recognize only one or very few pheromonal substances (Leinders-Zufall *et al.*, 2000). In addition, we complement these results by showing that a vomeronasal receptor (V1RD3) is able to respond to more than one substance, provided the substances share common structural features. For instance, 4-ethylphenol, 3-ethylphenol, 2-ethylphenol, ethylbenzene, ethylcyclohexane and cis-4-ethylcyclohexanol all consist of a six carbon ring with an ethyl group and activate V1RD3 in heterologous cells. We showed that 4-ethylphenol, 3-ethylphenol and 2-ethylphenol were also able to elicit Ca^{2+} transients in the dendritic knob of the same VSN (Fig.3.15). Therefore, this novel V1R receptor-ligand pair(s) could provide a valuable tool to investigate the signal transduction cascade in VSNs. Direct proof of the V1RD3 / 4-ethylphenol interaction, however, will require genetic ablation of the V1RD3 locus in gene-targeted animals.

It is known that the VNO detects both volatile and nonvolatile stimuli (O'Connell and Meredith, 1984). V2R-expressing VSNs respond to nonvolatile stimuli such as MUPs (Cheetham *et al*., 2007; Sherborne *et al.,* 2007), ESP-1 (Kimoto *et al*., 2005; Kimchi *et al.,* 2007; Haga *et al*., 2010), and MHC peptides (Leinders-Zufall *et al.,* 2004), whereas V1R-expressing VSNs respond to more volatile stimuli (Leinders-Zufall *et al.,* 2000; Nodari *et al.,* 2008). Our results for V1RD3 confirm this functional segregation of the VNO.

How do pheromones affect innate behavior? Currently, there is increasing interest in understanding how complex stimuli mixtures such as urine activate VSNs. In 2008, He *et al*. discovered a population of VSNs that uniquely identify the sex of an animal. They revealed both male urine-specific and female urine-specific VSNs (He *et al.,* 2008). Two years later, the same group used physiological recording methods to show that different VSNs react on different urine concentrations (He *et al*., 2010). These findings contradict previous results (Leinders-Zufall *et al*., 2000) that showed that VSN pheromone responses are narrowly tuned without broadening of their tuning curves at high stimulus concentrations. He *et al.* identified four different populations of cells being activated when different dilutions of male and female urine were applied (He *et al.,* 2010). The authors speculated on the mechanisms

underlying this dose dependent activation of distinct cell populations. The authors assume that synergistic and antagonistic interactions among pheromone components with their receptors could produce complex response patterns. Furthermore, the authors conclude that pheromones in a complex stimuli mixture such as urine could mask each other (He *et al.,* 2010). Thus, their results indicate that peripheral pheromone sensing is more complicated than previously expected. Indeed, most bodily secretions are complex stimulus mixtures consisting of peptides, proteins and volatile compounds. It appears that rather a blend of various stimuli encodes for complex innate behaviors.

4.3 The role of mitochondrial Ca^{2+} in mouse olfactory sensory neurons

Cytosolic Ca^{2+} concentration is tightly controlled by complex interactions of pumps, channels, exchangers and binding proteins. Local changes of Ca^{2+} regulate a wide range of intracellular processes. The Ca^{2+} concentration in the cytoplasm is maintained around ~100 - 200 nM, significantly lower than in the extracellular medium (1-2 mM) (Pietrobon *et al.,* 1990). The low intracellular Ca^{2+} concentration is ensured by the low permeability of the plasma membrane to ions and by the activity of plasma membrane Ca^{2+} - ATPases (PMCAs) which transport Ca^{2+} outside the cell (Strehler and Treiman, 2004). Intracellular regulation of Ca^{2+} was long thought to be an exclusive task of the endoplasmic reticulum (ER) (Park *et al*., 2000; Jones *et al.,* 2008). The ER membrane contains high affinity Ca^{2+} pumps, the sarcoplasmic / endoplasmic reticulum calcium ATPases (SERCAs) and is ultimately responsible for recovering basal cytoplasmic Ca^{2+} levels (Pietrobon *et al.,* 1990).

I show here, that OSN mitochondria sequester Ca^{2+} upon odor application and influence Ca^{2+} homeostasis by shaping the kinetics of the cytosolic Ca^{2+} signal. First, I show that Ca^{2+} transients are elicited in both the cytoplasm and mitochondria upon odor stimulation in OSNs. These Ca^{2+} transients are mediated by canonical cAMP-dependent signaling pathways. Inhibition of the ACIII or removal of extracellular Ca^{2+} abolished Ca^{2+} influx into the cytoplasm and mitochondria, showing that mitochondrial Ca^{2+} entry depends on extracellular Ca^{2+}.

Why do mitochondria sequester Ca^{2+}? Uptake of Ca^{2+} into mitochondria is an electrogenic process mediated by mitochondrial Ca^{2+} channels (MiCa). The negative mitochondrial membrane potential is the driving force for Ca^{2+} accumulation into the matrix (Gunter *et al.,* 1990, Bernardi *et al.,* 1999). Mitochondrial Ca^{2+} signaling appears to be fundamental in the control of mitochondrial metabolism. The main physiological role of mitochondrial Ca^{2+} uptake is to stimulate oxidative phosphorylation, i.e. ATP production (Territo *et al.,* 2001). The effects of Ca^{2+} for mitochondrial ATP synthesis illustrate the functional significance of mitochondrial Ca^{2+} sequestration and explain how a cell can accommodate the increasing energy demand during stimulated states.

We show here that mitochondrial Ca^{2+} uptake has profound consequences for specific characteristics of odor-dependent cytosolic Ca^{2+} transients and, thus, may influence neuronal phenotype. Using the protonophore FCCP (Trenker *et al.,* 2007), we demonstrate that perturbation of the mitochondrial membrane potential totally abolishes odor-mediated Ca^{2+} transients in mitochondria and significantly prolongs Ca^{2+} transients in the cytoplasm. Temporal characteristics of cytosolic Ca^{2+} signals can be influenced by mitochondrial Ca^{2+} uptake. This often manifests in alterations of the cytosolic Ca^{2+} signal (Herrington *et al.,* 1996). The lack of the proton gradient and the resulting absence of the membrane potential stops ATP production by the ATP synthase (ATPase). The ATPase can turn into reverse

mode, resulting in degradation of ATP to ADP + Pi. To prevent such ATP degradation, we coapplied oligomycin as an inhibitor for the ATPase. Mitochondrial Ca^{2+} extrusion is mediated by Na^{+}/Ca^{2+} exchangers (NCX) located at the inner mitochondrial membrane. NCX are responsible for low resting mitochondrial Ca^{2+} by removing a single Ca^{2+} ion from the mitochondrial matrix in exchange for the import of three Na^{+} ions. We show that inhibition of mitochondrial NCX with CGP37157 leads to a significant increase in odor response duration in OSN mitochondria, confirming that Ca^{2+} extrusion is inhibited and, therefore, Ca^{2+} is trapped in the mitochondrial matrix for a prolonged time. In cytosolic fluorescence imaging, we observed that cytosolic odor response duration is also significantly prolonged when NCX is inhibited. We conclude that Ca^{2+} accumulates in the mitochondrial matrix until the cytoplasm / mitochondria Ca^{2+} concentration 'gradient' reaches equilibrium and that happens faster when Ca^{2+} extrusion from mitochondria is inhibited.

With respect to brief Ca^{2+} transients, the ER appears to function as the primary storage organelle (Rizzuto *et al.,* 2004). The idea that the ER function as Ca^{2+} store arose in 1984 and is based on different experimental observations including the accumulation of Ca^{2+} in the ER of live cells and isolated microsomes (ER vesicles) (Somlyo *et al.,* 1984). To investigate Ca^{2+} sequestration of the ER in OSNs, we inhibited SERCA pumps at ER membranes using thapsigargin and investigated odor-mediated Ca^{2+} transients in the cytoplasm. Inhibition of Ca^{2+} sequestration by the ER showed prolonged odor-mediated cytosolic Ca^{2+} transients, indicating that the ER is also responsible for Ca^{2+} uptake during odor stimulation.

Next, we investigated the odor-dependent cytosolic Ca^{2+} elevation time course when Ca^{2+} sequestration by both the ER and mitochondria is simultaneously inhibited by coapplication of FCCP and thapsigargin. Our results illustrate that both organelles function synergistically as Ca^{2+} buffer systems in activated OSNs. Resting cytosolic Ca^{2+} conditions, however, are maintained by the activity of PMCAs and plasma membrane Na^{+}/Ca^{2+} exchangers.

It has been hypothesized that mitochondria and ER establish functional contacts. Tight morphological and functional links between both organelles were demonstrated (Rizzuto *et al.,* 1993; Csordas *et al.,* 2006). A close association between ER membranes and mitochondria has been clearly shown by electron tomography techniques which allowed to estimate distances around 10 – 25 nm as well as the presence of tethers between the mitochondrial and the ER membrane in rat liver cells (Csordas *et al.,* 2006). 5% to 20% of total mitochondrial membranes are colocalized with the ER (Rizzuto *et al.,* 1998; Csordas *et al.,* 2006). Direct 'tunneling' of Ca^{2+} from ER to mitochondria, essentially by-passing the cytoplasm, has been proposed by Darios *et al.* in 2003. Furthermore, a chaperone-mediated coupling of the ER and mitochondrial Ca^{2+} channels has been described. A reversible organelle junction that allows rapid and efficient Ca^{2+} transfer from the ER to mitochondria and *vice versa* was described (Szabadkai *et al.,* 2006; Malli *et al.,* 2007). While our data

show that both mitochondria and ER share Ca^{2+} buffer function within one OSN, further experiments are necessary to investigate the presence of tethers between them. Studies utilizing the electron tomography technique could reveal possible tethers between OSN mitochondria and ER.

Our findings suggest a critical role for mitochondria in shaping the temporal characteristic of odor-mediated cytosolic Ca^{2+} transients. Therefore, we investigated the mitochondrial role in Ca^{2+} signal rise time. We show that the 'late' Ca^{2+} rise time from 70% to 90% of an odor response amplitude is significantly prolonged when mitochondrial function is inhibited by FCCP. Yet, 'early' Ca^{2+} rise time from 10% to 70% was not altered. By contrast, the Ca^{2+} rise time from 10% to 70% is significantly decreased when Ca^{2+} sequestration by the ER is inhibited using thapsigargin. In this case, Ca^{2+} rise time from 70% to 90% was not altered. Our results indicate that Ca^{2+} sequestration by mitochondria and the ER differs on the temporal scale. The ER begins to sequester Ca^{2+} immediately when Ca^{2+} concentration is increasing in the cytoplasm. By contrast, mitochondria start to sequester Ca^{2+} later, when Ca^{2+} concentration is locally high and the ER is working to full capacity. Most reports indicate that mitochondria are more efficient in accumulating Ca^{2+} when the Ca^{2+} concentration is locally high (Wang *et al.,* 2000). Ca^{2+} pump mechanisms of the ER via SERCAs are relatively slow and consume ATP, but have a high affinity for Ca^{2+}. The MiCa ion channel has a low affinity for Ca^{2+} but permits Ca^{2+} to flow rapidly into the matrix without ATP consumption. Due to its low affinity for Ca^{2+}, MiCa is not sensitive to low cytosolic free Ca^{2+} concentrations. The channel does not conduct Ca^{2+} below a cytoplasmic concentration of around 200 - 300nM (Gunter *et al.,* 1990; Sparagna *et al.,* 1995). Under physiological conditions, mitochondrial Ca^{2+} accumulation thus depends on the cytosolic Ca^{2+} concentration to which the organelle is exposed. The proximity of mitochondria to Ca^{2+} sources is therefore an important determinant of Ca^{2+} uptake by these organelles (Mannella *et al.,* 1989). In OSNs, odor response-mediated Ca^{2+} influx via cyclic nucleotide-gated (CNG) channel is a hallmark of the primary signal transduction cascade (Nakamura and Gold, 1987; Firestein and Werblin, 1989; Zufall *et al*., 1994; Kleene, 2008). Here, we show that in dendritic knobs odor-mediated Ca^{2+} transients in the cytoplasm are significantly prolonged, when mitochondrial Ca^{2+} sequestration is inhibited, showing that mitochondria modulate the signal transduction in dendritic knobs.

In highly complex neuronal morphologies with long axons and dendrites, it is essential that mechanisms exist to transport mitochondria throughout the neuron and recruit mitochondria to regions with high metabolic demands such as presynaptic terminals (Hollenbeck and Saxton, 2005). Mitochondria develop at the cell soma (Davis *et al.,* 1996) and form a dynamic network (Yaffe *et al.,* 1999). Due to complex cytoskeletal transport mechanisms, individual neuronal mitochondria are highly mobile in both anterograde and retrograde

directions (Hollenbeck and Saxton, 2005). Directed transport along microtubules is mediated by the dynein-kinesin system, while mitochondria also move along actin filaments using myosin motors (Hollenbeck and Saxton, 2005). The velocity of mitochondria in neurons is about 0.3 – 0.6 µm/s (Kovacs *et al.,* 2005). Mitochondrial transport together with the dynamic processes of mitochondrial fission and fusion facilitate energy transmission across long distances. Mitochondrial fission allows for mitochondrial renewal, redistribution and proliferation, whereas the competing process, mitochondrial fusion, allows mitochondria to interact and communicate with each other (Hoppins *et al.,* 2007).

Since we showed the presence and function of mitochondria in both OSN somata and dendritic knob endings, we next investigated mitochondrial trafficking. Studies of mitochondrial movements in axons and dendrites of various neurons (Ligon and Steward, 2000; Morris and Hollenbeck, 1995; Overly *et al.,* 1996) indicate that the majority of neuronal mitochondria are largely immobile, whereas few organelles move bidirectionally with intermittent stops (Hollenbeck and Saxton, 2005). Moreover, it has been shown that mitochondria are able to translocate upon stimulation. Focal application of nerve growth factor (NGF) to growing axons results in the accumulation of mitochondria near the stimulation site (Chada and Hollenbeck, 2004).

Here, we illustrate mitochondrial trafficking by loading mitochondria in dissociated OSNs from mOR-EG / OMP-GFP mice with a mitochondria specific dye, MitoTracker® Red FM. Mitochondrial movement was observed using a confocal laser-scanning microscope. The results show that mitochondria display net movement from apical parts of the soma to dendritic parts of OSNs upon odor stimulation at a velocity of ~0.1 µm/s. It is difficult to investigate the velocity of singular mitochondria because mitochondria undergo continuous fusion and fission events. Therefore, we can only estimate OSNs mitochondrial velocity. Furthermore, these data indicate that mitochondria translocate to dendritic knobs to provide energy and to regulate Ca^{2+} at or close to sites of signal transduction and Ca^{2+} entry.

What initiates mitochondrial translocation to dendritic knobs? In OSNs, odor stimulation initiates multiple signaling pathways. Primary signal transduction in the cilia triggers different secondary cascades. Our results suggest that rather global Ca^{2+} elevation acts as a signal to activate mitochondrial translocation. More specifically, the rise of intracellular Ca^{2+} deriving from odor stimulation could activate the translocation of mitochondria to dendritic knobs. Interestingly, translocation of mitochondria is not observed immediately after stimulation. It takes a few seconds (up to 10 s) to detect odor-dependent translocation. In 2007, it was shown, that mitochondria translocate to the ER during Ca^{2+} release from internal stores (Kolikova *et al*., 2007), indicating that mitochondrial translocation is controlled by Ca^{2+}. The same study demonstrated that mitochondria of cultured hippocampal astrocytes translocate to the plasma membrane when transmitters such as ATP or glutamate are applied. The

authors showed that this translocation was depended on the rise of intracellular Ca^{2+}. They could inhibit this mitochondrial translocation by pre-incubation of the astrocytes with BAPTA-AM, a potent cytoplasmic Ca^{2+} chelator. Furthermore, Kolikova and coworkers showed that the rise of extracellular Ca^{2+} alone also caused mitochondrial translocation to the plasma membrane (Kolikova *et al*., 2007). These results are confirmed by a study on mitochondrial transport in T-cells that showed mitochondrial translocation as a direct consequence of Ca^{2+} influx (Quintana *et al.,* 2006). The results of Kolikova *et al*. and Quintana *et al* indicate that mitochondrial translocation in OSNs could derive from intracellular Ca^{2+} increase elicited by odor stimulation.

Do mitochondria enter the cilia of OSNs? OSN dendritic knobs contain numerous mitochondria (Cuschieri and Bannister 1975; Menco and Farbman 1985; Menco and Morrison 2003). But olfactory cilia do not possess mitochondria (Lidow & Menco, 1984). Cilia are microtubule-based organelles, with a thickness of around 300 nm (Menco, 1997), whereas the sizes of mitochondria range from 500 nm to 1 µm diameter (Mitchell *et al.,* 1961). First, mitochondria do not fit into the small ciliary compartments and, second, olfactory cilia lack microtubule-attached structures in proximal parts (Lidow & Menco, 1984). Hence, mitochondria cannot be transported into the small ciliary compartments. In the present dissertation, we characterized mitochondrial distribution in dissociated OMP-GFP positive OSNs. We observed mitochondrial staining in dendritic knobs and at the base of the cilia of OSNs (Fig.4.1). As expected, however, we never observed mitochondria in ciliary compartments.

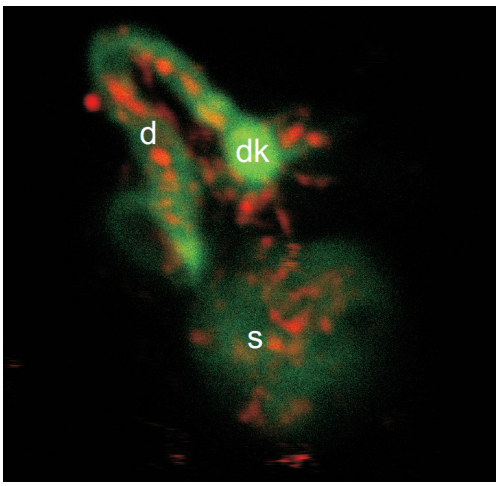


Fig.4.1: Merged fluorescence image of a dissociated OSN of an OMP-GFP mice (green) and MitoTracker® Red FM labeled mitochondria (red). Mitochondria are redistributed all over the cell. Mitochondria are located in dendritic knobs and at the base of cilia. s = soma, d = dendrite, dk = dendritic knob

Ongoing experiments try to reveal the mitochondrial role for the electrical output in OSNs. Are mitochondria involved e.g. in adaptation mechanisms or do mitochondria influence gene expression? We hypothesize that mitochondrial Ca^{2+} buffering modulates action potential output in OSNs. We address this question using whole-cell patch clamp recordings in OSNs of mOR-EG mice.

A study in 2006 investigated mitochondrial output in rat dorsal root ganglion neurons. The uncoupling of the electron transport with FCCP or inhibiting mitochondrial NCX with CGP37157 revealed that mitochondrial buffering of intracellular Ca^{2+} slowed Ca^{2+} oscillation frequency, decreased spike amplitude, and increased spike width (Jackson and Thayer, 2006). These findings illustrate the complex interaction of mitochondria and Ca^{2+}-regulated processes in sensory neurons.

Another study investigated the mitochondrial role in AP generation in parasympathetic neurons that were dissociated from mudpuppy (*Necturus maculosus*) cardiac ganglia. Here, exposure to the protonophore FCCP increased the latency of AP generation, indicating that mitochondria are involved in the regulation of AP generation (Barstow *et al.,* 2004).

4.3.1 Measurements of mitochondrial Ca^{2+}

So far, measurements of mitochondrial Ca^{2+} have been exclusively performed in biochemical assays or in cultured cells. These studies have undoubtedly led to a deeper understanding of mechanisms underlying Ca^{2+} regulation in mitochondria. However, spatio-temporal kinetics of fast Ca^{2+} transients and the *in-situ* organization of mitochondrial networks are difficult to assess *in vitro*. To date, there are several different techniques that allow measuring of Ca^{2+} in mitochondria, i.e., on the one hand, small molecule fluorescent reporters and, on the other hand, genetically encoded probes.

The most frequently used chemical probes are cationic dyes that accumulate in the mitochondrial matrix due to the negative mitochondrial membrane potential. Rhod-2 is a relatively selective mitochondrial Ca^{2+} sensor (Minta *et al*., 1989). Rhod-2 has been used in a number of studies investigating mitochondrial Ca^{2+} regulation in cultured cells. It is usually applied in its cell-permeant form as an acetoxymethylester (AM) and accumulates within the mitochondrial matrix where it is hydrolyzed to the active compound (Tsien, 1981). However, Rhod-2/AM labeling shows major disadvantages. Uneven distribution of the dye within mitochondria was observed (Launikonis *et al.*, 2005) and non-specific accumulation in the cytosol has also been reported (Rutter *et al.*, 1996). Tissue-dependent activity of cytosolic esterases may explain the variable efficacy of dye accumulation in mitochondria of different tissues (Trollinger *et al.*, 2000).

A major advantage of genetically encoded Ca^{2+} probes is that they can be efficiently targeted to subcellular compartments such as mitochondria. In 1962, biochemically isolated aequorin was used for the first time to measure intracellular Ca^{2+} transients (Ridgway *et al.*, 1967; Blinks *et al.*, 1976). Aequorin is an ideal sensor for (mitochondrial) Ca^{2+} measurements, because it can be genetically expressed and introduced into model organisms. In 2007, Rogers *et al.* described the first aequorin-based *in vivo* monitoring of mitochondrial Ca^{2+}

regulation in a conditional knock-in mouse line that ubiquitously expresses a mitochondrially targeted GFP-aequorin (mtGA) fusion protein. mtGA folds efficiently into a functional protein in most cell types and can be directed to any specific location inside the cell (Brini *et al.*, 1999). Moreover, aequorin actively produces light upon binding of Ca^{2+}. No excitation light is needed and no background signals are observed (Rogers *et al.*, 2007). In mtGA, aequorin acts as the Ca^{2+} sensor which delivers emission energy to the GFP acceptor molecule in a bioluminescence resonance energy transfer (BRET) process. Although BRET leads to a partial loss of emission energy, addition of the GFP is beneficial because it emits longer wavelength light with higher tissue penetration depth. Upon systemic application of coelenterazine, mitochondrial Ca^{2+} signaling was studied in different tissues using a bioluminescence imaging device (Rogers *et al.*, 2007, Pozzan *et al.*, 2009).

In the present dissertation, we established a different tool to measure Ca^{2+} in mitochondria. Our collaborators (Axxam Inc., Milan) generated a novel derivate of the photoprotein aequorin, i.e. c-Photina®, targeted to the inner mitochondrial membrane. They performed random mutagenesis of *Clytin*, a natural photoprotein isolated from *Clytia gregaria* jellyfish. One of those modified photoproteins displayed the desired characteristics and was called c-Photina®. To improve the transduction efficiency in mammalian cells, the *c-Photina* gene was optimized for mammalian codon usage and then fused to a mitochondrial tag (human *Cytochrome C Oxidase*) (Cainarca *et al.*, 2010). Compared to aequorin, the photoprotein c-Photina displays improved characteristics e.g. high affinity for Ca^{2+} and stable expression over time. This is important since several mammalian cells transfected with other natural or recombinant photoproteins tend to lose function over time (Cainarca *et al.*, 2010). By contrast, we here demonstrate successful application of c-Photina to detection of Ca^{2+} induced quanta of light using optical systems both in stem cells (Cainarca *et al.*, 2010) and in the MOE (Fluegge *et al.*, in preparation) from transgenic PhotoTopo animals.

The advantage of a BRET approach is to overcome the low light quantum yield of a single photoprotein. The combination of two partner proteins in BRET assays permits the detection of the Ca^{2+}-mediated signal, even with unavoidable loss of energy during the transfer. In comparison to the BRET approach, the c-Photina system alone is more direct and simpler without loss of energy. Moreover, using a bioluminescent reporter gene instead of a fusion construct avoids folding and translation problems.

The combination of *PhotoTopo* mice with the dedicated live-cell imaging bioluminescence microscope LV200 provides a powerful tool to detect bioluminescence signals directly emitted by aequorin. The LV200 is equipped with a highly sensitive EM-CCD camera. No additional mirrors, filters or lenses are added to prevent absorption of the low levels of light emitted by aequorin. In addition, the high numerical aperture of the tube lens affords an increase in sensitivity.

However, a bioluminescence imaging approach also has a few disadvantages. Quantitative recording is limited. Cells have to be loaded with coelenterazine, the photoprotein substrate. Coelenterazine consumption restricts sustained generation of bioluminescence even in the presence of Ca^{2+}. Moreover, coelenterazine incubation is required for several hours to load cells.

Compared to 'conventional' imaging approaches that employ Ca^{2+} dyes such as fluo-4/AM and fura-2/AM to investigate cytosolic Ca^{2+}, the c-Photina® system offers several advantages. First, there is no phototoxicity because there is no illumination of a fluorescent probe allowing us to perform high frequency measurements without cell damage. Second, there are no bleaching artefacts and no background signals, greatly improving sensitivity and ensuring a high signal to noise ratio. Thus, it is possible to detect even small Ca^{2+} changes. Fluo-4/AM and fura-2/AM are Ca^{2+} chelators and buffer Ca^{2+} with high affinity and, therefore, interfere to the Ca^{2+} homeostasis of the cell. Bioluminescence imaging does not interfere with cellular Ca^{2+} homeostasis. Therefore, possible Ca^{2+} chelating effects on downstream signaling can be excluded. Furthermore, we perform bioluminescence imaging with a high temporal resolution up to 25 Hz allowing detailed characterization of fast Ca^{2+} kinetics. By contrast, Ca^{2+} dye excitation and limits the frame rate of fluorescence Ca^{2+} imaging experiments in OSNs.

In this thesis, we utilize the advantages of both techniques, i.e. cytosolic fluorescence and mitochondrial bioluminescence imaging. This combination of cytosolic Ca^{2+} dyes and the c-Photina® system is an optimal tool to investigate the involvement of mitochondria in the OSN Ca^{2+} homeostasis *in situ.* Using these techniques, we can speculate about the interdependency of mitochondrial and cytosolic Ca^{2+} changes and shed light on the role of mitochondria in odor-induced cellular activity.

5 Summary

The general aim of my thesis was to gain a deeper understanding of sensory signaling in the mouse olfactory system. Specifically, my research focused on three important aspects of vomeronasal and olfactory signaling: Two projects addressed signaling mechanisms in the VNO, whereas another project focused on the role of mitochondria in olfactory sensory neurons.

In the first part of my thesis, we engaged in a collaborative approach with colleagues from the University of Geneva to identify a novel family of chemosensory receptors in the VNO, the formyl peptide receptor (FPR)-like proteins. FPR-like proteins are common immune system GPCRs. During inflammatory reactions, they initiate targeted movement (chemotaxis) of specific immune cells to sites of bacterial infection. We identified the FPR family in the VNO by qRT-PCR and *in situ* hybridizations. Next, we discovered a new class of vomeronasal agonists. I used recombinant *in vitro* expression of mouse FPR-like proteins to investigate sensitivity to disease and inflammation-related ligands. Moreover, I established an *in situ* approach that combines a whole-mount VNO preparation with dendritic Ca^{2+} imaging in the intact sensory epithelium. With this technique, I analyzed putative FPR-mediated signals in native vomeronasal tissue. Our results indicate that mice functionally express FPRs in VSNs to evaluate the health status of conspecifics.

In the second part of this thesis, I characterized a previously unidentified vomeronasal receptor-ligand pair using both recombinant receptor expression in a heterologous cell system and physiological recording methods in the mouse model. We showed increased vomeronasal expression of *V1rd3* after prolonged exposure of sexually naïve male mice to social chemostimuli such as male urine. First, the *V1rd3* gene was cloned and recombinantly expressed *in vitro* to investigate receptor sensitivity to urine-related ligands. Next, I used the whole-mount VNO preparation to perform dendritic Ca^{2+} imaging and, thus, verify the *in situ* agonist profile of V1RD3. I found cognate V1RD3 / ligand pairs that will likely provide novel insight into the chemical identity of mammalian pheromones in future studies.

In the third part of this thesis, my interest focused on the functional characterization of the mitochondrial role in Ca^{2+} signaling in mouse OSNs. Here, I investigated the mitochondrial function during OSN activity in main olfactory epithelium tissue slices. Using a combination of bioluminescence imaging and transgenic mice that stably express a Ca^{2+}-sensitive photoprotein selectively in mitochondria, I established a novel imaging approach to record mitochondrial Ca^{2+} signals at high temporal resolution. I showed that mitochondria shape the odor-induced cytosolic Ca^{2+} transients and translocate to dendritic compartments upon odor stimulation. On-going electrophysiological recordings from identified OSNs aim to reveal the functional consequences of mitochondrial perturbation on the odor-mediated electrical output signal.

Together, the data generated in this thesis will likely provide new insights into olfactory physiology and its impact on social behavior in mice. The majority of the FPR data presented in this thesis have been published (Rivière*, Challet*, Fluegge*, Spehr and Rodriguez, Formyl receptors-like are a novel family of vomeronasal chemosensors, *equal contribution, *Nature* 459, 574-577, 22 April 2009). Two other publications on the V1RD3 receptive field and on mitochondrial Ca^{2+} signaling in OSNs, respectively, are currently in preparation.

6 Abbreviations

A.dest	Aqua destillata
AC III	Adenylate cyclase III
ADP	Adenosinediphosphat
ANO2	Anoctamin 2
AOB	Accessory olfactory bulb
AP	Action potential
ATP	Adenosine-triphosphate
BK	large-conductance Ca^{2+}-activated K^+ channels
BV	Blood vessel
CaCC	Ca^{2+}-activated Cl^--channel
cAMP	Cyclic adenosinmonophosphat
CHO-cells	Chinese hamster ovary cells
CNG	Cyclic nucleotide-gated ion channel
CRAMP	antimicrobial peptide
Con A	Concanavalin A
DAG	Diacylglycerole
DTT	Dithiothreitol
E.coli	Escherichia coli
EGTA	Ethylene glycol tetraacetic acid
ER	Endoplasmic reticulum
ESP1	Exocrine gland-secreting peptide 1
ETC	Electron transport chain
EVG	Electro-vomeronasogram
Fab	Fragment antigen binding
$FADH_2$	Flavin-adenin-dinucleotid
FBS	Fetal bovine serum
FCCP	4-(trifluoromethoxyl) s-phenyl-hydrazone
FPRs	Formyl peptide receptor like proteins
fMLF	*N*-formyl-methionyl-leucyl-phenylalanine
GC – MS	Gas chromatography- mass spectroscopy
GG	Grueneberg Ganglion
G proteins	GTP binding proteins
GFP	Green fluorescent protein
GPCR	G protein-coupled receptor

GTP	Guanosine-5'-triphosphate
HEK 293	Human embryonal kidney cells
HEPES	4-(2-hydroxyethyl)-1-piperazineethanesulfonic acid
IP3	Inositol 1,4,5-trisphosphate
L	Lumen
LB medium	Lysogeny broth medium
MiCa	Mitochondrial Ca^{2+} channel
MHC	Major histocompatibility complex
MOB	Main olfactory bulb
MOE	Main olfactory epithelium
mtDNA	Mitochondrial DNA
MUP	Major urinary proteins
NADH	Nicotinamid-adenin-dinucleotid
NCX	Na^{+}/ Ca^{2+} exchanger
NGS	Normal goat serum
NFkB	Nuclear factor 'kappa-light-chain-enhancer' of activated B-cells
OMP	Olfactory marker protein
OR	Olfactory receptor
OSN	Olfactory sensory neuron
PBS	Phosphate buffered saline
PFA	Paraformaldehyde
PIP2	Phosphatidylinositol-4,5-biphosphate
PLC	Phospholipase C
PMCA	Plasma membrane Ca^{2+} ATPase
Pmol	Picomol
PUFAs	Polyunsaturated fatty acids
ROI	Region of interest
rpm	Rotation per minute
RT	Room temperature
RyR	Ryanodine receptor
SAA	Acute phase protein serum amyoloid A
SO	Septal organ
SERCA	Smooth endoplasmic reticular Ca^{2+} ATPase
TAAR	Trace amine-associated receptors
TRPC2	Transient receptor potential cation channel,

	subfamily C, member 2
U	Unit
UPAR	Urokinase plasminogen activator
V1R	Vomeronasal receptor type 1
V2R	Vomeronasal receptor type 2
VGCC	Voltage gated Ca^{2+} channels
VNO	Vomeronasal organ
VSN	Vomeronasal sensory neuron
β2M	β2 Microglobulin

7 References

Achiraman,S. and Archunan,G. (2002). Characterization of urinary volatiles in Swiss male mice (Mus musculus): bioassay of identified compounds. J. Biosci. *27*, 679-686.

Achiraman,S. and Archunan,G. (2002). Urinary proteins and pheromonal communication in mammals. Indian J. Exp. Biol. *40*, 1077-1078.

Bacchini,A., Gaetani,E., and Cavaggioni,A. (1992). Pheromone binding proteins of the mouse, Mus musculus. Experientia *48*, 419-421.

Bakalyar,H.A. and Reed,R.R. (1990). Identification of a specialized adenylyl cyclase that may mediate odorant detection. Science *250*, 1403-1406.

Bargmann,C.I. (2006). Comparative chemosensation from receptors to ecology. Nature *444*, 295-301.

Barker,S.A., Caldwell,K.K., Hall,A., Martinez,A.M., Pfeiffer,J.R., Oliver,J.M., and Wilson,B.S. (1995). Wortmannin blocks lipid and protein kinase activities associated with PI 3-kinase and inhibits a subset of responses induced by Fc epsilon R1 cross-linking. Mol. Biol. Cell *6*, 1145-1158.

Bassler,B.L. (2002). Small talk. Cell-to-cell communication in bacteria. Cell *109*, 421-424.

Belluscio,L., Gold,G.H., Nemes,A., and Axel,R. (1998). Mice deficient in G(olf) are anosmic. Neuron *20*, 69-81.

Bereiter-Hahn,J. and Voth,M. (1994). Dynamics of mitochondria in living cells: shape changes, dislocations, fusion, and fission of mitochondria. Microsc. Res. Tech. *27*, 198-219.

Berghard,A., Buck,L.B., and Liman,E.R. (1996). Evidence for distinct signaling mechanisms in two mammalian olfactory sense organs. Proc. Natl. Acad. Sci. U. S. A *93*, 2365-2369.

Bernardi,P. (1999). Mitochondria in muscle cell death. Ital. J. Neurol. Sci. *20*, 395-400.

Bernardi,P., Scorrano,L., Colonna,R., Petronilli,V., and Di,L.F. (1999). Mitochondria and cell death. Mechanistic aspects and methodological issues. Eur. J. Biochem. *264*, 687-701.

Bhatnagar,K.P. and Meisami,E. (1998). Vomeronasal organ in bats and primates: extremes of structural variability and its phylogenetic implications. Microsc. Res. Tech. *43*, 465-475.

Binns,K.E. and Brennan,P.A. (2005). Changes in electrophysiological activity in the accessory olfactory bulb and medial amygdala associated with mate recognition in mice. Eur. J. Neurosci. *21*, 2529-2537.

Bockaert,J. and Pin,J.P. (1999). Molecular tinkering of G protein-coupled receptors: an evolutionary success. EMBO J. *18*, 1723-1729.

Boehm,N. and Aron,C. (1988). Facilitory effects of olfactory cues emitted by estrous females on mounting behavior in the female rat. Physiol Behav. *43*, 669-671.

Boehm,T. (2006). Quality control in self/nonself discrimination. Cell. 2006. Jun. 2;125. (5):845. -58. *125*, 845-858.

Boehm,T. and Zufall,F. (2006). MHC peptides and the sensory evaluation of genotype. Trends Neurosci. 2006. Feb. ;29. (2):100. -7. Epub. 2005. Dec. 6. *29*, 100-107.

Borowsky,B., Adham,N., Jones,K.A., Raddatz,R., Artymyshyn,R., Ogozalek,K.L., Durkin,M.M., Lakhlani,P.P., Bonini,J.A., Pathirana,S., Boyle,N., Pu,X., Kouranova,E., Lichtblau,H., Ochoa,F.Y., Branchek,T.A., and Gerald,C. (2001). Trace amines: identification of a family of mammalian G protein-coupled receptors. Proc. Natl. Acad. Sci. U. S. A *98*, 8966-8971.

Boschat,C., Pelofi,C., Randin,O., Roppolo,D., Luscher,C., Broillet,M.C., and Rodriguez,I. (2002). Pheromone detection mediated by a V1r vomeronasal receptor. Nat. Neurosci. *5*, 1261-1262.

Boskey,E.R., Moench,T.R., Hees,P.S., and Cone,R.A. (2003). A self-sampling method to obtain large volumes of undiluted cervicovaginal secretions. Sex Transm. Dis. *30*, 107-109.

Bradley,J., Li,J., Davidson,N., Lester,H.A., and Zinn,K. (1994). Heteromeric olfactory cyclic nucleotide-gated channels: a subunit that confers increased sensitivity to cAMP. Proc. Natl. Acad. Sci. U. S. A *91*, 8890-8894.

Brann,J.H. and Fadool,D.A. (2006). Vomeronasal sensory neurons from Sternotherus odoratus (stinkpot/musk turtle) respond to chemosignals via the phospholipase C system. J. Exp. Biol. *209*, 1914-1927.

Brann,J.H., Dennis,J.C., Morrison,E.E., and Fadool,D.A. (2002). Type-specific inositol 1,4,5-trisphosphate receptor localization in the vomeronasal organ and its interaction with a transient receptor potential channel, TRPC2. J. Neurochem. *83*, 1452-1460.

Breer,H., Boekhoff,I., and Tareilus,E. (1990). Rapid kinetics of second messenger formation in olfactory transduction. Nature *345*, 65-68.

Breer,H., Fleischer,J., and Strotmann,J. (2006). The sense of smell: multiple olfactory subsystems. Cell Mol. Life Sci. 2006. Jul;63. (13):1465. -75. *63*, 1465-1475.

Brennan,P.A. (2001). The vomeronasal system. Cell Mol. Life Sci. 2001. Apr;58. (4):546. -55. *58*, 546-555.

Brennan,P.A. (2004). The nose knows who's who: chemosensory individuality and mate recognition in mice. Horm. Behav. 2004. Sep. ;46. (3):231. -40. *46*, 231-240.

Brennan,P.A. and Kendrick,K.M. (2006). Mammalian social odours: attraction and individual recognition. Philos. Trans. R. Soc. Lond B Biol. Sci. *361*, 2061-2078.

Brennan,P.A. and Keverne,E.B. (2004). Something in the air? New insights into mammalian pheromones. Curr. Biol. 2004. Jan. 20. ;14(2):R81. -9. *14*, R81-R89.

Brennan,P.A. and Zufall,F. (2006). Pheromonal communication in vertebrates. Nature. 2006. Nov. 16. ;444. (7117.):308. -15. *444* , 308-315.

Briand,L., Blon,F., Trotier,D., and Pernollet,J.C. (2004). Natural ligands of hamster aphrodisin. Chem. Senses *29*, 425-430.

Brini,M., Pinton,P., Pozzan,T., and Rizzuto,R. (1999). Targeted recombinant aequorins: tools for monitoring [Ca2+] in the various compartments of a living cell. Microsc. Res. Tech. *46*, 380-389.

Browning,J.L., Sizing,I.D., Lawton,P., Bourdon,P.R., Rennert,P.D., Majeau,G.R., Ambrose,C.M., Hession,C., Miatkowski,K., Griffiths,D.A., Ngam-ek,A., Meier,W., Benjamin,C.D., and Hochman,P.S. (1997). Characterization of lymphotoxin-alpha beta complexes on the surface of mouse lymphocytes. J. Immunol. *159*, 3288-3298.

Brunet,L.J., Gold,G.H., and Ngai,J. (1996). General anosmia caused by a targeted disruption of the mouse olfactory cyclic nucleotide-gated cation channel. Neuron *17*, 681-693.

Buck,L. and Axel,R. (1991). A novel multigene family may encode odorant receptors: a molecular basis for odor recognition. Cell *65*, 175-187.

Caggiano,M., Kauer,J.S., and Hunter,D.D. (1994). Globose basal cells are neuronal progenitors in the olfactory epithelium: a lineage analysis using a replication-incompetent retrovirus. Neuron *13*, 339-352.

Cainarca,S., Fenu,S., Ferri,C., Nucci,C., Arioli,P., Menegon,A., Piemonti,L., Lohmer,S., Wrabetz,L., and Corazza,S. (2010). A photoprotein in mouse embryonic stem cells measures Ca2+ mobilization in cells and in animals. PLoS. One. *5*, e8882.

Camps,M., Carozzi,A., Schnabel,P., Scheer,A., Parker,P.J., and Gierschik,P. (1992). Isozyme-selective stimulation of phospholipase C-beta 2 by G protein beta gamma-subunits. Nature *360*, 684-686.

Cariboni,A., Hickok,J., Rakic,S., Andrews,W., Maggi,R., Tischkau,S., and Parnavelas,J.G. (2007). Neuropilins and their ligands are important in the migration of gonadotropin-releasing hormone neurons. J. Neurosci. *27*, 2387-2395.

Carlsson MA, Hansson BS. 2002. Responses in highly selective sensory neurons to blends of pheromone components in the moth Agrotis segetum.J Insect Physiol. 48:443–451.

Carroll,L.S., Penn,D.J., and Potts,W.K. (2002). Discrimination of MHC-derived odors by untrained mice is consistent with divergence in peptide-binding region residues. Proc. Natl. Acad. Sci. U. S. A *99*, 2187-2192.

Cavaggioni,A. and Mucignat-Caretta,C. (2000). Major urinary proteins, alpha(2U)-globulins and aphrodisin. Biochim. Biophys. Acta *1482*, 218-228.

Cavaggioni,A., Mucignat,C., and Tirindelli,R. (1999). Pheromone signalling in the mouse: role of urinary proteins and vomeronasal organ. Arch. Ital. Biol. *137*, 193-200.

Cavaggioni,A., Mucignat-Caretta,C., and Redaelli,M. (2008). Mice recognize recent urine scent marks by the molecular composition. Chem. Senses *33*, 655-663.

Cavaggioni,A., Mucignat-Caretta,C., and Zagotto,G. (2003). Absolute configuration of 2-sec-butyl-4,5-dihydrothiazole in male mouse urine. Chem. Senses *28*, 791-797.

Chada,S.R. and Hollenbeck,P.J. (2004). Nerve growth factor signaling regulates motility and docking of axonal mitochondria. Curr. Biol. *14*, 1272-1276.

Chamero,P., Marton,T.F., Logan,D.W., Flanagan,K., Cruz,J.R., Saghatelian,A., Cravatt,B.F., and Stowers,L. (2007). Identification of protein pheromones that promote aggressive behaviour. Nature *450*, 899-902.

Cheetham,S.A., Thom,M.D., Jury,F., Ollier,W.E., Beynon,R.J., and Hurst,J.L. (2007). The genetic basis of individual-recognition signals in the mouse. Curr. Biol. *17*, 1771-1777.

Chen,H., He,Z., and Tessier-Lavigne,M. (1998). Axon guidance mechanisms: semaphorins as simultaneous repellents and anti-repellents. Nat. Neurosci. *1*, 436-439.

Chen,T.Y. and Yau,K.W. (1994). Direct modulation by Ca(2+)-calmodulin of cyclic nucleotide-activated channel of rat olfactory receptor neurons. Nature *368*, 545-548.

Chess,A., Simon,I., Cedar,H., and Axel,R. (1994). Allelic inactivation regulates olfactory receptor gene expression. Cell *78*, 823-834.

Clapham,D.E. (2007). Calcium signaling. Cell *131*, 1047-1058.

Claxton, N., Fellers, and Davidson. Laser scanning confocal microscopy. Ref Type: Generic

Cloutier,J.F., Giger,R.J., Koentges,G., Dulac,C., Kolodkin,A.L., and Ginty,D.D. (2002). Neuropilin-2 mediates axonal fasciculation, zonal segregation, but not axonal convergence, of primary accessory olfactory neurons. Neuron *33*, 877-892.

Collins,T.J., Berridge,M.J., Lipp,P., and Bootman,M.D. (2002). Mitochondria are morphologically and functionally heterogeneous within cells. EMBO J. *21*, 1616-1627.

Cowan,W.M., Raisman,G., and Powell,T.P. (1965). The connexions of the amygdala. J. Neurol. Neurosurg. Psychiatry *28*, 137-151.

Csordas,A. (2006). Mitochondrial transfer between eukaryotic animal cells and its physiologic role. Rejuvenation. Res. *9*, 450-454.

Csordas,G. and Hajnoczky,G. (2003). Plasticity of mitochondrial calcium signaling. J. Biol. Chem. *278*, 42273-42282.

Csordas,G., Renken,C., Varnai,P., Walter,L., Weaver,D., Buttle,K.F., Balla,T., Mannella,C.A., and Hajnoczky,G. (2006). Structural and functional features and significance of the physical linkage between ER and mitochondria. J. Cell Biol. *174*, 915-921.

Csordas,G., Thomas,A.P., and Hajnoczky,G. (2001). Calcium signal transmission between ryanodine receptors and mitochondria in cardiac muscle. Trends Cardiovasc. Med. *11*, 269-275.

Darios,F., Corti,O., Lucking,C.B., Hampe,C., Muriel,M.P., Abbas,N., Gu,W.J., Hirsch,E.C., Rooney,T., Ruberg,M., and Brice,A. (2003). Parkin prevents mitochondrial swelling and cytochrome c release in mitochondria-dependent cell death. Hum. Mol. Genet. *12*, 517-526.

Darios,F., Lambeng,N., Troadec,J.D., Michel,P.P., and Ruberg,M. (2003). Ceramide increases mitochondrial free calcium levels via caspase 8 and Bid: role in initiation of cell death. J. Neurochem. *84*, 643-654.

Davis,A.F. and Clayton,D.A. (1996). In situ localization of mitochondrial DNA replication in intact mammalian cells. J. Cell Biol. *135*, 883-893.

Dedov,V.N. and Roufogalis,B.D. (1999). Organisation of mitochondria in living sensory neurons. FEBS Lett. *456*, 171-174.

Del,P.K., Leinders-Zufall,T., Rodriguez,I., Jukam,D., Wysocki,C.J., Ogawa,S., Zufall,F., and Mombaerts,P. (2002). Deficient pheromone responses in mice lacking a cluster of vomeronasal receptor genes. Nature *419*, 70-74.

DePierre,J.W. and Ernster,L. (1977). Enzyme topology of intracellular membranes. Annu. Rev. Biochem. *46*, 201-262.

Dhallan,R.S., Yau,K.W., Schrader,K.A., and Reed,R.R. (1990). Primary structure and functional expression of a cyclic nucleotide-activated channel from olfactory neurons. Nature *347*, 184-187.

Doty,R.L., Diez,J.M., Turnacioglu,S., McKeown,D.A., Gledhill,J., Armstrong,K., and Lee,W.W. (2003). Influences of feedback and ascending and descending trial presentations on perithreshold odor detection performance. Chem. Senses *28*, 523-526.

Doving,K.B. and Trotier,D. (1998). Structure and function of the vomeronasal organ. J. Exp. Biol. *201*, 2913-2925.

Dulac,C. and Axel,R. (1995). A novel family of genes encoding putative pheromone receptors in mammals. Cell *83*, 195-206.

Dulac,C. and Torello,A.T. (2003). Molecular detection of pheromone signals in mammals: from genes to behaviour. Nat. Rev. Neurosci. 2003. Jul;4(7.):551. -62. *4*, 551-562.

Dulac,C. and Wagner,S. (2006). Genetic analysis of brain circuits underlying pheromone signaling. Annu. Rev. Genet. *40*, 449-467.

Edwards,F.A., Konnerth,A., Sakmann,B., and Takahashi,T. (1989). A thin slice preparation for patch clamp recordings from neurones of the mammalian central nervous system. Pflugers Arch. *414*, 600-612.

Eggert,F., Luszyk,D., Haberkorn,K., Wobst,B., Vostrowsky,O., Westphal,E., Bestmann,H.J., Muller-Ruchholtz,W., and Ferstl,R. (1998). The major histocompatibility complex and the chemosensory signalling of individuality in humans. Genetica *104*, 265-273.

Eisner,D.A. and Lederer,W.J. (1985). Na-Ca exchange: stoichiometry and electrogenicity. Am. J. Physiol *248*, C189-C202.

Eisthen,H.L. and Wyatt,T.D. (2006). The vomeronasal system and pheromones. Curr. Biol. 2006. Feb. 7. ;16. (3):R73. -4. *16*, R73-R74.

Fadool Debra Ann. Mammalian Pheromones. 23-9-2005. Ref Type: Report

Firestein,S. (2001). How the olfactory system makes sense of scents. Nature *413*, 211-218.

Firestein,S. and Werblin,F. (1989). Odor-induced membrane currents in vertebrate-olfactory receptor neurons. Science *244*, 79-82.

Firestein,S. and Zufall,F. (1994). The cyclic nucleotide gated channel of olfactory receptor neurons. Semin. Cell Biol. *5*, 39-46.

Gao,J.L., Lee,E.J., and Murphy,P.M. (1999). Impaired antibacterial host defense in mice lacking the N-formylpeptide receptor. J. Exp. Med. *189*, 657-662.

Getchell,T.V. (1986). Functional properties of vertebrate olfactory receptor neurons. Physiol Rev. *66*, 772-818.

Getchell,T.V., Margolis,F.L., and Getchell,M.L. (1984). Perireceptor and receptor events in vertebrate olfaction. Prog. Neurobiol. *23*, 317-345.

Goodwin,T.E., Rasmussen,E.L., Guinn,A.C., McKelvey,S.S., Gunawardena,R., Riddle,S.W., and Riddle,H.S. (1999). African elephant sesquiterpenes. J Nat. Prod. *62*, 1570-1572.

Graier,W.F., Frieden,M., and Malli,R. (2007). Mitochondria and Ca(2+) signaling: old guests, new functions. Pflugers Arch. *455*, 375-396.

Graul,R.C. and Sadee,W. (2001). Evolutionary relationships among G protein-coupled receptors using a clustered database approach. AAPS. PharmSci. *3*, E12.

Graziadei,P.P. (1993). Olfactory organ culture in vivo and in vitro. Cytotechnology *11*, 3-6.

Graziadei,P.P. and Graziadei,G.A. (1979). Neurogenesis and neuron regeneration in the olfactory system of mammals. I. Morphological aspects of differentiation and structural organization of the olfactory sensory neurons. J. Neurocytol. *8*, 1-18.

Grill,R.J., Jr. and Pixley,S.K. (1993). 2-Mercaptoethanol is a survival factor for olfactory, cortical and hippocampal neurons in short-term dissociated cell culture. Brain Res. *613*, 168-172.

Grus,W.E. and Zhang,J. (2006). Origin and evolution of the vertebrate vomeronasal system viewed through system-specific genes. Bioessays. 2006. Jul;28. (7.):709. -18. *28*, 709-718.

Gunter,T.E. and Pfeiffer,D.R. (1990). Mechanisms by which mitochondria transport calcium. Am. J. Physiol *258*, C755-C786.

Gunter,T.E., Buntinas,L., Sparagna,G., Eliseev,R., and Gunter,K. (2000). Mitochondrial calcium transport: mechanisms and functions. Cell Calcium *28*, 285-296.

Hagendorf,S., Fluegge,D., Engelhardt,C., and Spehr,M. (2009). Homeostatic control of sensory output in basal vomeronasal neurons: activity-dependent expression of ether-a-go-go-related gene potassium channels. J. Neurosci. *29*, 206-221.

Hamilton,W.D. and Zuk,M. (1982). Heritable true fitness and bright birds: a role for parasites? Science *218*, 384-387.

Hashiguchi,Y. and Nishida,M. (2006). Evolution and origin of vomeronasal-type odorant receptor gene repertoire in fishes. BMC. Evol. Biol. 2006. Oct. 3;6. :76. *6*, 76.

He,J., Ma,L., Kim,S., Nakai,J., and Yu,C.R. (2008). Encoding gender and individual information in the mouse vomeronasal organ. Science *320*, 535-538.

He,J., Ma,L., Kim,S., Schwartz,J., Santilli,M., Wood,C., Durnin,M.H., and Yu,C.R. (2010). Distinct signals conveyed by pheromone concentrations to the mouse vomeronasal organ. J. Neurosci. *30*, 7473-7483.

Heimer,L. (1972). The olfactory connections of the diencephalon in the rat. An experimental light- and electron-microscopic study with special emphasis on the problem of terminal degeneration. Brain Behav. Evol. *6*, 484-523.

Hermann,G.J. and Shaw,J.M. (1998). Mitochondrial dynamics in yeast. Annu. Rev. Cell Dev. Biol. *14*, 265-303.

Herrington,J., Park,Y.B., Babcock,D.F., and Hille,B. (1996). Dominant role of mitochondria in clearance of large Ca2+ loads from rat adrenal chromaffin cells. Neuron *16*, 219-228.

Hoeflich,K.P. and Ikura,M. (2002). Calmodulin in action: diversity in target recognition and activation mechanisms. Cell *108*, 739-742.

Hofmann,T., Schaefer,M., Schultz,G., and Gudermann,T. (2000). Cloning, expression and subcellular localization of two novel splice variants of mouse transient receptor potential channel 2. Biochem. J. *351*, 115-122.

Holekamp,T.F., Turaga,D., and Holy,T.E. (2008). Fast three-dimensional fluorescence imaging of activity in neural populations by objective-coupled planar illumination microscopy. Neuron *57*, 661-672.

Holland,M., Rhodes,G., DalleAve,M., Wiesler,D., and Novotny,M. (1983). Urinary profiles of volatile and acid metabolites in germfree and conventional rats. Life Sci. *32*, 787-794.

Hollenbeck,P.J. and Saxton,W.M. (2005). The axonal transport of mitochondria. J. Cell Sci. *118*, 5411-5419.

Holy,T.E., Dulac,C., and Meister,M. (2000). Responses of vomeronasal neurons to natural stimuli. Science *289*, 1569-1572.

Hoppins,S., Lackner,L., and Nunnari,J. (2007). The machines that divide and fuse mitochondria. Annu. Rev. Biochem. *76*, 751-780.

Huck,U.W., Carter,C.S., and Banks,E.M. (1982). Natural or hormone-induced sexual and social behaviors in the female brown lemming (Lemmus trimucronatus). Horm. Behav. *16*, 199-207.

Hussain,A., Saraiva,L.R., and Korsching,S.I. (2009). Positive Darwinian selection and the birth of an olfactory receptor clade in teleosts. Proc. Natl. Acad. Sci. U. S. A *106*, 4313-4318.

Imai,T., Suzuki,M., and Sakano,H. (2006). Odorant receptor-derived cAMP signals direct axonal targeting. Science *314*, 657-661.

Inamura,K., Kashiwayanagi,M., and Kurihara,K. (1999). Regionalization of Fos immunostaining in rat accessory olfactory bulb when the vomeronasal organ was exposed to urine. Eur. J. Neurosci. *11*, 2254-2260.

Ishii,T. and Mombaerts,P. (2008). Expression of nonclassical class I major histocompatibility genes defines a tripartite organization of the mouse vomeronasal system. J Neurosci. *28*, 2332-2341.

Ishii,T., Hirota,J., and Mombaerts,P. (2003). Combinatorial coexpression of neural and immune multigene families in mouse vomeronasal sensory neurons. Curr. Biol. 2003. Mar. 4;13(5):394. -400. *13*, 394-400.

Jackson JG, Thayer SA (2006) Mitochondrial modulation of Ca2+ -induced Ca2+ -release in rat sensory neurons. J Neurophysiol 1093-104

Jacob S, McClintock MK, Zelano B, Ober C. (2002) Paternally inherited HLA alleles are associated with women's choice of male odor. Nat Genet. Feb;30(2):175-9. Epub 2002 Jan 22.

Janeway,C.A., Jr. (1993). How the immune system recognizes invaders. Sci. Am. *269*, 72-79.

Janeway,C.A., Jr. and Golstein,P. (1993). Lymphocyte activation and effector functions. Editorial overview. The role of cell surface molecules. Curr. Opin. Immunol. *5*, 313-323.

Jin,W., Lo,T.M., Loh,H.H., and Thayer,S.A. (1994). U73122 inhibits phospholipase C-dependent calcium mobilization in neuronal cells. Brain Res. *642*, 237-243.

Jones,D.T. and Reed,R.R. (1989). Golf: an olfactory neuron specific-G protein involved in odorant signal transduction. Science *244*, 790-795.

Jones,P.P., Jiang,D., Bolstad,J., Hunt,D.J., Zhang,L., Demaurex,N., and Chen,S.R. (2008). Endoplasmic reticulum Ca2+ measurements reveal that the cardiac ryanodine receptor mutations linked to cardiac arrhythmia and sudden death alter the threshold for store-overload-induced Ca2+ release. Biochem. J. *412*, 171-178.

Joost,P. and Methner,A. (2002). Phylogenetic analysis of 277 human G-protein-coupled receptors as a tool for the prediction of orphan receptor ligands. Genome Biol. *3*, RESEARCH0063.

Josefsson,L.G. (1999). Evidence for kinship between diverse G-protein coupled receptors. Gene *239*, 333-340.

Kaba,H. and Nakanishi,S. (1995). Synaptic mechanisms of olfactory recognition memory. Rev. Neurosci. *6*, 125-141.

Karlson,P. and Luscher,M. (1959). Pheromones': a new term for a class of biologically active substances. Nature *183*, 55-56.

Kavaliers M, Choleris E, Pfaff DW, Recognition and avoidance of the odors of parasitized conspecifics and predators: differential genomic correlates. Neurosci. Biobehav. Rev. 2005; 29(8):1347-59

Kelliher,K.R. (2007). The combined role of the main olfactory and vomeronasal systems in social communication in mammals. Horm. Behav. *52*, 561-570.

Kelliher,K.R., Spehr,M., Li,X.H., Zufall,F., and Leinders-Zufall,T. (2006). Pheromonal recognition memory induced by TRPC2-independent vomeronasal sensing. Eur. J. Neurosci. *23*, 3385-3390.

Kelliher,K.R., Ziesmann,J., Munger,S.D., Reed,R.R., and Zufall,F. (2003). Importance of the CNGA4 channel gene for odor discrimination and adaptation in behaving mice. Proc. Natl. Acad. Sci. U. S. A *100*, 4299-4304.

Keverne,E.B. (1999). The vomeronasal organ. Science. *286*, 716-720.

Keverne,E.B. (2002). Mammalian pheromones: from genes to behaviour. Curr. Biol. 2002 Dec. 10;12. (23):R807. -9. *12*, R807-R809.

Keverne,E.B., Levy,F., Poindron,P., and Lindsay,D.R. (1983). Vaginal stimulation: an important determinant of maternal bonding in sheep. Science *219*, 81-83.

Kevin R.Kelliher, * Marc Spehr * Xiao-Hong Li Frank Zufall and Trese Leinders-Zufall. Pheromonal recognition memory induced independent vomeronasal sensing. 2006. Ref Type: Report

Kimchi,T., Xu,J., and Dulac,C. (2007). A functional circuit underlying male sexual behaviour in the female mouse brain. Nature.

Kimoto,H. and Touhara,K. (2005). Induction of c-Fos Expression in Mouse Vomeronasal Neurons by Sex-specific Non-volatile Pheromone(s). Chem. Senses. 2005. Jan. ;30. Suppl 1:i146. -i147. *30 Suppl 1*, i146-i147.

Kimoto,H., Haga,S., Sato,K., and Touhara,K. (2005). Sex-specific peptides from exocrine glands stimulate mouse vomeronasal sensory neurons. Nature. 2005. Oct. 6. ;437. (7060.):898. -901. *437*, 898-901.

Kimoto,H., Sato,K., Nodari,F., Haga,S., Holy,T.E., and Touhara,K. (2007). Sex- and Strain-Specific Expression and Vomeronasal Activity of Mouse ESP Family Peptides. Curr. Biol.

Kleene,S.J. (1993). Origin of the chloride current in olfactory transduction. Neuron *11*, 123-132.

Kleene,S.J. (2008). The electrochemical basis of odor transduction in vertebrate olfactory cilia. Chem. Senses *33*, 839-859.

Kobayakawa,K., Kobayakawa,R., Matsumoto,H., Oka,Y., Imai,T., Ikawa,M., Okabe,M., Ikeda,T., Itohara,S., Kikusui,T., Mori,K., and Sakano,H. (2007). Innate versus learned odour processing in the mouse olfactory bulb. Nature.

Kolikova, Afzalov, Giniatullina,Surin, Giniatullin and Khiroug (2007) Calcium-dependent trapping of mitochondria near plasma membrane in stimulated astrocytes. Brain Cell Biol 75-86

Kovacs,R., Kardos,J., Heinemann,U., and Kann,O. (2005). Mitochondrial calcium ion and membrane potential transients follow the pattern of epileptiform discharges in hippocampal slice cultures. J. Neurosci. *25*, 4260-4269.

Krieger,J., Schmitt,A., Lobel,D., Gudermann,T., Schultz,G., Breer,H., and Boekhoff,I. (1999). Selective activation of G protein subtypes in the vomeronasal organ upon stimulation with urine-derived compounds. J. Biol. Chem. *274*, 4655-4662.

Kurosaka,K., Chen,Q., Yarovinsky,F., Oppenheim,J.J., and Yang,D. (2005). Mouse cathelin-related antimicrobial peptide chemoattracts leukocytes using formyl peptide receptor-like 1/mouse formyl peptide receptor-like 2 as the receptor and acts as an immune adjuvant. J. Immunol. *174*, 6257-6265.

Laing DG, Cain WS, McBride RL, Ache BW. editors. (1989). Perception of complex smells and tastes. Sydney, Australia: Academic Press.

Launikonis,B.S., Zhou,J., Royer,L., Shannon,T.R., Brum,G., and Rios,E. (2005). Confocal imaging of [Ca2+] in cellular organelles by SEER, shifted excitation and emission ratioing of fluorescence. J. Physiol *567*, 523-543.

Le,Y., Murphy,P.M., and Wang,J.M. (2002). Formyl-peptide receptors revisited. Trends Immunol. *23*, 541-548.

Le,Y., Oppenheim,J.J., and Wang,J.M. (2001). Pleiotropic roles of formyl peptide receptors. Cytokine Growth Factor Rev. *12*, 91-105.

Le,Y., Wetzel,M.A., Shen,W., Gong,W., Rogers,T.J., Henderson,E.E., and Wang,J.M. (2001). Desensitization of chemokine receptor CCR5 in dendritic cells at the early stage of differentiation by activation of formyl peptide receptors. Clin. Immunol. *99*, 365-372.

Le,Y., Yang,Y., Cui,Y., Yazawa,H., Gong,W., Qiu,C., and Wang,J.M. (2002). Receptors for chemotactic formyl peptides as pharmacological targets. Int. Immunopharmacol. *2*, 1-13.

Lee,C.J., Fraser,B.A., Szu,S., and Lin,K.T. (1981). Chemical structure of and immune response to polysaccharides of Streptococcus pneumoniae. Rev. Infect. Dis. *3*, 323-331.

Lee,H.Y., Kang,H.K., Jo,E.J., Kim,J.I., Lee,Y.N., Lee,S.H., Park,Y.M., Ryu,S.H., Kwak,J.Y., and Bae,Y.S. (2004). Trp-Lys-Tyr-Met-Val-Met stimulates phagocytosis via phospho-lipase D-dependent signaling in mouse dendritic cells. Exp. Mol. Med. *36*, 135-144.

Leinders-Zufall,T. and Zufall,F. (1995). Block of cyclic nucleotide-gated channels in salamander olfactory receptor neurons by the guanylyl cyclase inhibitor LY83583. J. Neurophysiol. *74*, 2759-2762.

Leinders-Zufall,T., Brennan,P., Widmayer,P., PC,S., Maul-Pavicic,A., Jager,M., Li,X.H., Breer,H., Zufall,F., and Boehm,T. (2004). MHC class I peptides as chemosensory signals in the vomeronasal organ. Science. 2004. Nov. 5;306. (5698.):1033. -7. *306*, 1033-1037.

Leinders-Zufall,T., Cockerham,R.E., Michalakis,S., Biel,M., Garbers,D.L., Reed,R.R., Zufall,F., and Munger,S.D. (2007). Contribution of the receptor guanylyl cyclase GC-D to chemosensory function in the olfactory epithelium. Proc. Natl. Acad. Sci. U. S. A.

Leinders-Zufall,T., Greer,C.A., Shepherd,G.M., and Zufall,F. (1998). Visualizing odor detection in olfactory cilia by calcium imaging. Ann. N. Y. Acad. Sci. *855*, 205-207.

Leinders-Zufall,T., Greer,C.A., Shepherd,G.M., and Zufall,F. (1998). Imaging odor-induced calcium transients in single olfactory cilia: specificity of activation and role in transduction. J. Neurosci. *18*, 5630-5639.

Leinders-Zufall,T., Ishii,T., Mombaerts,P., Zufall,F., and Boehm,T. (2009). Structural requirements for the activation of vomeronasal sensory neurons by MHC peptides. Nat. Neurosci. *12*, 1551-1558.

Leinders-Zufall,T., Lane,A.P., Puche,A.C., Ma,W., Novotny,M.V., Shipley,M.T., and Zufall,F. (2000). Ultrasensitive pheromone detection by mammalian vomeronasal neurons. Nature *405*, 792-796.

Leinders-Zufall,T., Ma,M., and Zufall,F. (1999). Impaired odor adaptation in olfactory receptor neurons after inhibition of Ca2+/calmodulin kinase II. J. Neurosci. *19*, RC19.

Leinders-Zufall,T., Rand,M.N., Shepherd,G.M., Greer,C.A., and Zufall,F. (1997). Calcium entry through cyclic nucleotide-gated channels in individual cilia of olfactory receptor cells: spatiotemporal dynamics. J. Neurosci. *17*, 4136-4148.

Leinders-Zufall,T., Rosenboom,H., Barnstable,C.J., Shepherd,G.M., and Zufall,F. (1995). A calcium-permeable cGMP-activated cation conductance in hippocampal neurons. Neuroreport *6*, 1761-1765.

Leinders-Zufall,T., Shepherd,G.M., and Zufall,F. (1995). Regulation of cyclic nucleotide-gated channels and membrane excitability in olfactory receptor cells by carbon monoxide. J. Neurophysiol. *74*, 1498-1508.

Leinders-Zufall,T., Shepherd,G.M., and Zufall,F. (1996). Modulation by cyclic GMP of the odour sensitivity of vertebrate olfactory receptor cells. Proc. Biol. Sci. *263*, 803-811.

Leon,M. (1974). Maternal pheromone. Physiol Behav. *13*, 441-453.

Levai,O., Feistel,T., Breer,H., and Strotmann,J. (2006). Cells in the vomeronasal organ express odorant receptors but project to the accessory olfactory bulb. J Comp Neurol. 2006. Oct. 1;498. (4):476. -90. *498*, 476-490.

Leypold,B.G., Yu,C.R., Leinders-Zufall,T., Kim,M.M., Zufall,F., and Axel,R. (2002). Altered sexual and social behaviors in trp2 mutant mice. Proc. Natl. Acad. Sci. U. S. A *99*, 6376-6381.

Li,Z., Okamoto,K., Hayashi,Y., and Sheng,M. (2004). The importance of dendritic mitochondria in the morphogenesis and plasticity of spines and synapses. Cell *119*, 873-887.

Liberles,S.D. and Buck,L.B. (2006). A second class of chemosensory receptors in the olfactory epithelium. Nature *442*, 645-650.

Licht,G. and Meredith,M. (1987). Convergence of main and accessory olfactory pathways onto single neurons in the hamster amygdala. Exp. Brain Res. *69*, 7-18.

Ligon,L.A. and Steward,O. (2000). Movement of mitochondria in the axons and dendrites of cultured hippocampal neurons. J. Comp Neurol. *427*, 340-350.

Ligon,L.A. and Steward,O. (2000). Role of microtubules and actin filaments in the movement of mitochondria in the axons and dendrites of cultured hippocampal neurons. J. Comp Neurol. *427*, 351-361.

Liman,E.R. and Buck,L.B. (1994). A second subunit of the olfactory cyclic nucleotide-gated channel confers high sensitivity to cAMP. Neuron *13*, 611-621.

Liman,E.R., Corey,D.P., and Dulac,C. (1999). TRP2: a candidate transduction channel for mammalian pheromone sensory signaling. Proc. Natl. Acad. Sci. U. S. A *96*, 5791-5796.

Lin,D.Y., Zhang,S.Z., Block,E., and Katz,L.C. (2005). Encoding social signals in the mouse main olfactory bulb. Nature *434*, 470-477.

Lin,W., Arellano,J., Slotnick,B., and Restrepo,D. (2004). Odors detected by mice deficient in cyclic nucleotide-gated channel subunit A2 stimulate the main olfactory system. J. Neurosci. *24*, 3703-3710.

Liu,M., Chen,T.Y., Ahamed,B., Li,J., and Yau,K.W. (1994). Calcium-calmodulin modulation of the olfactory cyclic nucleotide-gated cation channel. Science *266*, 1348-1354.

Lledo,P.M., Somasundaram,B., Morton,A.J., Emson,P.C., and Mason,W.T. (1992). Stable transfection of calbindin-D28k into the GH3 cell line alters calcium currents and intracellular calcium homeostasis. Neuron *9*, 943-954.

Loconto,J., Papes,F., Chang,E., Stowers,L., Jones,E.P., Takada,T., Kumanovics,A., Fischer,L.K., and Dulac,C. (2003). Functional expression of murine V2R pheromone receptors involves selective association with the M10 and M1 families of MHC class Ib molecules. Cell. 2003. Mar. 7. ;112. (5):607. -18. *112*, 607-618.

Lucas,P., Ukhanov,K., Leinders-Zufall,T., and Zufall,F. (2003). A diacylglycerol-gated cation channel in vomeronasal neuron dendrites is impaired in TRPC2 mutant mice: mechanism of pheromone transduction. Neuron *40*, 551-561.

Luo,M. and Katz,L.C. (2004). Encoding pheromonal signals in the mammalian vomeronasal system. Curr. Opin. Neurobiol. 2004. Aug. ;14(4):428. -34. *14*, 428-434.

Ma,J. and Lowe,G. (2004). Action potential backpropagation and multiglomerular signaling in the rat vomeronasal system. J. Neurosci. *24*, 9341-9352.

Ma,M. (2007). Encoding olfactory signals via multiple chemosensory systems. Crit Rev. Biochem. Mol. Biol. *42*, 463-480.

MacDermott,A.B., Mayer,M.L., Westbrook,G.L., Smith,S.J., and Barker,J.L. (1986). NMDA-receptor activation increases cytoplasmic calcium concentration in cultured spinal cord neurones. Nature *321*, 519-522.

Maenaka,K. and Jones,E.Y. (1999). MHC superfamily structure and the immune system. Curr. Opin. Struct. Biol. *9*, 745-753.

Malli,R., Frieden,M., Hunkova,M., Trenker,M., and Graier,W.F. (2007). Ca2+ refilling of the endoplasmic reticulum is largely preserved albeit reduced Ca2+ entry in endothelial cells. Cell Calcium *41*, 63-76.

Martel,K.L. and Baum,M.J. (2009). Adult testosterone treatment but not surgical disruption of vomeronasal function augments male-typical sexual behavior in female mice. J. Neurosci. *29*, 7658-7666.

Martini,S., Silvotti,L., Shirazi,A., Ryba,N.J., and Tirindelli,R. (2001). Co-expression of putative pheromone receptors in the sensory neurons of the vomeronasal organ. J Neurosci. 2001. Feb. 1;21(3):843. -8. *21*, 843-848.

Mashukova,A., Spehr,M., Hatt,H., and Neuhaus,E.M. (2006). Beta-arrestin2-mediated internalization of mammalian odorant receptors. J Neurosci. 2006. Sep. 27. ;26. (39.):9902. -12. *26*, 9902-9912.

Matsunami,H. and Buck,L.B. (1997). A multigene family encoding a diverse array of putative pheromone receptors in mammals. Cell *90*, 775-784.

Matthews,H.R. and Reisert,J. (2003). Calcium, the two-faced messenger of olfactory transduction and adaptation. Curr. Opin. Neurobiol. *13*, 469-475.

Menco,B.P. (1997). Ultrastructural aspects of olfactory signaling. Chem. Senses *22*, 295-311.

Menco,B.P. and Jackson,J.E. (1997). Neuron-like cells on the apical surface of the developing rat olfactory epithelium. Neurosci. Lett. *239*, 117-120.

Menco,B.P., Carr,V.M., Ezeh,P.I., Liman,E.R., and Yankova,M.P. (2001). Ultrastructural localization of G-proteins and the channel protein TRP2 to microvilli of rat vomeronasal receptor cells. J. Comp Neurol. *438*, 468-489.

Menco,B.P., Cunningham,A.M., Qasba,P., Levy,N., and Reed,R.R. (1997). Putative odour receptors localize in cilia of olfactory receptor cells in rat and mouse: a freeze-substitution ultrastructural study. J. Neurocytol. *26*, 691-706.

Michel,V., Monnier,Z., Cvetkovic,V., and Math,F. (1999). Organotypic culture of neuroepithelium attached to olfactory bulb from adult mouse as a tool to study neuronal regeneration after ZnSO4 neuroepithelial trauma. Neurosci. Lett. *271*, 195-198.

Michelangeli,F., Ogunbayo,O.A., and Wootton,L.L. (2005). A plethora of interacting organellar Ca2+ stores. Curr. Opin. Cell Biol. *17*, 135-140.

Minta,A., Kao,J.P., and Tsien,R.Y. (1989). Fluorescent indicators for cytosolic calcium based on rhodamine and fluorescein chromophores. J. Biol. Chem. *264*, 8171-8178.

Mironov,S.L. (2006). Spontaneous and evoked neuronal activities regulate movements of single neuronal mitochondria. Synapse *59*, 403-411.

Mironov,S.L. and Symonchuk,N. (2006). ER vesicles and mitochondria move and communicate at synapses. J. Cell Sci. *119*, 4926-4934.

Mombaerts,P. (1996). Targeting olfaction. Curr. Opin. Neurobiol. *6*, 481-486.

Mombaerts,P. (2001). How smell develops. Nat. Neurosci. *4 Suppl*, 1192-1198.

Mombaerts,P. (2004). Genes and ligands for odorant, vomeronasal and taste receptors. Nat. Rev. Neurosci. 2004. Apr;5(4):263. -78. *5*, 263-278.

Mombaerts,P. (2006). Axonal wiring in the mouse olfactory system. Annu. Rev. Cell Dev. Biol. *22*, 713-737.

Mombaerts,P., Wang,F., Dulac,C., Chao,S.K., Nemes,A., Mendelsohn,M., Edmondson,J., and Axel,R. (1996). Visualizing an olfactory sensory map. Cell *87*, 675-686.

Mombaerts,P., Wang,F., Dulac,C., Vassar,R., Chao,S.K., Nemes,A., Mendelsohn,M., Edmondson,J., and Axel,R. (1996). The molecular biology of olfactory perception. Cold Spring Harb. Symp. Quant. Biol. *61*, 135-145.

Morris,R.L. and Hollenbeck,P.J. (1995). Axonal transport of mitochondria along microtubules and F-actin in living vertebrate neurons. J. Cell Biol. *131*, 1315-1326.

Moulton,D.G. and Beidler,L.M. (1967). Structure and function in the peripheral olfactory system. Physiol Rev. *47*, 1-52.

Munger,S.D., Lane,A.P., Zhong,H., Leinders-Zufall,T., Yau,K.W., Zufall,F., and Reed,R.R. (2001). Central role of the CNGA4 channel subunit in Ca2+-calmodulin-dependent odor adaptation. Science *294*, 2172-2175.

Munger,S.D., Leinders-Zufall,T., and Zufall,F. (2008). Subsystem Organization of the Mammalian Sense of Smell. Annu. Rev. Physiol.

Muramoto,K., Osada,T., Kato-Negishi,M., Kuroda,Y., and Ichikawa,M. (2003). Increase in the number of tyrosine hydroxylase-containing neurons in a primary culture system of the rat accessory olfactory bulb by co-culture with vomeronasal pockets. Neuroscience *116*, 985-994.

Murphy,P.G., Ogilvy,A.J., and Whiteley,S.M. (1996). The effect of propofol on the neutrophil respiratory burst. Eur. J. Anaesthesiol. *13*, 471-473.

Murphy,P.M., Ozcelik,T., Kenney,R.T., Tiffany,H.L., McDermott,D., and Francke,U. (1992). A structural homologue of the N-formyl peptide receptor. Characterization and chromosome mapping of a peptide chemoattractant receptor family. J. Biol. Chem. *267*, 7637-7643.

Nakamura,T. and Gold,G.H. (1987). A cyclic nucleotide-gated conductance in olfactory receptor cilia. Nature *325*, 442-444.

Neupert,W. (1997). Protein import into mitochondria. Annu. Rev. Biochem. *66*, 863-917.

Nicholls,D. and Akerman,K. (1982). Mitochondrial calcium transport. Biochim. Biophys. Acta *683*, 57-88.

Nicholls,D.G. (2005). Mitochondria and calcium signaling. Cell Calcium *38*, 311-317.

Nodari,F. and Holy,T.E. (2005). Olfactory coding: sniffing out signals. Nat. Neurosci. 2005. Apr;8. (4):406. -7. *8*, 406-407.

Nodari,F., Hsu,F.F., Fu,X., Holekamp,T.F., Kao,L.F., Turk,J., and Holy,T.E. (2008). Sulfated steroids as natural ligands of mouse pheromone-sensing neurons. J Neurosci. *28*, 6407-6418.

Nomura,T., Takahashi,S., and Ushiki,T. (2004). Cytoarchitecture of the normal rat olfactory epithelium: light and scanning electron microscopic studies. Arch. Histol. Cytol. 2004. Jun. ;67. (2):159. -70. *67*, 159-170.

Novotny,M.V., Ma,W., Wiesler,D., and Zidek,L. (1999). Positive identification of the puberty-accelerating pheromone of the house mouse: the volatile ligands associating with the major urinary protein. Proc. Biol. Sci. *266*, 2017-2022.

Nunnari,J., Fox,T.D., and Walter,P. (1993). A mitochondrial protease with two catalytic subunits of nonoverlapping specificities. Science *262*, 1997-2004.

Ober C, Aldrich CL (1997) HLA-G polymorphismus: neutral evolution or novel function? J Reprod Immunol;36(1-2):1-21

Olender,T., Lancet,D., and Nebert,D.W. (2008). Update on the olfactory receptor (OR) gene superfamily. Hum. Genomics *3*, 87-97.

Olson,R., Huey-Tubman,K.E., Dulac,C., and Bjorkman,P.J. (2005). Structure of a pheromone receptor-associated MHC molecule with an open and empty groove. PLoS. Biol. 2005. Aug. ;3(8.):e257. Epub. 2005. Jul 12. *3*, e257.

Otis,T.S., De Koninck,Y., and Mody,I. (1993). Characterization of synaptically elicited GABAB responses using patch-clamp recordings in rat hippocampal slices. J Physiol. *463*, 391-407.

Overly,C.C., Rieff,H.I., and Hollenbeck,P.J. (1996). Organelle motility and metabolism in axons vs dendrites of cultured hippocampal neurons. J. Cell Sci. *109 (Pt 5)*, 971-980.

Pankevich,D., Baum,M.J., and Cherry,J.A. (2003). Removal of the superior cervical ganglia fails to block Fos induction in the accessory olfactory system of male mice after exposure to female odors. Neurosci. Lett. *345*, 13-16.

Pankevich,D.E., Baum,M.J., and Cherry,J.A. (2004). Olfactory sex discrimination persists, whereas the preference for urinary odorants from estrous females disappears in male mice after vomeronasal organ removal. J. Neurosci. *24*, 9451-9457.

Papes,F., Logan,D.W., and Stowers,L. (2010). The vomeronasal organ mediates interspecies defensive behaviors through detection of protein pheromone homologs. Cell *141*, 692-703.

Park,M.K., Petersen,O.H., and Tepikin,A.V. (2000). The endoplasmic reticulum as one continuous Ca(2+) pool: visualization of rapid Ca(2+) movements and equilibration. EMBO J. *19*, 5729-5739.

Phillips,M., Gleeson,K., Hughes,J.M., Greenberg,J., Cataneo,R.N., Baker,L., and McVay,W.P. (1999). Volatile organic compounds in breath as markers of lung cancer: a cross-sectional study. Lancet *353*, 1930-1933.

Pietrobon,D., Di,V.F., and Pozzan,T. (1990). Structural and functional aspects of calcium homeostasis in eukaryotic cells. Eur. J. Biochem. *193*, 599-622.

Pifferi,S., Dibattista,M., Sagheddu,C., Boccaccio,A., Al,Q.A., Ghirardi,F., Tirindelli,R., and Menini,A. (2009). Calcium-activated chloride currents in olfactory sensory neurons from mice lacking bestrophin-2. J. Physiol *587*, 4265-4279.

Pozzan,T. and Rudolf,R. (2009). Measurements of mitochondrial calcium in vivo. Biochim. Biophys. Acta *1787*, 1317-1323.

Pro-Sistiaga,P., Mohedano-Moriano,A., Ubeda-Banon,I., Del,M.A.-J., Marcos,P., rtacho-Perula,E., Crespo,C., Insausti,R., and Martinez-Marcos,A. (2007). Convergence of olfactory and vomeronasal projections in the rat basal telencephalon. J. Comp Neurol. *504*, 346-362.

Prossnitz,E.R. and Ye,R.D. (1997). The N-formyl peptide receptor: a model for the study of chemoattractant receptor structure and function. Pharmacol. Ther. *74*, 73-102.

Quill,T.A., Ren,D., Clapham,D.E., and Garbers,D.L. (2001). A voltage-gated ion channel expressed specifically in spermatozoa. Proc. Natl. Acad. Sci. U. S. A *98*, 12527-12531.

Quintana A, Schwarz EC, Schwindling C, Lipp P, Kaestner L, Hoth M. (2006) Sustained activity of calcium release-activated calcium channels requires translocation of mitochondria to the plasma membrane. J Biol Chem 281(52):40302-9

Rasche,S., Toetter,B., Adler,J., Tschapek,A., Doerner,J.F., Kurtenbach,S., Hatt,H., Meyer,H., Warscheid,B., and Neuhaus,E.M. (2010). Tmem16b is specifically expressed in the cilia of olfactory sensory neurons. Chem. Senses *35*, 239-245.

Reed,R.R. (2004). After the holy grail: establishing a molecular basis for Mammalian olfaction. Cell. 2004. Jan. 23;116. (2):329. -36. *116*, 329-336.

Regnier,F.E. and Wilson,E.O. (1971). Chemical communication and "propaganda" in slave-maker ants. Science *172*, 267-269.

Resnati,M., Pallavicini,I., Wang,J.M., Oppenheim,J., Serhan,C.N., Romano,M., and Blasi,F. (2002). The fibrinolytic receptor for urokinase activates the G protein-coupled chemotactic receptor FPRL1/LXA4R. Proc. Natl. Acad. Sci. U. S. A *99*, 1359-1364.

Ressler,K.J., Sullivan,S.L., and Buck,L.B. (1994). Information coding in the olfactory system: evidence for a stereotyped and highly organized epitope map in the olfactory bulb. Cell *79*, 1245-1255.

Restrepo,D., Arellano,J., Oliva,A.M., Schaefer,M.L., and Lin,W. (2004). Emerging views on the distinct but related roles of the main and accessory olfactory systems in responsiveness to chemosensory signals in mice. Horm. Behav. *46*, 247-256.

Restrepo,D., Lin,W., Salcedo,E., Yamazaki,K., and Beauchamp,G. (2006). Odortypes and MHC peptides: Complementary chemosignals of MHC haplotype? Trends Neurosci. 2006. Nov. ;29. (11):604. -9. Epub. 2006. Aug. 14. *29*, 604-609.

Rice,S.E. and Gelfand,V.I. (2006). Paradigm lost: milton connects kinesin heavy chain to miro on mitochondria. J. Cell Biol. *173*, 459-461.

Ridgway,E.B. and Ashley,C.C. (1967). Calcium transients in single muscle fibers. Biochem. Biophys. Res. Commun. *29*, 229-234.

Riviere,S., Challet,L., Fluegge,D., Spehr,M., and Rodriguez,I. (2009). Formyl peptide receptor-like proteins are a novel family of vomeronasal chemosensors. Nature *459*, 574-577.

Rizzuto,R. (2003). Calcium mobilization from mitochondria in synaptic transmitter release. J. Cell Biol. *163*, 441-443.

Rizzuto,R. (2003). The collagen-mitochondria connection. Nat. Genet. *35*, 300-301.

Rizzuto,R. and Pozzan,T. (2003). When calcium goes wrong: genetic alterations of a ubiquitous signaling route. Nat. Genet. *34*, 135-141.

Rizzuto,R. and Pozzan,T. (2006). Microdomains of intracellular Ca2+: molecular determinants and functional consequences. Physiol Rev. *86*, 369-408.

Rizzuto,R., Bastianutto,C., Brini,M., Murgia,M., and Pozzan,T. (1994). Mitochondrial Ca2+ homeostasis in intact cells. J. Cell Biol. *126*, 1183-1194.

Rizzuto,R., Brini,M., and Pozzan,T. (1993). Intracellular targeting of the photoprotein aequorin: a new approach for measuring, in living cells, Ca2+ concentrations in defined cellular compartments. Cytotechnology *11 Suppl 1*, S44-S46.

Rizzuto,R., Brini,M., and Pozzan,T. (1994). Targeting recombinant aequorin to specific intracellular organelles. Methods Cell Biol. *40*, 339-358.

Rizzuto,R., Brini,M., Bastianutto,C., Marsault,R., and Pozzan,T. (1995). Photoprotein-mediated measurement of calcium ion concentration in mitochondria of living cells. Methods Enzymol. *260*, 417-428.

Rizzuto,R., Brini,M., Pizzo,P., Murgia,M., and Pozzan,T. (1995). Chimeric green fluorescent protein as a tool for visualizing subcellular organelles in living cells. Curr. Biol. *5*, 635-642.

Rizzuto,R., Carrington,W., and Tuft,R.A. (1998). Digital imaging microscopy of living cells. Trends Cell Biol. *8*, 288-292.

Rizzuto,R., Marchi,S., Bonora,M., Aguiari,P., Bononi,A., De,S.D., Giorgi,C., Leo,S., Rimessi,A., Siviero,R., Zecchini,E., and Pinton,P. (2009). Ca(2+) transfer from the ER to mitochondria: when, how and why. Biochim. Biophys. Acta *1787*, 1342-1351.

Rizzuto,R., Pinton,P., Brini,M., Chiesa,A., Filippin,L., and Pozzan,T. (1999). Mitochondria as biosensors of calcium microdomains. Cell Calcium *26*, 193-199.

Rizzuto,R., Pinton,P., Carrington,W., Fay,F.S., Fogarty,K.E., Lifshitz,L.M., Tuft,R.A., and Pozzan,T. (1998). Close contacts with the endoplasmic reticulum as determinants of mitochondrial Ca2+ responses. Science *280*, 1763-1766.

Rizzuto,R., Pinton,P., Ferrari,D., Chami,M., Szabadkai,G., Magalhaes,P.J., Di,V.F., and Pozzan,T. (2003). Calcium and apoptosis: facts and hypotheses. Oncogene *22*, 8619-8627.

Rizzuto,R., Simpson,A.W., Brini,M., and Pozzan,T. (1992). Rapid changes of mitochondrial Ca2+ revealed by specifically targeted recombinant aequorin. Nature *358*, 325-327.

Rodriguez,I. (2005). Remarkable diversity of mammalian pheromone receptor repertoires. Proc. Natl. Acad. Sci. U. S. A. 2005. May. 10;102. (19.):6639. -40. Epub. 2005. May. 3. *102*, 6639-6640.

Rodriguez,I. and Mombaerts,P. (2002). Novel human vomeronasal receptor-like genes reveal species-specific families. Curr. Biol. *12*, R409-R411.

Rodriguez,I., Del,P.K., Rothman,A., Ishii,T., and Mombaerts,P. (2002). Multiple new and isolated families within the mouse superfamily of V1r vomeronasal receptors. Nat. Neurosci. *5*, 134-140.

Rodriguez,I., Greer,C.A., Mok,M.Y., and Mombaerts,P. (2000). A putative pheromone receptor gene expressed in human olfactory mucosa. Nat. Genet. *26*, 18-19.

Rogers,K.S., Friend,W.H., and Higgins,E.S. (1986). Metabolic and mitochondrial disturbances in streptozotocin-treated Sprague-Dawley and Sherman rats. Proc. Soc. Exp. Biol. Med. *182*, 167-175.

Rogers,K.S., Higgins,E.S., and Loria,R.M. (1986). Influence of genetic predisposition to diabetes and obesity on mitochondrial function. Biochem. Med. Metab Biol. *35*, 72-76.

Rossler,P., Kroner,C., Krieger,J., Lobel,D., Breer,H., and Boekhoff,I. (2000). Cyclic adenosine monophosphate signaling in the rat vomeronasal organ: role of an adenylyl cyclase type VI. Chem. Senses *25*, 313-322.

Rowley and Turner (1964). Increase in macroglobulin antibodies of mouse and pig following injection of bacterial lipopolysaccharide. Immunology 394-402

Ryba,N.J. and Tirindelli,R. (1997). A new multigene family of putative pheromone receptors. Neuron *19*, 371-379.

Saito,H., Kubota,M., Roberts,R.W., Chi,Q., and Matsunami,H. (2004). RTP family members induce functional expression of mammalian odorant receptors. Cell *119*, 679-691.

Sam,M., Vora,S., Malnic,B., Ma,W., Novotny,M.V., and Buck,L.B. (2001). Neuropharmacology. Odorants may arouse instinctive behaviours. Nature *412*, 142.

Scalia,F. and Winans,S.S. (1975). The differential projections of the olfactory bulb and accessory olfactory bulb in mammals. J. Comp Neurol. *161*, 31-55.

Scott,K. (2003). Sex and the MHC. Dev. Cell. 2003. Mar. ;4(3):290. -1. *4*, 290-291.

Sekaran,S., Lall,G.S., Ralphs,K.L., Wolstenholme,A.J., Lucas,R.J., Foster,R.G., and Hankins,M.W. (2007). 2-Aminoethoxydiphenylborane is an acute inhibitor of directly photosensitive retinal ganglion cell activity in vitro and in vivo. J. Neurosci. *27*, 3981-3986.

Serizawa,S., Miyamichi,K., and Sakano,H. (2004). One neuron-one receptor rule in the mouse olfactory system. Trends Genet. *20*, 648-653.

Shaw,P.H., Held,W.A., and Hastie,N.D. (1983). The gene family for major urinary proteins: expression in several secretory tissues of the mouse. Cell *32*, 755-761.

Shimazaki,R., Boccaccio,A., Mazzatenta,A., Pinato,G., Migliore,M., and Menini,A. (2006). Electrophysiological properties and modeling of murine vomeronasal sensory neurons in acute slice preparations. Chem. Senses *31*, 425-435.

Silvotti,L., Giannini,G., and Tirindelli,R. (2005). The vomeronasal receptor V2R2 does not require escort molecules for expression in heterologous systems. Chem. Senses. 2005. Jan. ;30. (1):1-8. *30*, 1-8.

Singer,A.G., Macrides,F., Clancy,A.N., and Agosta,W.C. (1986). Purification and analysis of a proteinaceous aphrodisiac pheromone from hamster vaginal discharge. J. Biol. Chem. *261*, 13323-13326.

Singh,P.B., Brown,R.E., and Roser,B. (1987). MHC antigens in urine as olfactory recognition cues. Nature *327*, 161-164.

Skeen,J.T. and Thiessen,D.D. (1977). Scent of gerbil cuisine. Physiol Behav. *19*, 11-14.

Skulachev,V.P. (2001). Mitochondrial filaments and clusters as intracellular power-transmitting cables. Trends Biochem. Sci. *26* , 23-29.

Slotnick,B., Sanguino,A., Husband,S., Marquino,G., and Silberberg,A. (2007). Olfaction and olfactory epithelium in mice treated with zinc gluconate. Laryngoscope *117*, 743-749.

Somlyo,A.P. (1984). Cell physiology: cellular site of calcium regulation. Nature *309*, 516-517.

Sparagna,G.C., Gunter,K.K., Sheu,S.S., and Gunter,T.E. (1995). Mitochondrial calcium uptake from physiological-type pulses of calcium. A description of the rapid uptake mode. J. Biol. Chem. *270*, 27510-27515.

Spehr,J., Hagendorf,S., Weiss,J., Spehr,M., Leinders-Zufall,T., and Zufall,F. (2009). Ca2+ -calmodulin feedback mediates sensory adaptation and inhibits pheromone-sensitive ion channels in the vomeronasal organ. J. Neurosci. *29*, 2125-2135.

Spehr,M. and Leinders-Zufall,T. (2005). One neuron--multiple receptors: increased complexity in olfactory coding? Sci. STKE. *2005*, e25.

Spehr,M., Hatt,H., and Wetzel,C.H. (2002). Arachidonic acid plays a role in rat vomeronasal signal transduction. J. Neurosci. *22*, 8429-8437.

Spehr,M., Kelliher,K.R., Li,X.H., Boehm,T., Leinders-Zufall,T., and Zufall,F. (2006). Essential role of the main olfactory system in social recognition of major histocompatibility complex peptide ligands. J. Neurosci. *26*, 1961-1970.

Spehr,M., Spehr,J., Ukhanov,K., Kelliher,K.R., Leinders-Zufall,T., and Zufall,F. (2006). Parallel processing of social signals by the mammalian main and accessory olfactory systems. Cell Mol. Life Sci. *63*, 1476-1484.

Spehr,M., Wetzel,C.H., Hatt,H., and Ache,B.W. (2002). 3-phosphoinositides modulate cyclic nucleotide signaling in olfactory receptor neurons. Neuron *33*, 731-739.

Stachecki,J.J. and Armant,D.R. (1996). Regulation of blastocoele formation by intracellular calcium release is mediated through a phospholipase C-dependent pathway in mice. Biol. Reprod. *55*, 1292-1298.

Stephan,A.B., Shum,E.Y., Hirsh,S., Cygnar,K.D., Reisert,J., and Zhao,H. (2009). ANO2 is the cilial calcium-activated chloride channel that may mediate olfactory amplification. Proc. Natl. Acad. Sci. U. S. A *106*, 11776-11781.

Stewart,R. and Lane,R.P. (2007). V1R promoters are well conserved and exhibit common putative regulatory motifs. BMC. Genomics *8*, 253.

Stowers,L. and Marton,T.F. (2005). What is a pheromone? Mammalian pheromones reconsidered. Neuron. 2005. Jun. 2;46. (5):699. -702. *46*, 699-702.

Stowers,L., Holy,T.E., Meister,M., Dulac,C., and Koentges,G. (2002). Loss of sex discrimination and male-male aggression in mice deficient for TRP2. Science *295*, 1493-1500.

Strehler,E.E. and Treiman,M. (2004). Calcium pumps of plasma membrane and cell interior. Curr. Mol. Med. *4*, 323-335.

Stuart,G.J., Dodt,H.U., and Sakmann,B. (1993). Patch-clamp recordings from the soma and dendrites of neurons in brain slices using infrared video microscopy. Pflugers Arch. *423*, 511-518.

Su,S.B., Gong,W., Gao,J.L., Shen,W., Murphy,P.M., Oppenheim,J.J., and Wang,J.M. (1999). A seven-transmembrane, G protein-coupled receptor, FPRL1, mediates the chemotactic activity of serum amyloid A for human phagocytic cells. J. Exp. Med. *189*, 395-402.

Szabadkai,G., Bianchi,K., Varnai,P., De,S.D., Wieckowski,M.R., Cavagna,D., Nagy,A.I., Balla,T., and Rizzuto,R. (2006). Chaperone-mediated coupling of endoplasmic reticulum and mitochondrial Ca2+ channels. J. Cell Biol. *175*, 901-911.

Szabadkai,G., Simoni,A.M., Bianchi,K., De,S.D., Leo,S., Wieckowski,M.R., and Rizzuto,R. (2006). Mitochondrial dynamics and Ca2+ signaling. Biochim. Biophys. Acta *1763*, 442-449.

Takami,S. (2002). Recent progress in the neurobiology of the vomeronasal organ. Microsc. Res. Tech. *58*, 228-250.

Takano,T., Fiore,S., Maddox,J.F., Brady,H.R., Petasis,N.A., and Serhan,C.N. (1997). Aspirin-triggered 15-epi-lipoxin A4 (LXA4) and LXA4 stable analogues are potent inhibitors of acute inflammation: evidence for anti-inflammatory receptors. J. Exp. Med. *185*, 1693-1704.

Territo,P.R., French,S.A., and Balaban,R.S. (2001). Simulation of cardiac work transitions, in vitro: effects of simultaneous Ca2+ and ATPase additions on isolated porcine heart mitochondria. Cell Calcium *30* , 19-27.

Territo,P.R., French,S.A., Dunleavy,M.C., Evans,F.J., and Balaban,R.S. (2001). Calcium activation of heart mitochondrial oxidative phosphorylation: rapid kinetics of mVO2, NADH, AND light scattering. J. Biol. Chem. *276*, 2586-2599.

Thompson,R.N., Robertson,B.K., Napier,A., and Wekesa,K.S. (2004). Sex-specific responses to urinary chemicals by the mouse vomeronasal organ. Chem. Senses *29*, 749-754.

Thorne,N. and Amrein,H. (2003). Vomeronasal organ: pheromone recognition with a twist. Curr. Biol. 2003. Mar. 18. ;13(6.):R220. -2. *13*, R220-R222.

Tirindelli,R., Dibattista,M., Pifferi,S., and Menini,A. (2009). From pheromones to behavior. Physiol Rev. *89*, 921-956.

Toescu,E.C. and Verkhratsky,A. (2000). Parameters of calcium homeostasis in normal neuronal ageing. J. Anat. *197 Pt 4*, 563-569.

Touhara,K. and Vosshall,L.B. (2009). Sensing odorants and pheromones with chemosensory receptors. Annu. Rev. Physiol *71*, 307-332.

Trenker,M., Malli,R., Fertschai,I., Levak-Frank,S., and Graier,W.F. (2007). Uncoupling proteins 2 and 3 are fundamental for mitochondrial Ca2+ uniport. Nat. Cell Biol. *9*, 445-452.

Trinh,K. and Storm,D.R. (2003). Vomeronasal organ detects odorants in absence of signaling through main olfactory epithelium. Nat. Neurosci. *6*, 519-525.

Trollinger,D.R., Cascio,W.E., and Lemasters,J.J. (2000). Mitochondrial calcium transients in adult rabbit cardiac myocytes: inhibition by ruthenium red and artifacts caused by lysosomal loading of Ca(2+)-indicating fluorophores. Biophys. J. *79*, 39-50.

Tsien,R.Y. and Rink,T.J. (1981). Ca2+-selective electrodes: a novel PVC-gelled neutral carrier mixture compared with other currently available sensors. J. Neurosci. Methods *4*, 73-86.

Ui,M., Okada,T., Hazeki,K., and Hazeki,O. (1995). Wortmannin as a unique probe for an intracellular signalling protein, phosphoinositide 3-kinase. Trends Biochem. Sci. *20*, 303-307.

Ukhanov,K., Leinders-Zufall,T., and Zufall,F. (2007). Patch-clamp analysis of gene-targeted vomeronasal neurons expressing a defined V1r or V2r receptor: ionic mechanisms underlying persistent firing. J. Neurophysiol. *98*, 2357-2369.

Vandenbergh,J.G. (1975). Proceedings: Pheromonal stimulation of puberty in female mice. J. Endocrinol. *64*, 38P.

Vandenbergh,J.G., Whitsett,J.M., and Lombardi,J.R. (1975). Partial isolation of a pheromone accelerating puberty in female mice. J. Reprod. Fertil. *43*, 515-523.

Vosshall,L.B. (2005). Social signals: the secret language of mice. Curr. Biol. *15*, R255-R257.

Wagner,S., Gresser,A.L., Torello,A.T., and Dulac,C. (2006). A multireceptor genetic approach uncovers an ordered integration of VNO sensory inputs in the accessory olfactory bulb. Neuron. 2006. Jun. 1;50. (5):697. -709. *50*, 697-709.

Wang,H.J., Guay,G., Pogan,L., Sauve,R., and Nabi,I.R. (2000). Calcium regulates the association between mitochondria and a smooth subdomain of the endoplasmic reticulum. J. Cell Biol. *150*, 1489-1498.

Wang,Z., Balet,S.C., Li,V., Nudelman,A., Chan,G.C., and Storm,D.R. (2006). Pheromone detection in male mice depends on signaling through the type 3 adenylyl cyclase in the main olfactory epithelium. J. Neurosci. *26*, 7375-7379.

Watson,R.P., Demmer,J., Baker,E.N., and Arcus,V.L. (2007). Three-dimensional structure and ligand binding properties of trichosurin, a metatherian lipocalin from the milk whey of the common brushtail possum Trichosurus vulpecula. Biochem J *408*, 29-38.

Wedekind C, Seebeck T, Bettens F, Paepke AJ. (1995) MHC-dependent mate prefenrences in humans ProcBiolSci 1995;260(1359):245-9

Wekesa,K.S. and Anholt,R.R. (1997). Pheromone regulated production of inositol-(1, 4, 5)-trisphosphate in the mammalian vomeronasal organ. Endocrinology *138*, 3497-3504.

Wekesa,K.S., Miller,S., and Napier,A. (2003). Involvement of G(q/11) in signal transduction in the mammalian vomeronasal organ. J. Exp. Biol. *206*, 827-832.

White,R.J. and Reynolds,I.J. (1997). Mitochondria accumulate Ca2+ following intense glutamate stimulation of cultured rat forebrain neurones. J. Physiol *498 (Pt 1)*, 31-47.

Willis,C.M., Church,S.M., Guest,C.M., Cook,W.A., McCarthy,N., Bransbury,A.J., Church,M.R., and Church,J.C. (2004). Olfactory detection of human bladder cancer by dogs: proof of principle study. BMJ *329*, 712.

Witt,M. and Hummel,T. (2006). Vomeronasal versus olfactory epithelium: is there a cellular basis for human vomeronasal perception? Int. Rev. Cytol. *248*, 209-259.

Wong,S.T., Trinh,K., Hacker,B., Chan,G.C., Lowe,G., Gaggar,A., Xia,Z., Gold,G.H., and Storm,D.R. (2000). Disruption of the type III adenylyl cyclase gene leads to peripheral and behavioral anosmia in transgenic mice. Neuron *27*, 487-497.

Woodley,S.K., Cloe,A.L., Waters,P., and Baum,M.J. (2004). Effects of vomeronasal organ removal on olfactory sex discrimination and odor preferences of female ferrets. Chem. Senses *29*, 659-669.

Wysocki,C.J. and Lepri,J.J. (1991). Consequences of removing the vomeronasal organ. J. Steroid Biochem. Mol. Biol. *39*, 661-669.

Wysocki,C.J. and Preti,G. (1998). Pheromonal influences. Arch. Sex Behav. *27*, 627-634.

Wysocki,C.J. and Preti,G. (2004). Facts, fallacies, fears, and frustrations with human pheromones. Anat. Rec. A Discov. Mol. Cell Evol. Biol. *281*, 1201-1211.

Wysocki,C.J., Yamazaki,K., Curran,M., Wysocki,L.M., and Beauchamp,G.K. (2004). Mice (Mus musculus) lacking a vomeronasal organ can discriminate MHC-determined odortypes. Horm. Behav. 2004. Sep. ;46. (3):241. -6. *46*, 241-246.

Yaffe,M.P. (1999). The machinery of mitochondrial inheritance and behavior. Science *283*, 1493-1497.

Yamaguchi,M., Yamazaki,K., Beauchamp,G.K., Bard,J., Thomas,L., and Boyse,E.A. (1981). Distinctive urinary odors governed by the major histocompatibility locus of the mouse. Proc. Natl. Acad. Sci. U. S. A *78*, 5817-5820.

Yamazaki,K., Beauchamp,G.K., Imai,Y., Bard,J., Phelan,S.P., Thomas,L., and Boyse,E.A. (1990). Odor types determined by the major histocompatibility complex in germfree mice. Proc. Natl. Acad. Sci. U. S. A *87* , 8413-8416.

Yang,C. and Delay,R.J. (2010). Calcium-activated chloride current amplifies the response to urine in mouse vomeronasal sensory neurons. J. Gen. Physiol *135*, 3-13.

Yildirim,E., Dietrich,A., and Birnbaumer,L. (2003). The mouse C-type transient receptor potential 2 (TRPC2) channel: alternative splicing and calmodulin binding to its N terminus. Proc. Natl. Acad. Sci. U. S. A *100*, 2220-2225.

Young,J.M., Kambere,M., Trask,B.J., and Lane,R.P. (2005). Divergent V1R repertoires in five species: Amplification in rodents, decimation in primates, and a surprisingly small repertoire in dogs. Genome Res. *15*, 231-240.

Yule,D.I., Ernst,S.A., Ohnishi,H., and Wojcikiewicz,R.J. (1997). Evidence that zymogen granules are not a physiologically relevant calcium pool. Defining the distribution of inositol 1,4,5-trisphosphate receptors in pancreatic acinar cells. J. Biol. Chem. *272*, 9093-9098.

Zagotta,W.N. and Siegelbaum,S.A. (1996). Structure and function of cyclic nucleotide-gated channels. Annu. Rev. Neurosci. *19*, 235-263.

Zhang,J.X., Sun,L., Zhang,J.H., and Feng,Z.Y. (2008). Sex- and gonad-affecting scent compounds and 3 male pheromones in the rat. Chem. Senses *33*, 611-621.

Zhang,P., Yang,C., and Delay,R.J. (2008). Urine stimulation activates BK channels in mouse vomeronasal neurons. J. Neurophysiol. *100*, 1824-1834.

Zucchi,R., Chiellini,G., Scanlan,T.S., and Grandy,D.K. (2006). Trace amine-associated receptors and their ligands. Br. J. Pharmacol. *149*, 967-978.

Zufall,F. (1993). Cyclic AMP-gated cation channels of olfactory receptor neurons. EXS *66*, 135-145.

Zufall,F. (2005). Connexins and olfactory synchronicity: toward the olfactory code. Neuron *46*, 693-694.

Zufall,F. (2005). The TRPC2 ion channel and pheromone sensing in the accessory olfactory system. Naunyn Schmiedebergs Arch. Pharmacol. *371*, 245-250.

Zufall,F. and Firestein,S. (1993). Divalent cations block the cyclic nucleotide-gated channel of olfactory receptor neurons. J. Neurophysiol. *69*, 1758-1768.

Zufall,F. and Hatt,H. (1991). Dual activation of a sex pheromone-dependent ion channel from insect olfactory dendrites by protein kinase C activators and cyclic GMP. Proc. Natl. Acad. Sci. U. S. A *88*, 8520-8524.

Zufall,F. and Leinders-Zufall,T. (1997). Identification of a long-lasting form of odor adaptation that depends on the carbon Monoxide/cGMP second-messenger system. J. Neurosci. *17*, 2703-2712.

Zufall,F. and Leinders-Zufall,T. (1998). Role of cyclic GMP in olfactory transduction and adaptation. Ann. N. Y. Acad. Sci. *855* , 199-204.

Zufall,F. and Leinders-Zufall,T. (2000). The cellular and molecular basis of odor adaptation. Chem. Senses *25*, 473-481.

Zufall,F. and Leinders-Zufall,T. (2007). Mammalian pheromone sensing. Curr. Opin. Neurobiol.

Zufall,F. and Munger,S.D. (2001). From odor and pheromone transduction to the organization of the sense of smell. Trends Neurosci. *24*, 191-193.

Zufall,F. and Munger,S.D. (2010). Receptor guanylyl cyclases in mammalian olfactory function. Mol. Cell Biochem. *334*, 191-197.

Zufall,F., Firestein,S., and Shepherd,G.M. (1991). Analysis of single cyclic nucleotide-gated channels in olfactory receptor cells. J. Neurosci. *11*, 3573-3580.

Zufall,F., Firestein,S., and Shepherd,G.M. (1994). Cyclic nucleotide-gated ion channels and sensory transduction in olfactory receptor neurons. Annu. Rev. Biophys. Biomol. Struct. *23*, 577-607.

Zufall,F., Hatt,H., and Firestein,S. (1993). Rapid application and removal of second messengers to cyclic nucleotide-gated channels from olfactory epithelium. Proc. Natl. Acad. Sci. U. S. A *90*, 9335-9339.

Zufall,F., Kelliher,K.R., and Leinders-Zufall,T. (2002). Pheromone detection by mammalian vomeronasal neurons. Microsc. Res. Tech. *58*, 251-260.

Zufall,F., Leinders-Zufall,T., and Greer,C.A. (2000). Amplification of odor-induced Ca(2+) transients by store-operated Ca(2+) release and its role in olfactory signal transduction. J. Neurophysiol. *83*, 501-512.

Zufall,F., Shepherd,G.M., and Barnstable,C.J. (1997). Cyclic nucleotide gated channels as regulators of CNS development and plasticity. Curr. Opin. Neurobiol. *7*, 404-412.

Zufall,F., Shepherd,G.M., and Firestein,S. (1991). Inhibition of the olfactory cyclic nucleotide gated ion channel by intracellular calcium. Proc. Biol. Sci. *246*, 225-230.

Zufall,F., Ukhanov,K., Lucas,P., Liman,E.R., and Leinders-Zufall,T. (2005). Neurobiology of TRPC2: from gene to behavior. Pflugers Arch. *451*, 61-71.

8 Acknowledgement

Abschließend möchte ich mich bei allen bedanken, die zum Gelingen dieser Doktorarbeit beigetragen haben.

An erster Stelle möchte ich mich bei meinem Doktorvater Prof. Dr. Marc Spehr für die Überlassung des interessanten Themas dieser Arbeit und die mir entgegenbrachte Unterstützung bedanken. Weiterhin danke ich für die konstruktive Kritik, die mir persönlich und fachlich viel gebracht hat. Danke für die vielen spannende Konferenzen, die ich besuchen durfte und mir ermöglicht haben, mich mit internationalen Wissenschaftlern austauschen zu können. Danke, dass mir das Vertrauen entgegengebracht wurde meine Arbeit auf einer Vortragsreise in Liverpool präsentieren zu dürfen. Ich habe während der letzten Jahre sehr viel gelernt, habe interessante Erfahrungen sammeln dürfen und hatte viel Spaß dabei.

Herrn Prof. Dr. Dr. Frank Zufall möchte ich für die vielen wertvollen Tipps auf Konferenzen und besonders für die Übernahme des Koreferats danken.

Für die finanzielle Förderung bei Kongressreisen danke ich der „Ruhr-University Research School“.

Ein herzliches Dankeschön gilt allen Mitarbeitern der AG Chemosensorik, die mir hilfreich mit Rat und Tat zur Seite gestanden haben.

Mein ganz besonderer Dank gilt meinen Eltern und meiner Familie, die mir das Studium und die Promotion ermöglicht und mich immer liebevoll unterstützt haben. Ohne diese Hilfe und Aufmunterung in schwierigen Phasen wäre das alles nicht möglich gewesen.

Vielen Dank!

9 Curriculum vitae

Personal Data Daniela Patrizia Flügge

Jülicherstraße 86
D-52146 Würselen
Tel.: +49 163 2379736

D.Fluegge@sensorik.rwth-aachen.de

Birth Sept. 26, 1983 – Mainz

Education and academic degrees

March 2007 – October 2010	**PhD thesis** – Ruhr-University Bochum / RWTH Aachen "Physiological investigation of signaling mechanisms in the mouse olfactory and vomeronasal system"
May 2005 – January 2007	**Master of Science** – Ruhr-University Bochum "Overexpression of lysosomal cysteine proteases in murine microglial cells using lentiviral vectors"
October 2002 – May 2005	**Bachelor of Science** – Ruhr-University Bochum "Examination of mitochondrial function in *parkin* deficient mice"
August 1993 – June 2002	**General qualification for university entrance** (Abitur) Märkisches Gymnasium Schwelm / NRW
August 1991 – June 1993	Grundschule Westfalendamm Schwelm / NRW
August 1989 – June 1991	Gustav-Brunner Grundschule Gustavsburg / Hessen

Language skills German, English, Italian, French

Scholarships Research School at Ruhr-University Bochum
International Graduate School of Biosciences

Publications

S. Riviére*, L. Challet*, **D. Fluegge***, M. Spehr and I. Rodriguez, "Formyl receptors-like are a novel family of vomeronasal chemosensors" (*equal contribution) *Nature* (22nd April 2009)

S. Hagendorf, **D. Fluegge**, C.H. Engelhardt and M. Spehr "Homeostatic control of sensory output in basal vomeronasal neurons: Activity-dependent expression of ether-à-go-go related gene potassium channel" *Journal of Neuroscience* (7th January 2009)

Talks

Liverpool, 15 – 17, 2010: University of Liverpool, Faculty of Veterinary Science

D. Fluegge
"Characterization of the mitochondrial role in calcium homeostasis in olfactory sensory neurons"

Participation to conferences

Poster presentations:

Washington, May 23- 26, 2010: Janelia Farms

Fluegge, D., Herling, S., Cainarca, S., Corazza S. and Spehr, M
"On the role of mitochondrial calcium in mouse olfactory sensory neurons"

Chicago, October 16 – 21, 2009: Neuroscience 2009

D. Fluegge, S. Rivière, L. Challet, M. Spehr, I. Rodriguez
"Identification and Functional Characterization of Formyl receptor-like proteins in the mouse vomeronasal organ"

Göttingen, March 25 – 29, 2009: 8th Göttingen Meeting of the German Neuroscience Society

D. Fluegge, M. Spehr
"An intact whole organ preparation of the mouse vomeronasal organ: confocal life cell imaging in the microvillous layer of the sensory epithelium"

S. Hagendorf, **D. Fluegge**, C.H. Engelhardt and M. Spehr:
"Homeostatic Control of Sensory Output in Basal Vomeronasal Neurons: Activity-Dependent Expression of Ether-à-Go-Go Related Gene Potassium Channels"

San Francisco, July 21 - 26, 2008: International Symposium on Olfaction and Taste/AChemS Meeting

D. Fluegge, C.H. Engelhardt, S. Hagendorf and M. Spehr
"An intact whole organ preparation of the mouse vomeronasal organ: confocal life cell imaging in the microvillous layer of the sensory epithelium"

S. Hagendorf, C.H. Engelhardt, **D. Fluegge** and M. Spehr:
"Intrinsic plasticity in the mouse vomeronasal organ: The role of the ether-à-gogo related gene ion channel"

Cologne, March 02 - 05, 2008: 87th Annual Meeting of the German Physiological Society

D. Fluegge, C.H. Engelhardt, S. Hagendorf and M. Spehr
"Functional characterization of recombinant vomeronasal receptors"

S. Hagendorf, C.H. Engelhardt, **D. Fluegge** and M. Spehr:
"Characterization of the ether-à-gogo related gene ion channel in the mouse vomeronasal organ"

Heidelberg, Sept. 28-29, 2007: Symposium Olfactory Information Processing, University of Heidelberg

D. Fluegge, C.H. Engelhardt, S. Hagendorf and M. Spehr
"Functional characterization of recombinant vomeronasal receptors"

S. Hagendorf, C. H. Engelhardt, **D. Fluegge**, L. Klein-Hitpass and M. Spehr:
"Regulation of ion channel gene expression in the mouse VNO''